EXPERIMENTAL VALIDATION OF A NOVEL FISCHER-TROPSCH TUBULAR FIXED BED REACTOR UNDER SUPERCRITICAL CONDITIONS

A Thesis

by

AMRO ISMAIL ESSA KASHT

Submitted to the Office of Graduate and Professional Studies of
Texas A&M University
in partial fulfillment of the requirements for the degree of

MASTER OF SCIENCE

Chair of Committee,	Nimir Elbashir
Committee Members,	Luc Véchot
	Mohamed Aggour
Head of Department,	Nazmul Karim

August 2015

Major Subject: Chemical Engineering

ABSTRACT

Selecting a reactor technology for the Fischer-Tropsch Synthesis (FTS) is a trade-off since each reactor type (reaction phase) has its strengths and weaknesses. In order to overcome many of the limitations of the conventional FTS reactors, supercritical fluids (SCF) were proposed to be used as a reaction medium. SCF act as a unique reaction media, offering single-phase operation with diffusivities similar to those of gases and solubilities and heat transfer properties similar to those of liquids.

Even though SCF were applied in a number of studies showing promising enhancements since the late 1980s, none of these studies were able to move the supercritical Fischer-Tropsch (SC-FTS) technology beyond the lab-scale. The aim of this project was to overcome this by commissioning a bench-scale, high-pressure reactor unit that can provide better understanding of the FTS reaction, optimize the reaction behavior for typical large-scale FTS processes, and investigate/validate the potentials of enhancements of the FTS under supercritical phase.

This thesis describes the methods followed in commissioning and operating this unique reactor unit. In addition, to accomplish the project goals, a sophisticated experimental campaign was developed, starting with the catalyst (15 wt% Co/Al_2O_3) preparation and finishing with the product analysis using multiple gas chromatographs (GCs). The validation study showed that under SC-FTS operation, CO conversion increased by 14 %, methane selectivity decreased from 15 to 2.2 normalized wt%, middle distillates and wax selectivities increased by 35 wt% and 75 wt%, respectively, and the

chain growth probability increased from 0.76 to 0.85, while total olefin formation rate increased by 62 %. The aforementioned improvements were attributed to the *in-situ* wax extraction ability of SC solvents, their ability to extract olefins before they undergo secondary reactions, and their liquid-like heat capacity allowing for better reaction heat removal. The obtained results demonstrate that the SC-FTS technology has the potential to substitute conventional FTS processes. Nevertheless, deeper understanding of the reaction mechanism and the reaction mixture thermo-physical properties under SC phase as well as techno-economic evaluation of this technology are required before it can be commercialized.

DEDICATION

Mum and Dad, thanks for everything I am, for your relentless support and for carrying me through each and every step of my life.

My beloved Sanah, thank you for the joy and happiness you brought to my life; you have been my source of motivation and strength thru moments of despair and discouragement.

My buddy Ghazi the cat who is to be blamed for any typo in this work. Thank you for distracting me with your cuteness overload and playful nature.

Dear family and friends, thank you for bearing with me through all these years and for being there for me when I needed you the most.

I dedicate my past, present and future to you all. Thank you!

ACKNOWLEDGEMENTS

The realization of this project was made possible thru the generous financial fund offered by Qatar National Research Fund and Texas A&M University. The Office of Graduate and Professional Studies at Texas A&M University at Qatar are also sincerely acknowledged for their support and effort in facilitating resources that enabled the construction and operation of the novel FTS reactor unit. In addition, I am profoundly grateful for the research fellowship awarded by Itochu Corporation.

I would like to thank my advisor, Dr. Nimir Elbashir and my committee members, Dr. Luc Véchot and Prof. Mohamed Aggour, for their guidance and support throughout the course of this work. I am also grateful to Dr. Jan Blank for his helpful discussions and his assistance in running the experimental campaign. I also extend my gratitude to Rehan Hussain for his assistance in performing the FTS calculations. I am sincerely thankful to all members of our research team for their valuable scientific discussions and for assistance in commissioning, startup and operating the high-pressure bench-scale reactor unit. We also appreciate the generosity of Prof. Dragomir Bukur for providing the initial catalyst samples. I would also like to express my gratitude to the faculty and staff at the chemical engineering program and the Academic Success Center for their valuable assistance and reviews. Finally, I would like to thank my friends and colleagues at Texas A&M University for making my time here a lively experience.

NOMENCLATURE

3WV	Three Way Valve
6WV	Six Way Valve
8WVS	Eight Way Selecting Valve
AG	Air Generator
Al_2O_3	Alumina
Ar	Argon
ASF	Anderson-Schulz-Flory
ASME	American Society of Mechanical Engineers
bpd	Barrel per day
BTL	Biomass-to-Liquid
CH_4	Methane
Co	Cobalt
CO	Carbon monoxide
CO_2	Carbon dioxide
CNG	Crude Natural Gas
CTL	Coal To Liquid
CV	Check Valve
F	Furnace
FBR	Fluidized Bed Reactors
Fe	Iron

FI	Flow Indicator
FID	Flame Ionization Detector
FTS	Fischer-Tropsch Synthesis
GB	Gas Booster
GC	Gas Chromatograph
GTL	Gas-to-Liquid
H_2	Hydrogen
He	Helium
HT	Heating Tape
HTFT`	High Temperature Fischer-Tropsch
KV	Automatic Shut-off Valve
KY	Solenoid Valve
LHC	Light Hydrocarbons
LNG	Liquefied Natural Gas
LTFT	Low-Temperature-Fischer-Tropsch
MD	Middle Distillates
MFC	Mass Flow Controller
MgO	Magnesia
MS	Mass Spectroscopy
NG	Natural Gas
N_2	Nitrogen
Ni	Nickel

NO_x	Nitrogen Oxides
PCV	Pressure Control Valve
PI	Pressure Indicator
PLC	Programmable Logic Controllers
PPE	Personal Protective Equipment
PSV	Pressure Safety Valve
PT	Pressure Transmitter
PV	Pressure Valve
QNRF	Qatar National Research Fund
QP	Qatar Petroleum
R	Reactor
Ru	Ruthenium
SC	Supercritical
SCADA	Supervisory Control And Data Acquisition
SCF	Supercritical Fluids
SC-FTS	Supercritical Fischer-Tropsch Synthesis
SiO_2	Silica
SM	Static Mixer
SMDS	Shell Middle distillates Synthesis
SNG	Sweet Natural Gas
SPK	Synthetic Paraffinic Kerosene
SPR	Slurry Phase Reactors

TAMUQ	Texas A&M University at Qatar
TCD	Thermal Conductivity Detector
TE	Temperature Element
TFBR	Tubular Fixed Bed Reactors
TiO_2	Titania
V	Vessel
WC	Water Chiller
WGS	Water Gas Shift
XTL	X-to-Liquid

TABLE OF CONTENTS

Page

LIST OF FIGURES

Page

Page

Page

Page

LIST OF TABLES

Page

I. INTRODUCTION AND LITERATURE REVIEW

I.1 Gas-to-Liquid Technology

Crude oil has been an important commodity for a long time. It has been extensively used for energy generation, as a transportation fuel and in the petrochemical industry. However, oil prices are escalating continuously while its natural resources are being depleted. In addition, population growth and industrial expansion in the developed countries have boosted our global rate of oil consumption and have created serious energy supply challenges [1]. As the future demand is expected to further increase, traditional sources of energy must be utilized more efficiently and sustainable alternative energy sources that can alleviate pressure on depleting oil resources must be investigated and developed to bridge the foreseen supply gap. Escalating concerns about the unstable oil prices and oil supply insecurity coupled with stricter environmental regulations have catalyzed the interest in the production of synthetic fuels from alternative resources such as natural gas (NG), coal and biomass via the X-to-Liquid (XTL) process, where X being G (referring to natural gas GTL), C (referring to coal CTL) and B (referring to biomass BTL) [2-7].

Being poor in petroleum resources but rich in coal resources, Germany intensely invested in developing coal-derived liquid fuels as an alternative to petroleum-based fuels. In 1923 two German scientists (Franz Fischer and Hans Tropsch) were able to convert a mixture carbon monoxide (CO) and hydrogen (H_2) called syngas into various hydrocarbons that can later be refined to obtain liquid fuels and other value added chemicals [8]. The first commercial CTL plant was operated by the German firm Brabag

between 1936 and 1938 in Braunkohle-Benzin, Germany and had a capacity of 660000 tons per year of primary products [9, 10]. During the Second World War, Germany needed liquid fuels to fulfill its military aspirations and drive its tank fleets. This uprise in the need for liquid fuels boosted the production of synthetic fuels via the CTL process, which accounted for more than 30 % of Germany's war period fuel [10]. After the war had ended, German FTS technology was transferred and further developed in the United States. However, in the 1950s and 1960s cheap oil prices forced US companies to discontinue their FTS research. On the contrary, in South Africa (a coal-rich country), Sasol continued FTS development efforts and in 1955 started the operation of SASOL 1 plant with 8000 barrel per day (bpd) production capacity [11]. Afterward, the 1970s oil crisis revived the interest in the FTS, and that is when major companies lead by Sasol and Shell seriously invested to improve the Fischer-Tropsch process. A more favorable route to CTL was found to be the GTL process, by which NG is reformed to produce syngas, which is then converted via the catalytic FTS reactor into value added chemicals and environmentally clean fuels [12]. In the mid-1990s Sasol commissioned the MossGas GLT plant (Mossel Bay, South Africa) that utilized Sasol's slurry technology, while Royal Dutch Shell completed the 12500 bpd Bintulu (Malaysia) plant, which produce middle distillates liquid fuels and chemicals using cobalt (Co) based catalyst in a tubular fixed bed reactor (TFBR) [11].

The synthetic crude oil produced via the GTL process is extremely pure and virtually free of sulfur and aromatics, which makes GTL fuels a cleaner option with reduced CO, nitrogen oxides NO_x, hydrocarbons and particulate emissions [13]. The

synthetic crude can then be refined/cracked into gasoline, diesel and Synthetic Paraffinic Kerosene (SPK). GTL fuels can be blended with petroleum-derived fuels in order to bring them up to compliance with aviation standards. Other than fuels, the FTS can be used as a source of high-value chemicals (α-olefins) that are produced with significant quantities during the FTS. These α-Olefins are used as a chemical intermediate for many chemical processes including polymer, plastic, detergent and lubricant manufacturing [14].

In the GTL process, NG molecules are torn apart and then reassembled to form longer chain hydrocarbon molecules following four distinct steps, as illustrated in Figure 1. The first step is gas sweetening, which include gas dehydration, acid gas removal, mercury removal, fractionation, nitrogen rejection and helium extraction. Next is syngas generation via steam reforming or partial oxidation of NG. This is followed by the catalytic FTS, by which syngas is converted into an array of hydrocarbons chains (C_1 to C_{40+}) including (*n*-paraffins, α-olefins, isomers, alkenes, oxygenates, ketones, carboxylic acids, etc.). So, in order to obtain the desired hydrocarbon cuts (generally middle distillates diesel, jet fuel and lubricants) [1], the formed products must be refined, by hydrocracking, isomerization, and/or hydro-isomerization processes [1].

The main reason behind the increased interest in GTL industry is that NG is considered to be relatively clean, cheap and easy to access. However, it fails to make any significant contribution as a transportation fuel in its gaseous state. The GTL process facilitates the transportation of NG as liquid fuels and chemicals when alternative transportation techniques, pipelines or liquefaction (LNG), are not economically or physically possible.

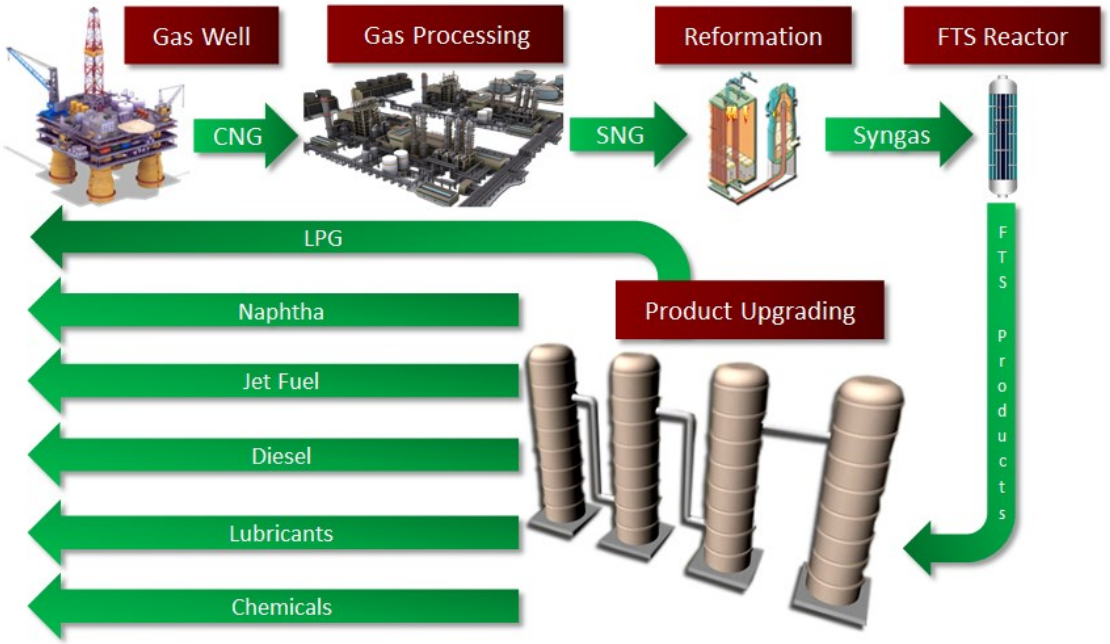

Figure 1. GTL process overview.

For countries with limited oil resources but considerable NG resources, the benefits of the GTL process are evident. The GTL technology can play a significant role in ensuring energy security for these countries as it brings more flexibility to NG investment and offers an alternative source of ultra-clean fuels and value added chemicals. The continuous increase of oil prices means that GTL derived fuel is becoming more economically attractive. Additionally, fuels produced via the GTL process have an environmental advantage over those produced from conventional crude oil since they have low sulfur and aromatic content. Abundant non-associated NG reserves led the way for the State of Qatar to become the world leader in GTL production and a globalized research center in GTL technology. Qatar's vision, of becoming the world capital of GTL, has met success through the inauguration of the Oryx GTL and Shell Pearl projects. The Oryx GTL

project is a joint venture between Qatar Petroleum (QP) and Sasol Limited of South Africa. The plant was commissioned in 2006 with a production capacity of 34000 bpd utilizing Sasol's slurry reactor technology [9]. Adjacent to the Oryx GTL plant, a more recent plant started operation in 2011, the Pearl GTL plant is a joint venture between QP and Royal Dutch Shell. The Pearl GTL is considered as the largest GTL plant in the world. The Pearl GTL plant is a scaled-up version of Shell Bintulu plant in Malaysia, which is based on Shell Middle Distillates Synthesis (SMDS) technology that utilize multi-tubular fixed bed reactors with cobalt-based catalyst to produce heavy wax that will later be hydrocracked into middle distillates and base oils. The plant is capable of producing above 250000 bbl/day of synthetic fuels and specialty chemicals [15]. The plant produces SPK, which is currently being mixed with petroleum-derived kerosene in order to meet the aviation industry standards. Even so, the primary future target is to satisfy the demand of Qatar Airways fleet operating at the Doha International Airport using the locally produced synthetic jet fuel. Through the utilization of ultra-clean fuels, Qatar is demonstrating its commitment to sustainable development and becoming a role model in the use of environmentally improved fuels.

I.2 The Fischer-Tropsch Synthesis

The Fischer-Tropsch synthesis (FTS) is considered as the heart of the GTL process responsible for converting NG derived syngas into ultra-clean fuels and value added chemicals [16]. The FTS is a surface catalyzed process (heterogeneous reaction) in which syngas (H_2 and CO) react on an active catalyst site; usually cobalt (Co) or iron (Fe), to produce longer chain gaseous, liquid and solid (wax) hydrocarbons composed mainly of

n-paraffins, α-olefins, isomers, alkenes and oxygenates [1, 17, 18]. The reaction of H_2 and CO during the FTS consists of a long and complex reaction sequence, nonetheless it has long been generalized as a polymerization process [8, 19, 20], by which a monomer is formed from the primary two reactants. Then the monomer building blocks joins by the successive addition of C_1 units to form longer chain hydrocarbon molecules, according to the following reaction equation:

$$nCO + 2nH_2 \rightarrow (-CH_2-)_n + nH_2O$$

The chain termination is either done by adding a hydrogen molecule to the chain and then detaching from the surface resulting in a paraffin molecule:

$$nCO + (2n+1)H_2 \rightarrow C_nH_{2n+2} + nH_2O$$

Or the termination can be done by directly detaching from the surface resulting in an olefin:

$$nCO + 2nH_2 \rightarrow C_nH_{2n} + nH_2O$$

Other undesirable reactions that usually accompany the FTS reaction are methanation and the Water Gas Shift (WGS) reaction. The methanation reaction takes place as follows:

$$CO + 3H_2 \rightarrow CH_4 + H_2O$$

While the WGS reaction occurs as follows:

$$CO + H_2O \rightarrow CO_2 + H_2$$

The WGS reaction converts carbon monoxide to carbon dioxide, which is an unwanted byproduct. The extent of the WGS reaction depends on the type of the catalyst used. For instance, the WGS reaction plays an important role when Fe-based catalysts are used. However, when cobalt or ruthenium based catalysts are used the WGS reaction can be neglected.

I.2.1 The Fischer-Tropsch Synthesis Catalysts

Mainly three transitions metals (iron, cobalt and ruthenium) proved to be useful as a catalyst for the FTS. Nickel (Ni) can be used as well, however under normal operating conditions it favors CH_4 formation; thus, it is rarely applied in the FTS. On the other hand, ruthenium (Ru) is far too expensive with limited reserves that make it unsuitable for large-scale process [9]. These factors only leave Fe and Co as industrially applicable FTS catalysts.

Fe is cheaper than Co and promotes the WGS reaction, hence can tolerate lower H_2/CO ratios [6]. This makes Fe catalyst preferred when using syngas derived from lower quality feedstock (coal and biomass) that tends to have low H_2/CO ratios. In addition, Fe catalysts can be used over a wide range of conditions (temperature, pressure and syngas ratios). Nevertheless, Fe is different from other FTS catalysts by means of metallic stability. Unlike the other metals that remain in the stable metallic state during the FTS, Fe forms a number of metallic phases that include oxides and carbides. Controlling these phase transitions play a critical role in sustaining the catalyst activity. Besides, Fe catalysts are less active towards hydrogenation and thus produce more light olefins and alcohols. Additionally, Fe-based catalysts have a shorter life span, are not worth regenerating, have a lower chain growth probability and form considerable amounts of carbon dioxide (CO_2), while water produced by the FTS reaction reduces the reaction rate on Fe catalysts to greater extent compared to Co catalysts [9].

Although Fe-based catalysts are cheaper and can better tolerate low H_2/CO ratios, Co-based catalysts are increasingly being used in industrial FTS reactors due to their higher activity and higher chain growth, as well cobalt catalysts can be regenerated and can last for years [21]. Co catalysts are found to provide the best compromise between cost and performance and are specifically preferred when the feedstock is NG, which can produce syngas with high H_2/CO ratios. The main features of Co-based catalysts are high product yields, long operation lifetime, and linear alkanes dominant product spectrum [22]. Additionally, in the case of Co catalysts, conversion is not affected by the formed water vapor during the FTS reaction. Due to that, a lower reactor temperature can be

applied to achieve similar conversion rates and provide safe thermal control of the reactor. The linear alkanes dominant product spectrum in the case of Co-based FTS is attributed to the ability of Co catalysts to readsorb α-olefins on the active sites, thus increasing the chain length through secondary reactions by either hydrogenation of the carbon-carbon double bond (C=C) or by isomerization reactions [23]. However, Co-based catalysts can only be used at lower reaction temperatures since at high temperatures Co favors CH_4 formation. Another negative side is that Co catalysts are difficult to dispose of due to environmental concerns. In addition, because of their higher price, Co is used in minimum amounts by dispersing it on a stable, low-priced, high-surface-area support such as alumina (Al_2O_3), silica (SiO_2), titania (TiO_2), magnesia (MgO) or zeolites [9]. The following table gives a rough comparison between the applicable FTS catalysts.

Table 1. General FTS catalysts comparison.

Parameter/Catalyst	**Nickel**	**Iron**	**Cobalt**	**Ruthenium**
Cost	Average	Low	Average	High
Life time (stability)	High	Low	High	High
Activity	Average	Average	High	High
Chain growth	Low	Average	High	High
H_2/CO ratio	-	0.5-2.5	2	-
CO_2 selectivity	High	High	Low	Low

I.2.2 The Fischer-Tropsch Synthesis Reactors

Despite of the long years of research on the FTS technology, only three reactor types were able to meet commercialization requirements. These are Fluidized Bed Reactor (FBR), Tubular Fixed Bed Reactor (TFBR) and Slurry Phase Reactor (SPR).

FTS reactors are divided into two groups according to their operating temperature, Low-Temperature-Fischer-Tropsch (LTFT) and High-Temperature-Fischer-Tropsch (HTFT). The LTFT is performed in TFBR or SPR at (200 to 250) °C, using Co or Fe-based catalysts, producing mainly middle distillates, diesel, jet fuel, lubricants and wax. The HTFT is performed in FBR at (300 to 350) °C, using Fe-based catalysts, producing mainly gasoline and short chain alkenes [5, 10, 18, 20, 21, 24, 25]. Conventional LTFT reactors operate with a three-phase system (Gaseous: syngas, water vapor and light hydrocarbons. Liquid: heavy hydrocarbons. Solid: wax and catalyst). HTFT reactors operate in the two-phase regime (Gaseous: syngas, hydrocarbons and water vapor. Solid: catalyst) [20]. The choice of the reactor type of preference depends on many factors; however, the primary factor is the desired product distribution.

1.2.2.1 Fluidized Bed Reactors (FBR)

FBR are vessels that contains a fluidized bed composed of iron-based catalyst. Syngas is bubbled up through the reactor where it is converted to hydrocarbon products. Enhanced heat transfer characteristics of the fluidized bed help to overcome temperature control difficulties faced using TFBR. However, in order to avoid catalyst agglomeration due to wax formation and to maintain bed fluidity, FBR are operated at higher temperatures (330 – 350) °C compared to SPR and TFBR. Operating the FTS at such elevated temperatures results in high CH_4 formation and poor selectivity towards the most desired products (middle distillates) [26].

1.2.2.2 Tubular Fixed Bed Reactors (TFBR)

In industrial TFBR, multiple tubes are used in parallel. The reactor resembles a shell and tube heat exchanger, with catalyst particles packed inside the tubes and Boiler Feed Water (BFW)/steam flowing on the shell side. The reactor heat exchanger is necessary to remove the heat generated by the FTS reaction while producing steam at the same time. Syngas flows through the catalyst filled tubes where it reacts forming a chain of hydrocarbon products. TFBR are usually operated at temperatures between 180 and 250 °C and at pressures between 10 and 45 bar. At these conditions, the TFBR operate in the three phase regime (gas-liquid-solid) [17, 27].

The main drawback of TFBR is the non-uniform temperature distribution along the catalyst bed (axial temperature gradient). Also, the temperature can vary from the center of the reactor tube to the wall where heat is removed (radial temperature gradient). Local hot spots formation is also problematic in TFBR as they can cause thermal runaway, catalyst deactivation or sintering and rise in CH_4 formation [28, 29]. To limit the effect of these drawbacks, high load heat exchangers must be employed to cool the reactor bed. Moreover, as the reaction proceeds wax starts to form and coat the catalyst pellets, which creates a mass transfer resistance between the catalyst pellet pore mouth and the active metal sites inside the pore, thus reducing catalyst activity with time on stream [30]. Furthermore, due to pressure drop constraints, catalysts used in TFBR must have diameters larger than 1 mm. This results in intra-particle diffusion limitation of both reactants and products. Despite that, TFBR are relatively easy to operate and scale-up and they do not require a separate system for catalyst-product separation [28]. Moreover,

TFBR (gas phase) offer excellent reactant diffusivity, which results in higher reaction rates and catalyst activity. Thus, TFBR are widely used in FTS applications, starting from laboratory uses in kinetics studies, catalyst development, catalyst deactivation studies, etc. and up to large fully commercial industrial scale FTS reactors.

1.2.2.3 Slurry Phase Reactors (SPR)

SPR are vessels containing slurry, which is mainly composed of the formed liquid and wax products (C_{20+}) with the catalyst particles suspended in the slurry. Syngas is bubbled up through the slurry and as it passes through the catalyst particles, it reacts and converts into hydrocarbon products. Gaseous products consisting of unreacted syngas and light hydrocarbons leaves from the top of the reactor and is further processed downstream. Heavier products remain in the reactor for a longer time as they become part of the slurry. The slurry is periodically extracted in order to separate the products and the catalyst that is recycled back to the reactor. Heat generated by the FTS reaction is removed using internal cooling coils emerged inside the reactor bed and used to generate steam at the same time [17, 27]. The operating temperature of SPR depends on whether Co or Fe is used as a catalyst. Nevertheless, temperature is kept below 250 °C to minimize methane selectivity, enhance chain growth probability, and prevent any internal wax hydrocracking [5].

SPR were designed to solve the temperature control problems faced in TFBR, they operate almost isothermally due to the enhanced heat capacity of the liquid medium (slurry). This is a significant advantage and as a result, SPR can be operated at moderate temperatures, which favor the formation of middle distillates. However, the introduction

of the liquid reaction media induces mass transfer limitations [29]. Therefore, SPR suffer from low conversion rate per pass since the diffusion of syngas in the catalyst pores is slow due to the presence of heavy slurry that fills the catalyst pores [31, 32]. Additionally, catalyst attrition and cumbersome extraction of catalyst from the slurry are major drawbacks in the SPR [30]. Nevertheless, this continuous catalyst extraction enables on-line catalyst regeneration or replacement.

1.2.2.4 Comparing Fischer-Tropsch Reactors

Each of the previously mentioned reactor technologies have their advantages and disadvantages. Thus, selecting a particular reactor design is usually a trade-off. For example, in TFBR the high diffusivity of the gas phase allows for high reaction rates and conversion per pass. Moreover, TFBR have a lower capital cost and a less sophisticated design. However, TFBR suffers from catalyst deactivation and difficulty in temperature control. On the other hand, in SPR the well-mixed slurry plays a vital role as it improves heat distribution and removal through the reactor. This enhance the temperature control of the reactor and allow for near isothermal operation, which provides better control over the product distribution and significantly increases the catalyst lifespan. On the downside, in SPR the catalyst suffers from significant friction that leads to catalyst attrition. Additionally, in SPR the wax-catalyst separation process needs to be of high efficiency, which is quite cumbersome to achieve [17].

Table 2. Comparing available commercial FTS reactor technologies [5, 17, 27, 30, 31, 33-41].

Reactor Technology	Fluidized Bed Reactor (FBR)	Tubular Fixed Bed Reactor (TFBR)	Slurry Phase Reactor (SPR)
Operating Conditions	• Temperature: 300-350 °C • Pressure: 20-40 bar • Catalyst: Fe <100 μm • Main products: α-olefins, gasoline fuel and oxygenates	• Temperature: 180-250 °C • Pressure: 10-45 bar • Catalyst: Fe or Co > 1 mm • Main products: middle distillates hydrocarbon (diesel fuel and jet fuel) and wax	• Temperature: 200-240 °C • Pressure: 20-40 bar • Catalyst: Fe or Co 20 μm <x<100 μm • Main products: middle distillates hydrocarbon (diesel fuel and jet fuel) and wax
Advantages	• High heat efficiency, thus less heat exchange area is required • Excellent reaction heat removal, efficient temperature control and isothermal operation • Small unit size • Ability for on-line catalyst regeneration and addition • Minimized diffusional resistances due to small catalyst size	• Simple to design, operate and scale-up • High reaction rates and conversion per pass due to the high diffusivity of reactants in the gas phase • Ideal plug flow concentration profile • Wide operating temperature range • Can be used at high pressures • Ability for large catalyst loading in the reactor • Minimum catalyst attrition • A specialized system for catalyst-wax separation is not required	• Compact unit design with reduced cost • Better heat transfer properties of the liquid phase improve reaction heat removal and makes axial and radial temperature gradients negligible (isothermal operation), which allows for higher average operating temperature. • Reduced catalyst deactivation rate, due to the high wax solubility in the liquid phase • Low pressure drops • Liquid phase is well mixed and provide good reactant distribution in the catalyst bed • Ability for on-line catalyst regeneration and addition, enhancing reactor availability • Limited intra-particle diffusion limitation since smaller catalyst particles are used.

Table 2. Continued.

Reactor Technology	Fluidized Bed Reactor (FBR)	Tubular Fixed Bed Reactor (TFBR)	Slurry Phase Reactor (SPR)
Disadvantages	• Complex design and operation • High capital and maintenance cost • Difficult reactor scale-up • Low chain growth probability and narrow hydrocarbon product range (low molecular weight C_1-C_{10}) due to high temperature operation, which is forced to avoid catalyst agglomeration • Catalyst attrition	• High capital cost • Poor heat transfer properties of the gas phase makes reaction heat removal difficult causing non-uniform reactor temperature profile and local hot spots. This in turn, increase CH_4 selectivity, lower chain growth probability, cause difficulties in controlling the product distribution, may lead to catalyst thermal degradation (deactivation due to carbon deposition and sintering) and reaction runaway. • Large catalyst particles are required to avoid high pressure drop, this reduce the effectiveness factor as diffusion of reactants into the catalyst particle core becomes more difficult • Wax accumulation over the catalyst eventually lead to pore plugging • Non-uniform flow patterns (channeling), leading to uneven distribution of reactants inside the catalyst bed • Catalyst replacement or regeneration is difficult and costly, requiring reactor shutdown	• Low mass transfer properties (low diffusion) in the liquid phase results in low conversion per pass • Complicated catalyst/slurry separation • Catalyst attrition, settling and agglomeration • Foam formation inside bed

Table 2 presents a comparison between the available commercial FTS reactors. From the table, it is evident that choosing a single reactor technology for the FTS will be a non-optimal compromise between the strengths and weaknesses of each available technology [42]. To overcome the limitation of the current conventional reactor technologies, an advanced novel approach must be developed and applied. Continuous studies are conducted to optimize the current available reactor technologies and further develop new alternative designs that may improve the FTS. This is not a simple task as it is challenged by the complicated synthesis mechanism and the difficulty in predicting the thermal and physical properties of the reaction mixture [26].

From the previous review of FTS reactors, it is understandable that the ideal FTS reactor has to combine the strength of the two main FTS reactors (TFBR and SPR), while at the same time mitigate their limitations. A step towards the combination of the advantages of TFBR and the SPR is the introduction of SCF as a reaction media for the FTS [43]. The SC reaction media combines the desired properties of the gas phase (high diffusion) and the liquid phase (high solubility and high heat transfer) along with the ability to maximize product selectivity within the desired product range.

I.3 Application of Supercritical Fluids in the Fischer-Tropsch Synthesis

The aforementioned shortcomings in the two key LTFT reactors have stimulated researchers to look for alternative reaction media. It makes sense that the idealistic FTS reaction medium should possess liquid-like densities and heat transfer properties for efficient product desorption and heat removal, and at the same time gas-like diffusivities to achieve high reaction rates and high product removal rate [44]. Such a combination was

found possible through the application of supercritical fluids (SCF) as a FTS reaction media [29, 45]. SCF are those fluids present at temperatures and pressures that exceed their thermodynamic vapor–liquid critical point [46]. Their utilization in industrial applications has been considered since the 1980s [47]. SCF are seen as a unique reaction media that offer single phase operation for the FTS, adequate density that allows for considerable dissolution power, greater diffusivity and lower viscosity than that of liquids, and improve the *in-situ* wax removal from the catalyst [17, 46].

Using SCF in FTS offers several advantages over the conventional gas phase and liquid phase FTS. These advantages are summarized as follows [2, 17, 36, 39, 41, 43, 44, 46-55]:

- *In-situ* wax (low volatility high molecular weight hydrocarbons) extraction from the catalyst surface and pores, due to the high solubility of heavy hydrocarbons in the SC solvents (liquid-like solubilities) [36, 43, 44]. The wax formed during the FTS does not vaporize under the reaction conditions, it can plug the catalyst pores and eventually the catalyst bed itself [49]. The *in-situ* wax extraction improves pore accessibility, helps in maintaining high catalyst activity, enhances catalyst stability, extends its life and increases the production of longer chain hydrocarbons [2, 46]. This may also improve the economics of the GTL process since a complex filtration system for catalyst removal from wax product is no longer required [36].
- Improved α-olefin (value added products) selectivity, due to the improved desorption of primary products from the catalyst pores, so that the residence time

of olefins inside the catalyst pores is reduced, hence lowering the probability of their participation in secondary reactions [36, 39, 41, 50, 53].

- Greater production of heavy hydrocarbons, due to the improved incorporation of primary products in the chain growth process (desorption of α-olefin before they undergo secondary reactions) and enhanced heat removal rates when compared to gas-phase reaction [36, 41, 43].
- Capability for selecting and controlling the product distribution, by temperature and pressure tuning around the critical point, which will switch the media from liquid-like to gas-like, and thus eliminate the interphase mass transfer limitations which in turn promotes reaction pathways toward the desirable product range [44].
- Increased syngas conversion rate, due to the gas-like diffusivity of SCF (reactant gases are readily miscible in SC solvents), which enhances reactant transport from the bulk fluid to the catalyst surface and then to the catalyst inner pores where the active sites are found.
- Uniform reactor temperature profile with minimized temperature gradients and inhibition of local hot spot formation, due to increased heat capacity of the SC phase compared to the gas phase. In SC-FTS, the bulk flow will be responsible for heat removal and thus saves energy and water required for cooling in the jacketed conventional gas phase FTS reactors. Better temperature control increases the production of long chain hydrocarbons and suppresses CH_4 formation [36, 41, 43].

I.3.1 Literature Review on the Supercritical Fischer-Tropsch Synthesis

The groundbreaking study that investigated the application of SCF in the FTS was carried out by Yokota and Fujimoto in 1989 [56]. In their study, they compared the FTS performance in TFBR operated at three different phases: SC phase (n-hexane), gas phase (nitrogen N_2 makeup) and liquid phase (hexadecane media) [43]. SC reaction media was reported to have unique characteristics that facilitates the *in-situ* wax removal from the catalyst pores, improved heat removal, resulted in higher reactants diffusion and increased α-olefin selectivity compared to the gas and liquid phases FTS [49, 52]. Later, Fan and Fujimoto [51], compared between n-pentane and n-hexane as a FTS SC solvents. They found that pentane is favored for wax production since low reaction temperature was applied while hexane is preferred for middle distillates production since higher reaction temperatures are required. Fujimoto research group [57] further studied the FTS performance when using n-pentane, n-hexane, n-heptane and n-octane as SC solvents. They found that the α-olefin selectivity was similar when n-pentane and n-hexane were used, and to some extent lower, when n-heptane was used, however when n-decane was used the α-olefin selectivity was considerably lower. This suggests that the α-olefins desorption capacity is lower in n-decane compared to that in SC *n*-pentane, *n*-hexane and *n*-heptane. Nonetheless, the research group stated that n-decane was well below the critical point at the reaction conditions, which may have caused the lower α-olefin selectivity [57].

Experiments carried by Bukur and co-workers indicated an increment in α-olefin selectivity when SCF were used as a reaction media [39, 50, 58]. Their findings showed that when using an iron-based catalyst, the olefin selectivity was temperature independent (at similar conversion) but significantly dependent on the reaction phase: either gas or SC.

Bochniak and Subramaniam [44] looked into the effect of pressure tuning on the catalyst pore diffusivity and effectiveness factor under SC n-hexane operation, using a TFBR with an iron-based catalyst at 240 °C and H_2:CO of 2:1 feed ratio. They also observed an increase in conversion, chain growth probability, and α-olefin selectivity under SC hexane. They explained this by the improved diffusivity of reactants and products and better desorption of heavy α-olefins from the catalyst pores before they undergo secondary reactions. Later, Subramaniam [46] discussed the various benefits of SCF as a reaction medium over the conventional (gas or liquid) media. He focused on the ability of SCF to extract hydrocarbon waxes from the catalyst pores, this *in-situ* extraction reduces coke formation and increases reactant accessibility to the internal active sites [46], which in turn reduces pore diffusion limitation and increases catalyst lifetime.

Jacobs et al. [36] similarly reported a rise in catalyst activity and α-olefin selectivity when they conducted the FTS under SC conditions (TFBR, Co/Al_2O_3, hexane 55 wt% and pentane 45 wt % mixture SCF, T = 220°C and 2:1 H_2 to CO). Moreover, they observed an enhancement in catalyst life and a reduction in CH_4 selectivity.

Roberts and Co, studied the advantages of SCF in the FTS, utilizing a number of Co-based catalysts (15 wt% Co), with different supports such as Al_2O_3 and SiO_2 [41, 54]. Roberts, Huang and Elbashir [41, 59] reported improvements in terms of conversion, α-

olefin selectivity, chain growth, catalyst stability and active site availability when conducting FTS under SC conditions (TFBR, Co/Al_2O_3 catalyst, n-hexane SC solvent, T = 250 °C and H_2:CO of 2:1 feed ratio).

II. RESEARCH PROBLEM AND OBJECTIVES

II.1 Research Problem

The FTS has received a great deal of interest as an alternative source of petroleum-based fuels as it utilizes the readily available natural gas, coal and biomass derived syngas to produce ultra-clean fuels and value added chemicals. Nonetheless, FTS is faced with many pitfalls, and based on the literature review covered in Chapter I, it is evident that choosing a FTS reactor technology is a non-optimum trade-off between the strengths and weaknesses of each available reactor technology [42]. Hence, it is of great value to design novel reactor technology that is capable of combining the advantages of commercial FTS reactors while simultaneously eliminating their disadvantages. The proposed SCF reaction media is assumed to provide superior fluid properties (diffusivity similar to those of gases with solubility and heat capacity similar to those of liquids), which enhance the *in-situ* wax extraction from catalyst pores and facilitate better reactor temperature control that typically results in enhancement of chain growth and olefin selectivity.

At present, all industrially commercialized FTS reactors are operated at either the gas phase or liquid phase. However, we seek novel technology that can combine the advantages of the two conventional LTFT reactors (TFBR – gas phase and SPR – liquid phase) and simultaneously mitigate their limitations. The utilization of SCF in the FTS as a reaction media has been investigated since the late 1980s [56], and even though a number of studies [2, 17, 36, 39, 41, 43, 44, 46-55] showed promising enhancements, as discussed in section I.3, none of these studies were able to move the SC-FTS technology beyond the lab-scale. The aim of this project is to tackle this problem by commissioning a state-of-

the-art bench-scale SC-FTS reactor unit (Figure 2), capable of running the FTS reaction at high pressures and temperatures under both the conventional gas phase and the unique SC phase. Such system will enable us to study and gain better understanding of the FTS reaction when carried under supercritical conditions, optimize the reaction behavior for typical large-scale FTS processes, investigate and validate the potentials of enhancements of the SCF-FTS over conventional gas phase FTS process.

Figure 2. The high-pressure bench-scale reactor unit during the construction and commissioning phase.

II.2 Research Objectives

This project is focused on the utilization of a unique reaction media that is capable of providing certain advantages over the currently available FTS commercial reactor technologies (TFBR and SPR) while simultaneously overcoming several of their main drawbacks. This medium is the near critical and supercritical phase that could be facilitated by solvent(s) that dominate the reaction mixture to bring the thermo-physical characteristics to gas-like diffusivities and transport properties, and liquid-like solubilities and heat transfer properties [2, 26, 43, 47]. As discussed in Chapter I several research activities have been conducted in this field but they were limited to lab-scale reactors [2]. The major objective of this research project is to explore the possibility of scaling up this technology from lab-scale to bench-scale by building sophisticated high-pressure reactor unit that can be safely operated on variety of conditions to compare conventional gas phase to near critical and supercritical phase conditions. To be specific the objectives of this research work are as follow:

1. Identify the role of supercritical solvents on the FTS in a bench-scale reactor that has been built for this purpose. The bench-scale is an intermediate unit scale that falls between the lab-scale and pilot plant.
2. Prepare an active and selective cobalt-based catalyst for the FTS reaction.
3. Develop a safe configuration and operational protocol for the high-pressure bench-scale reactor to run the FTS reactor up to 80 bar in the presence of supercritical solvent.

4. Investigate the mass and heat transfer contributions on the FTS reaction performance on a bench-scale reactor when conducting the FTS reaction in gas phase and in supercritical phase.
5. Develop analysis setup and protocol for the reactant and product using multiple gas chromatographs (GCs) to accurately measure the cobalt catalyst activity and selectivity under both gas phase and supercritical phase.
6. Compare the catalyst performance in the gas phase and supercritical phase, and compare results with those in literature.
7. Explain the differences in the performance and enhancement on the product distribution and activity under the supercritical phase FTS.

III. METHODOLOGY

The experimental campaign reported in this work was carried out in the Fuel Characterization Lab at Texas A&M University at Qatar, whereby the FTS reaction behavior under both conventional gas phase and non-conventional SC phase was studied over cobalt-based catalyst (including a 15 wt% Co/Al_2O_3) utilizing the novel high-pressure reactor unit.

Firstly, the work was focused on the design and commissioning of a novel bench-scale reactor unit, capable of performing various chemical reactions at high temperatures and high pressures. The researcher role was mainly focused on developing Process Flow Diagrams (PFDs) and Piping and Instrumentation Diagrams (P&IDs) for the reactor unit and associated utilities. These diagrams aid in representing the bench-scale reactor unit and identify all control, measuring and safety features of the process from the feed delivery system all the way to the product analysis units.

Secondly, the focus was on providing additional features to the reactor unit so that it can facilitate running the FTS reaction under near and supercritical conditions while sustaining safety and system stability. A SCF delivery system was designed; the delivery system consists of a solvent storage vessel connected to a nitrogen source in order to maintain an inert atmosphere within the tank. The solvent is introduced to the system by a high-pressure liquid pump. The liquid solvent is then passed through a vaporizer before it is mixed with the feed gases. A static mixer is used to ensure proper mixing of the feed gases and the SCF.

Thirdly, the research activities were focused on the preparation of cobalt-based catalyst for the FTS reaction. This catalyst is a 15 weight percent cobalt catalyst supported on alumina (15 wt% Co/Al_2O_3). The well-known impregnation technique was followed to prepare this catalyst, which has then been calcined and reduced under controlled conditions.

Fourthly, a detailed procedure was developed for safe reactor startup, shutdown and the activation of the prepared catalyst. Additionally, an experimental procedure was developed to run the FTS reaction under near and supercritical phase, as well as the conventional gas phase.

Simultaneously, a custom-made analysis system and method needed to be implemented to collect gaseous and liquid products from the reactor effluent for characterization. These samples were then analyzed and the data obtained was used to measure the catalyst activity and selectivity under the two different reaction mediums.

Finally, the experimental data collected was used to compare FTS in the gas phase and under the SCF conditions. Enhancements in catalyst activity, chain growth probability and olefin selectivity under SC phase operation have been observed.

This chapter contains several subsections that includes a detailed description of the newly commissioned reactor unit, the method used for the catalyst preparation, calcination and reduction. In addition, it contains the procedure followed to activate the catalyst/adsorbers employed in the feed purification system. The last subsection of this chapter contains a simplified Standard Operating Procedure (SOP) developed to run, operate and shut down the reactor unit.

III.1 Reactor System Description

The bench-scale reactor unit consist primarily of five sections. The first section involves the feed delivery setup for gas stream (e.g. syngas, CO, H_2, argon) and liquid stream (e.g. solvent hexane). The second section is the reaction zone where the FTS reaction takes place. The third section involves the product separation setup to separate permanent gases, liquid hydrocarbons and wax, using both hot and cold traps. The fourth section is composed of the reactants and products on-line GC analysis system. The fifth section is represented by the utilities that are necessary for safe reactor operation and control. The utility section is composed of three sub-sections: (1) pneumatic air, (2) chilled water system and (3) ventilation setup. For the supercritical phase testing, the reactor unit has liquid solvent delivery configuration that is composed of a 5.0 gallons hexane storage tank (V-100, Hedwin, WPB7252), a High Pressure Liquid Chromatography (HPLC) pump (P-101, LabAlliance, P40SFT01) and a vaporizer (V-110, Swagelok, 316L-50DF4-300) insulated with heating tape (HT-113, HTS Amptek, AWO-052-080) under controlled temperature.

This reactor unit was designed for safe unattained operation, which was made possible by the utilization of high-tech automation systems (Honeywell HC900 SCADA and C30 controller with ADAM-6051 Modbus). The Programmable Logic Controllers (PLC) system (Honeywell HC900) continuously records process variables (temperature, pressure, flow, etc.) and has several alarm settings with pre-programed alarm-triggered safety actions, which makes it possible to control the reactor unit within the allowable safety zones. All commands are stored on the PLC and as a result, failure of the computer

system will not lead to a failure of the reactor unit. Moreover, all the measurement and control devices (thermocouples, heating tapes, furnace, chiller, pressure transducers, pressure control valves, solvent pump, shut off valves, mass flow controllers) employed in the reactor unit are connected to the PLC system and controlled by the Supervisory Control And Data Acquisition (SCADA) system (GE, Proficy HMI/SCADA – iFIX), shown in Figure 4.

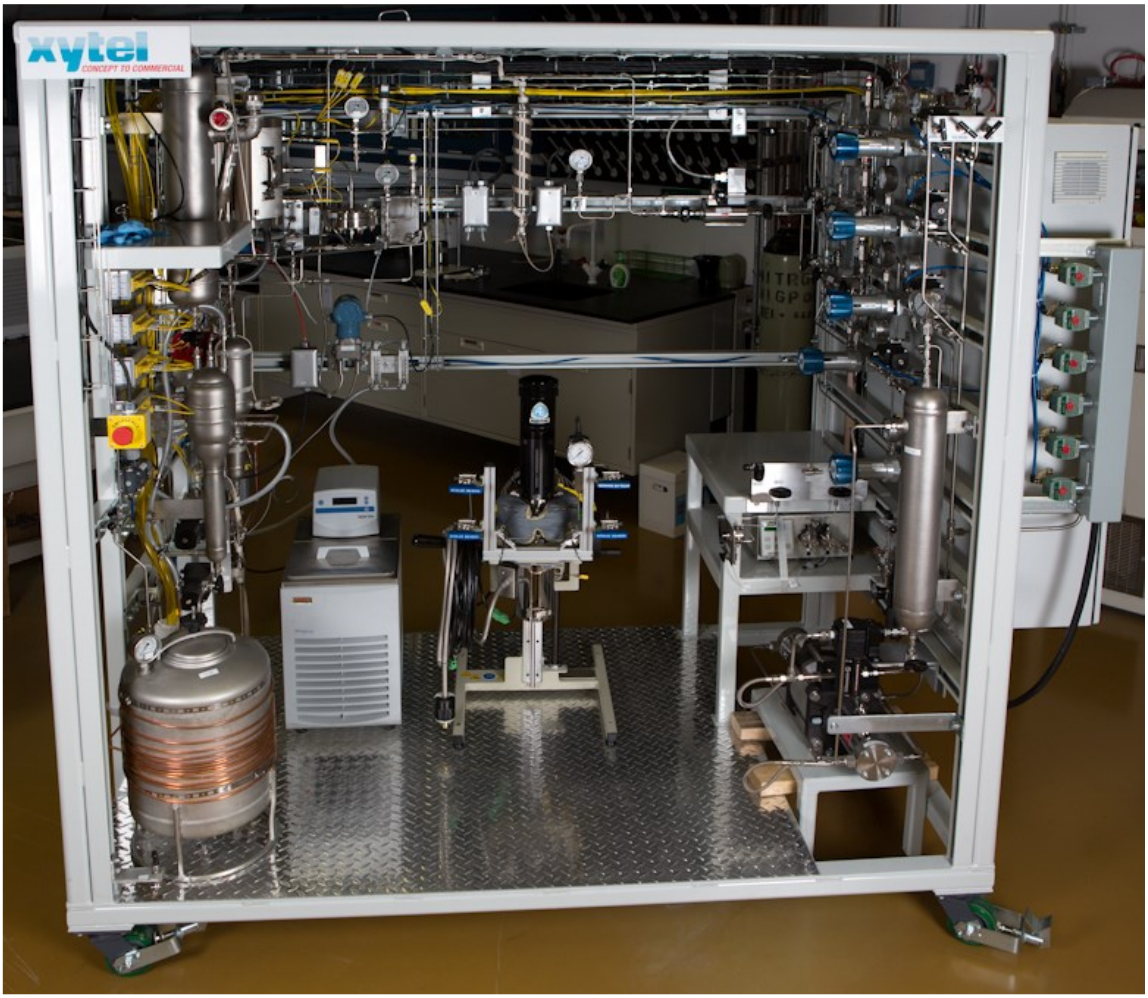

Figure 3. The high-pressure bench-scale reactor unit of Texas A&M University at Qatar.

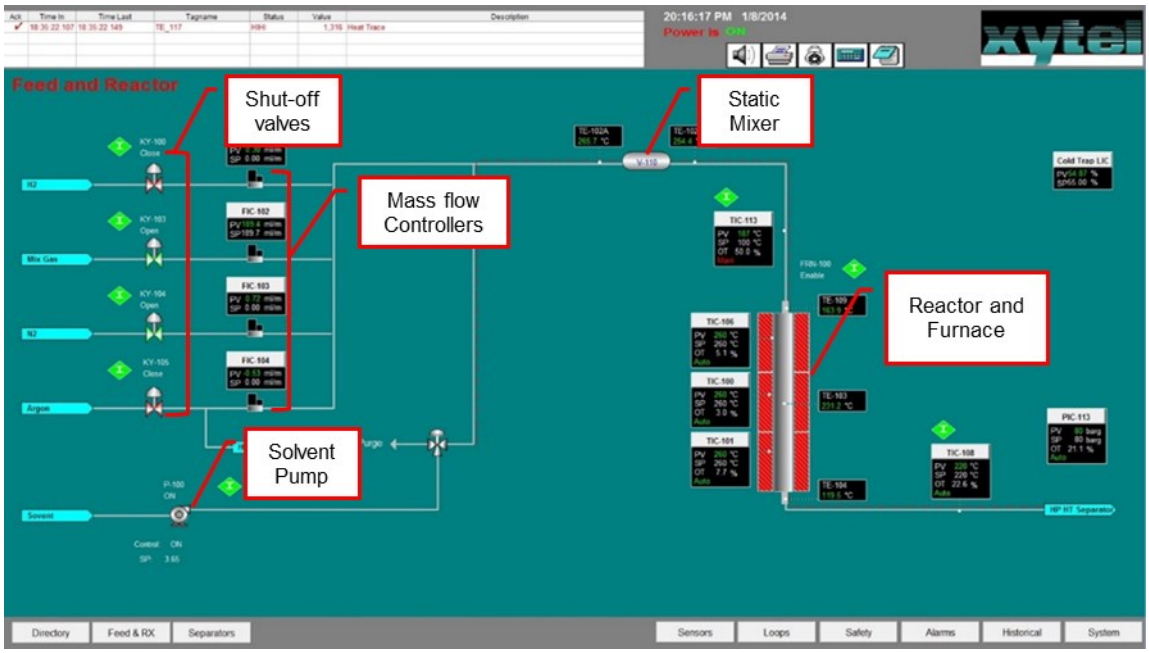

Figure 4. PLC/SCADA computer graphical interface.

Figure 5. Dräger Polytron 7000 Fixed CO gas detector with Dräger REGARD-1 Control System connected to the SC-FTS reactor unit.

Moreover, to ensure the safety of personnel working in the lab, toxic gas detectors (Dräger Polytron 7000 Fixed gas detector with Dräger REGARD-1 Control System), as shown in Figure 5, are distributed around the reactor unit to continuously monitor CO, H_2 and O_2 levels, and raise alarm if abnormal conditions are detected. This configuration will automatically shut down the reactor unit if the alarm goes off.

III.1.1 Feed Delivery Section

At the feed delivery section (Figures 6 and 8) raw materials necessary for the reaction are introduced into the system. Using pressure-regulating valves (PR-101, 102, 103, 104, Tescom, 44-1862-24), shown in Figure 8, the feed gases are allowed into the system at controlled pressure from their respective gas cylinders. The common gases for the FTS tests are: syngas (National Industrial Gas Plants, 150 bar, 50 L, 33.4 % CO and 66.6 H_2), carbon monoxide (Air Liquide, 200 bar, 50 L, 99.97 % CO), hydrogen (Quality Specialty Gases, 150 bar, 50 L, 99.999 % H_2), argon (Quality Specialty Gases, 150 bar, 50 L, 99.999 % Ar) and nitrogen (National Industrial Gas Plants, 150 bar, 50 L, 99.999 % N_2). For the supercritical phase testing, liquid solvent, hexane (Merck Chemicals, ≥ 98.5 % n-hexane) is delivered from the storage tank (V-100) at controlled volumetric flow rates using the HPLC pump (P-101), as shown in Figure 9.

After that, the solvent and each feed gas passes through a purification system (FP-101, 102, 103, 104, 105), shown in Figure 10. The feed purification system is composed of a cylindrical vessel (Swagelok, 316L-50DF4-500) filled with three layers of adsorbers/catalysts separated by glass wool (Supelco), as shown in Figure 9. The first layer is made by BASF Selexsorb COS adsorbents for the removal of COS, H_2S, CS_2, CO_2; the

second layer is made by BASF PuriStar R3-15 for the removal of acetylene, and O_2; the third layer is made by BASF E-315 for the removal of arsine and sulfur compounds. In addition, the gases pass through an inline gas filters (Swagelok, SS-SCF3-VR4-P-30) for particles and moisture removal.

Figure 6. High-pressure bench-scale reactor unit, Feed Delivery System.

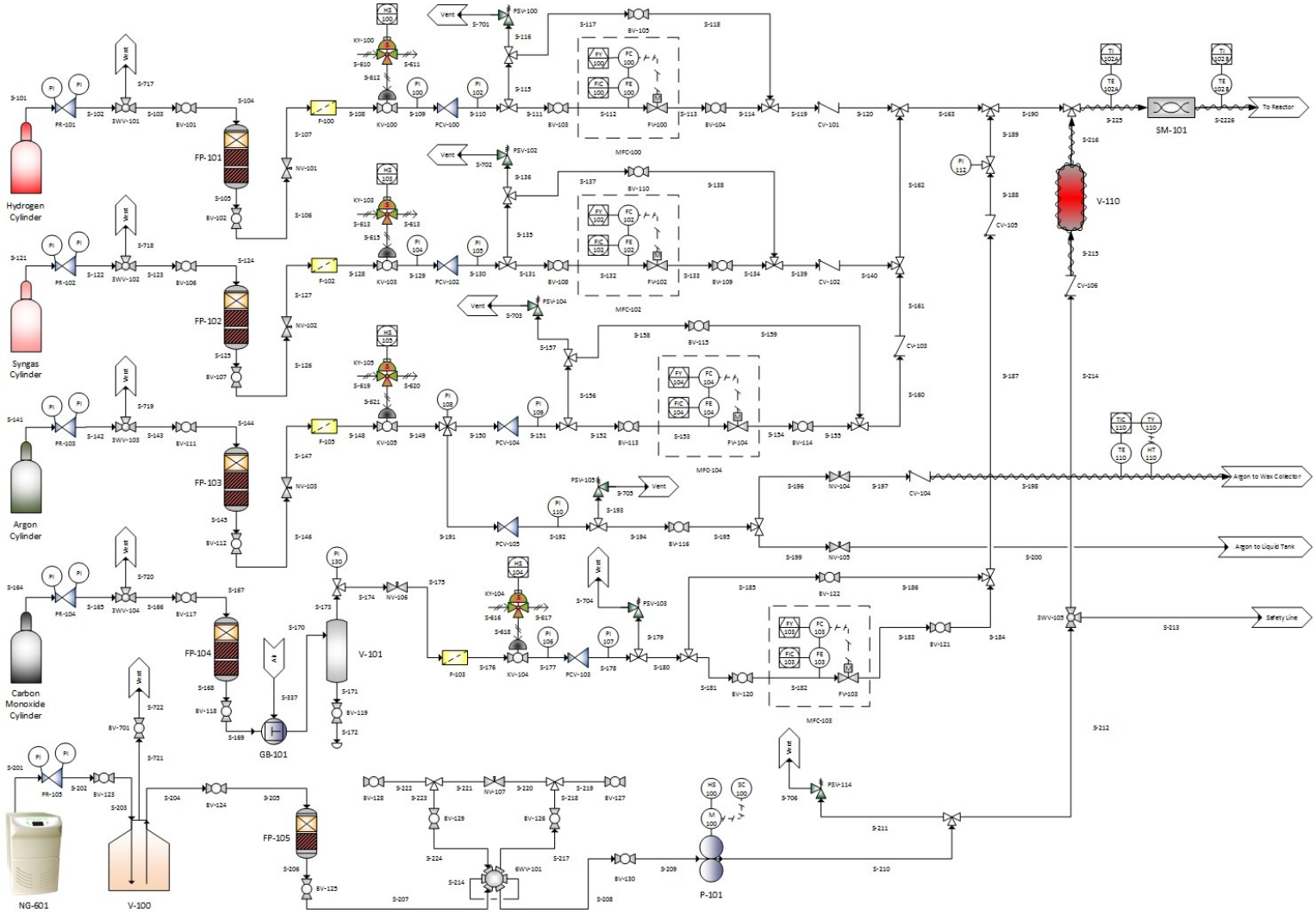

Figure 7. High-pressure bench-scale reactor unit, Feed Delivery System P&ID.

Figure 8. Gas supply cylinders (from left to right: H_2, syngas, CO, Ar) connected to the high-pressure bench-scale reactor unit.

Figure 9. Solvent delivery and feed purification systems.

Figure 10. Feed purification system, purging and depressurizing valves.

The feed gases enter the system at controlled flow rates (0 – 500 nmL/min) using four mass flow controllers (MFCs) (MFC-100, 102, 103, 104, Bronkhorst, EL-FLOW F-230M-AGD-22-V), calibrated specifically for each gas. The setup of these MFCs is shown in Figure 11.

The solvent enters the vaporizer vessel (V-110, Swagelok, 316L-50DF4-300) heated with a heating tape (HT-113, HTS Amptek, AWO-052-080) and insulated using glass wool tape and aluminum foil. After that, hexane vapor is mixed with the feed gases in the static mixer (SM-101, Koflo, Stratos 250 1/2-32) located upstream of the FTS reactor. The static mixer ensures proper solvent/syngas mixing prior being fed to the reactor.

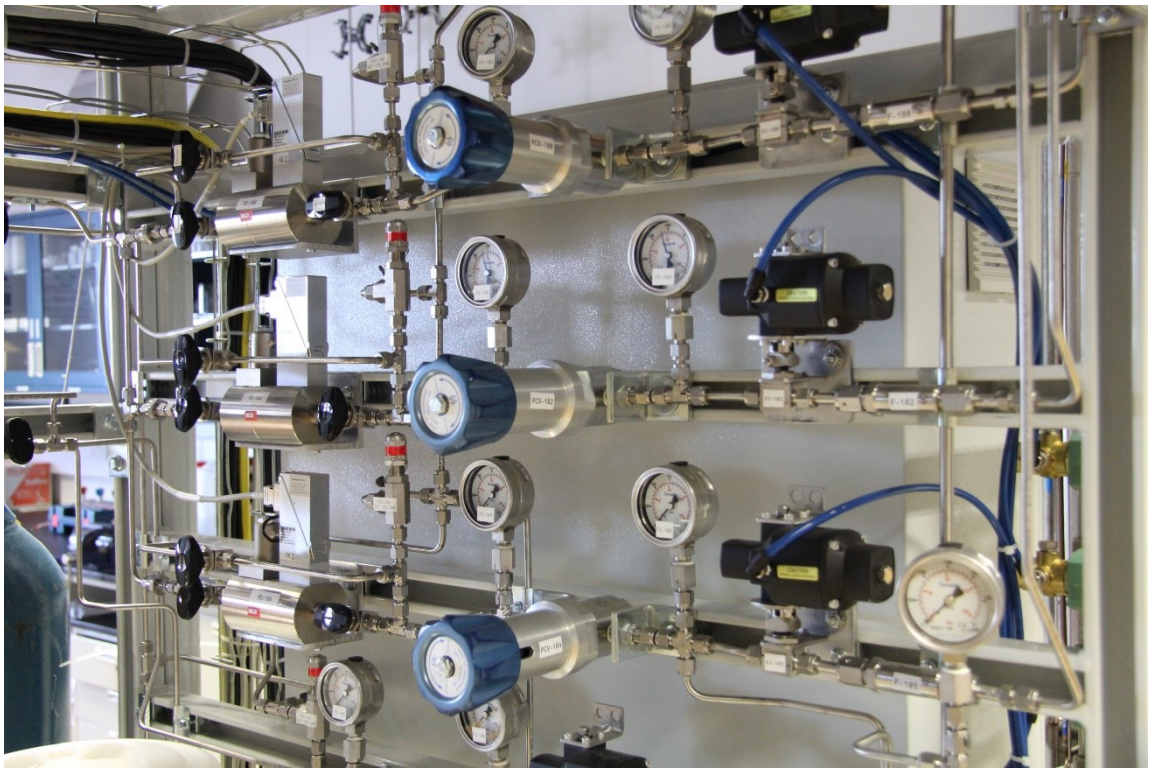

Figure 11. Feed delivery system, MFCs and Shut-off valves.

III.1.2 Reaction and Separation Section

Figure 10 shows the reaction and separation section, where the reactant/solvent mixture enters the custom made tubular fixed bed reactor (R-100, Autoclave Engineers, 16” overall length, 12” heated length, 2/3” internal diameter, 1.0” outer diameter, 70 cm^3 net volume in heated zone) at a controlled mass flow rate, inlet temperature, inlet pressure, H_2/CO ratio and syngas to solvent ratio.

The reactor tube is vertically embedded in a hollow ceramic insulated electric furnace (F-100, Applied Test Systems, Lab Furnace 3210) with three heating zones, capable of producing temperature up to 1000 °C, as shown in Figure 13. Each heating zone is supplied with a separate temperature control loop to minimize axial temperature

gradients and efficiently control the reactor temperature. The reactor temperature is monitored and controlled within ± 2.0 °C, at the inlet (Loop-113), the outlet (Loop-108) and the reactor surface (Loop-100, 101, 106). The internal reactor temperature is measured at three different positions using a temperature probe with three equally distributed thermocouples (TE-103, 104, 109, Omega, KMQXL-020G-12) in order to visualize the axial temperature profile inside the reactor bed.

The reactor pressure is controlled by the pressure control valve (PV-115, Badger Meter, 1001GCN36SVOSP01ST), as shown in Figure 14. The PV located between the reactor and the hot trap (V-102, Xytel, 1053-V102) builds up the pressure in the reactor by restricting the flow out of the reactor. It operates (open or close) to maintain the reactor pressure at the desired set point by using the pressure feedback measured by the pressure transducer (PT-133, WIKA, S10/0-3000 psi).

Two flash separation columns are placed downstream of the high-pressure reactor, as shown in Figure 15. The first one is the hot trap (V-102, Xytel, 1053-V102, 2.0 L) surrounded by a heating tape (HT-115, HTS Amptek, AWO-052-100) and insulated by glass wool and aluminum foil. The hot trap is operated at 150 °C and 0.9 barg to facilitate the condensation of heavy hydrocarbons (wax) prior to the on-line GC system. The formed wax is collected in a special pressure vessel (V-103, Buchiglasuster, Miniclave-Steel) for further analysis. All the lines connecting the reactor with the hot trap, the wax collection vessel and the on-line GC are heated to 150 °C to prevent any wax condensation.

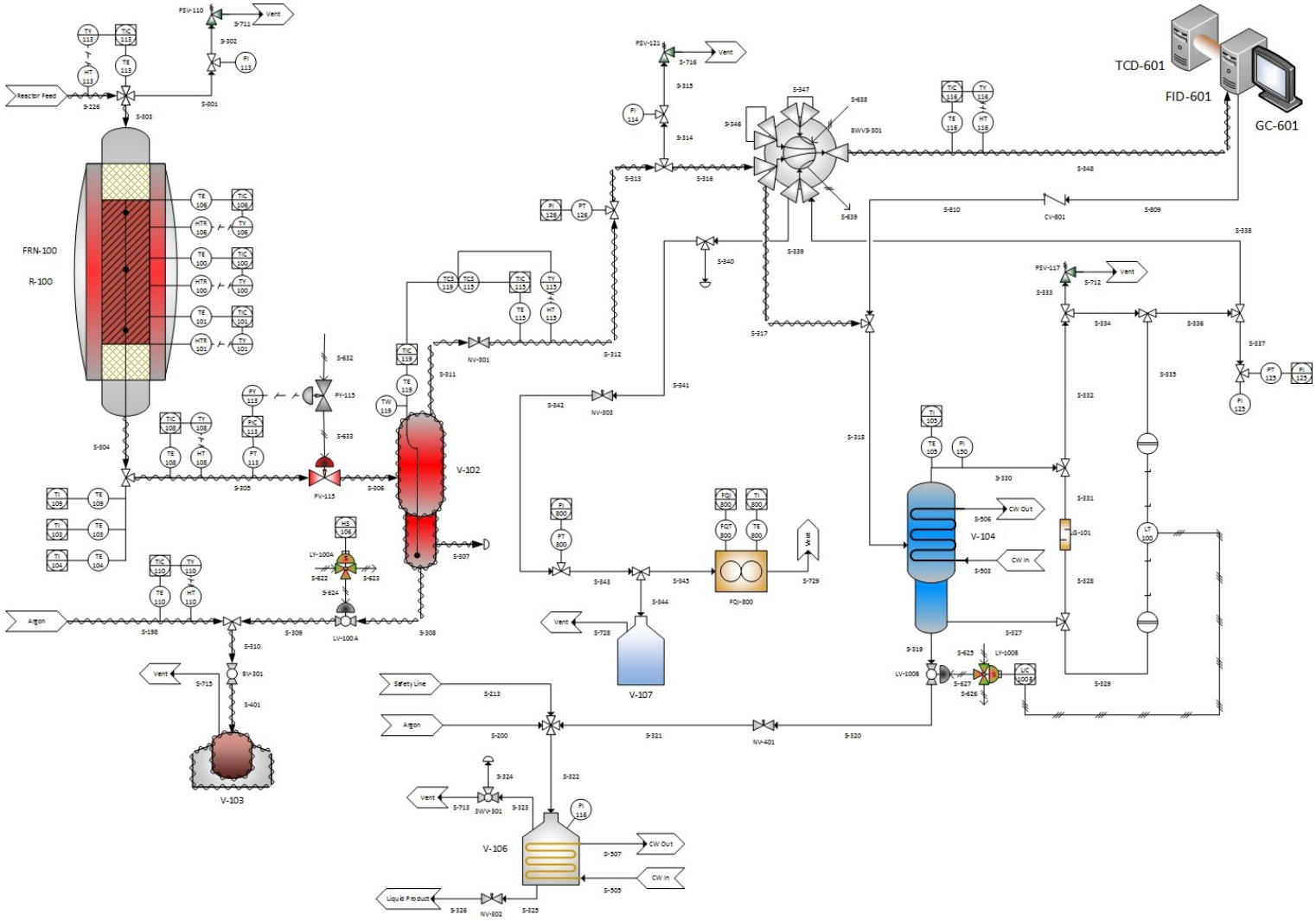

Figure 12. High-Pressure bench-scale reactor unit, Reaction and Separation System P&ID.

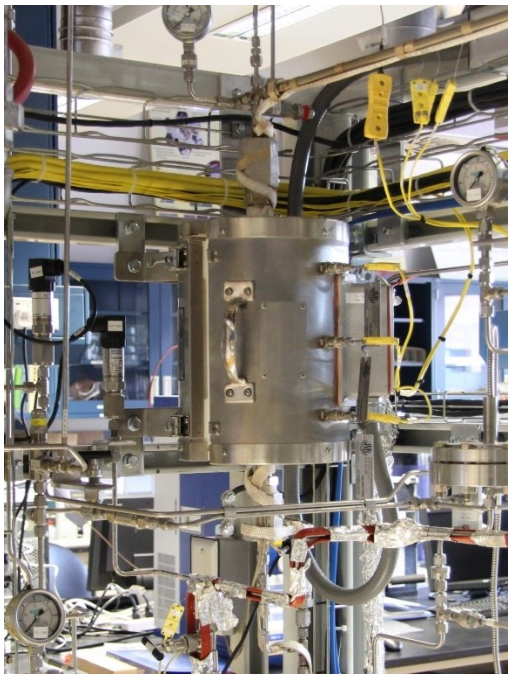

Figure 13. Reactor furnace.

Figure 14. Reactor pressure control valve.

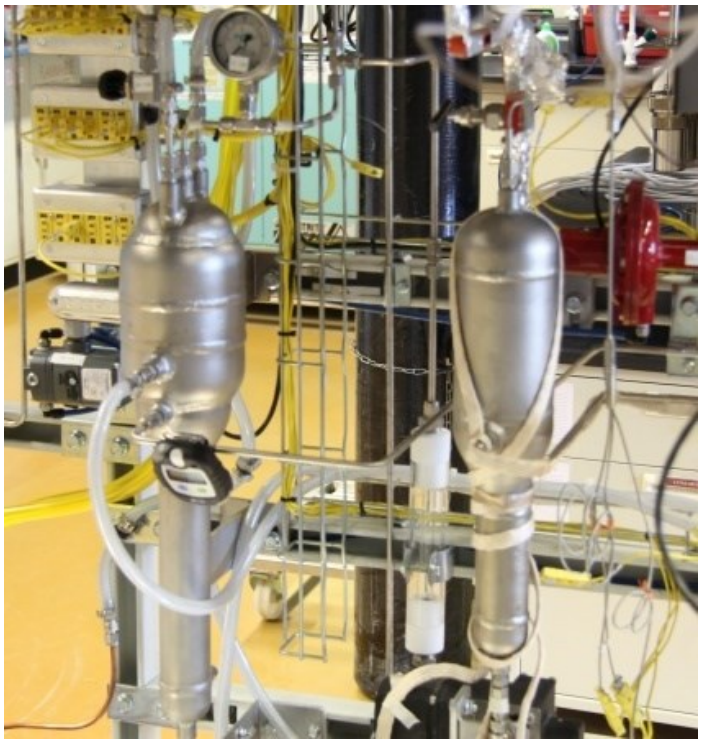

Figure 15. The hot trap (right) and cold trap (left).

A fraction of the gases leaving from the top of the hot trap is directed towards the on-line GC system through an air actuated 8 way Selecting Valve (8WVS-101, VICI, A3CSF4MWE). The remaining hot trap gas stream goes toward the cold trap (V-104, Xytel, 1053-V104) used to separate liquid hydrocarbons and permanent gases, as illustrated in Figure 15. After the on-line analysis, the gases return to the separation section through a check valve (CV-801, Swagelok, 6L-CW4S4) upstream the cold trap. The cold trap is internally cooled using cooling coils with chilled water flow at 4.0 °C, supplied by water chiller (WC-501, Thermo Scientific, NESLAB RTE 10). Hydrocarbons and water condensed by the cold trap are collected in a tank (V-106, APACHE, 12G-6, 7.0 gal) and liquid samples are periodically collected for off-line GC analysis. Permanent gases and

volatile hydrocarbons leave from the top of the cold trap and pass through a flow meter (FQI-800, Ritter, TG1-1.4571-PP) before being safely vented through the ventilation system.

III.1.3 Product Analysis System

The analytical system used in this project consists of dual on-line gas chromatograph (GC-801, Shimadzu, GC-2014) with both Thermal Conductivity Detector (TCD-801, Shimadzu, TCD-2014) and Flame Ionization Detector (FID-801, Shimadzu, FID-2014), The on-line GC setup which is shown in Figures 16 and 17 is used for product distribution profile, selectivity and conversion calculations. Additionally, an off-line GC/Mass Spectroscopy (Agilent GC/MS, 7890A) is used for identification of sample components and product distribution analysis, shown in Figure 19.

III.1.3.1 Shimadzu On-Line Analysis System

The gas coming from the hot trap pass through an 8 Way Selecting Valve (8WVS-101, VICI, A3CSF4MWE) used to inject samples at specified intervals into the on-line GC system. Operation of the sampling valves is controlled by Shimadzu GC Postrun software that acquires samples at preset times and record TCD and FID data. The lines connecting the hot trap and the GC system are kept at 150 °C to prevent any condensation or wax accumulation in the analysis system.

The on-line GC consists of three detectors, TCD-1, FID and TCD-2. TCD-1 detector analyzes permanent gases (O_2, N_2, CH_4, CO, CO_2, C_2 and H_2S) by utilizing two GC columns (MC-1, Restek, Molesieve 13X, 2.0 mmID (millimeter internal diameter), 2 m length, 1/8 inOD (inch outer diameter), SilcoSmooth Tubing, 80/100 mesh) and (MC-

2, Restek, Molesieve 5A, 2.0 mmID, 2 m length, 1/8 inOD, SilcoSmooth Tubing, 80/100 mesh). Both columns use helium (He) as a carrier gas at 5.0 mL/min and 4.0 bar.

On the other hand, the FID detector analyzes (C_3-C_{13}) hydrocarbons by utilizing a single fused silica capillary column (MC-3, Restek, Rtx-1, 60 m length, 0.53 mmID, 5.0 μmdf) to separate the hydrocarbons. MC-3 also uses He as a carrier gas at 5.0 mL/min and 4.0 bar, while air (350 mL/min, 4.0 bar) and H_2 (35 mL/min, 4.0 bar) are used to light the detector flame and N_2 as makeup gas at 25 mL/min and 4.0 bar. Hydrocarbon products heavier than C_{15} are not detected by the on-line FID. One more detector TCD-2 is used with a single packed column (MC-4, Restek, Porapak Q, 80/100 mesh) to detect H_2, where in this column N_2 was used as a carrier gas at 25 mL/min and 4.0 bar.

Figure 16. Shimadzu on-line GC system.

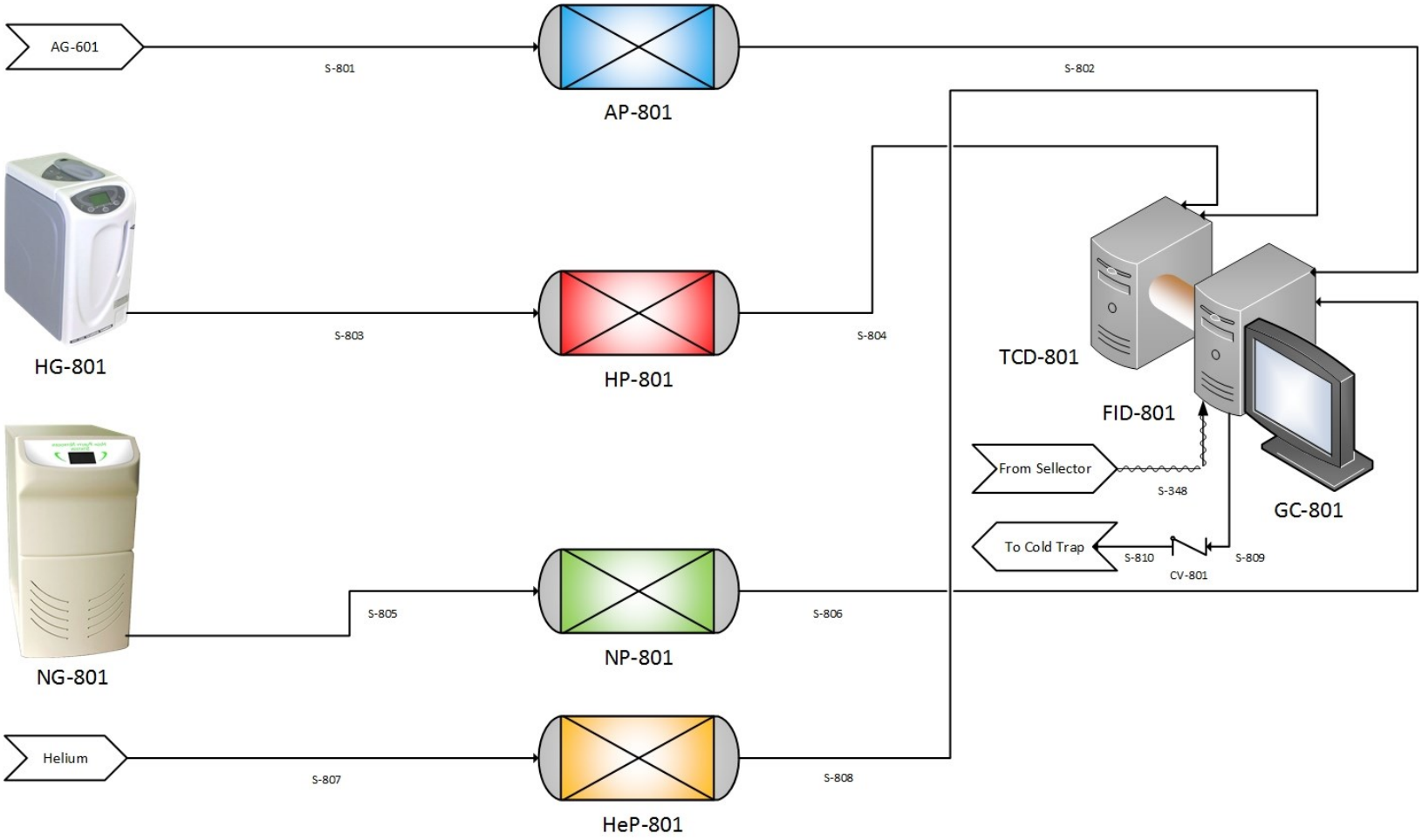

Figure 17. On-line GC Analysis System P&ID.

III.1.3.2 Agilent Off-Line Analysis System

Liquid products from the cold trap (Figure 19) are periodically collected for off-line analysis using GC/MS (Agilent, 7890A) system equipped with FID and Mass Spectroscopy (MS) that uses a capillary column (Agilent J&W, HP-5ms, 30 m, 0.25 mm, 0.25 μm) to separate (C_5-C_{30}) hydrocarbons, as shown in Figure 18. The column use He as carrier gas at 5.0 mL/min and 4.0 bar, air at 350 mL/min and 4.0 bar, and H_2 at 35 mL/min and 4.0 bar to light the FID flame and N_2 as makeup gas at 25 mL/min and 4.0 bar.

Figure 18. Agilent off-line analysis system.

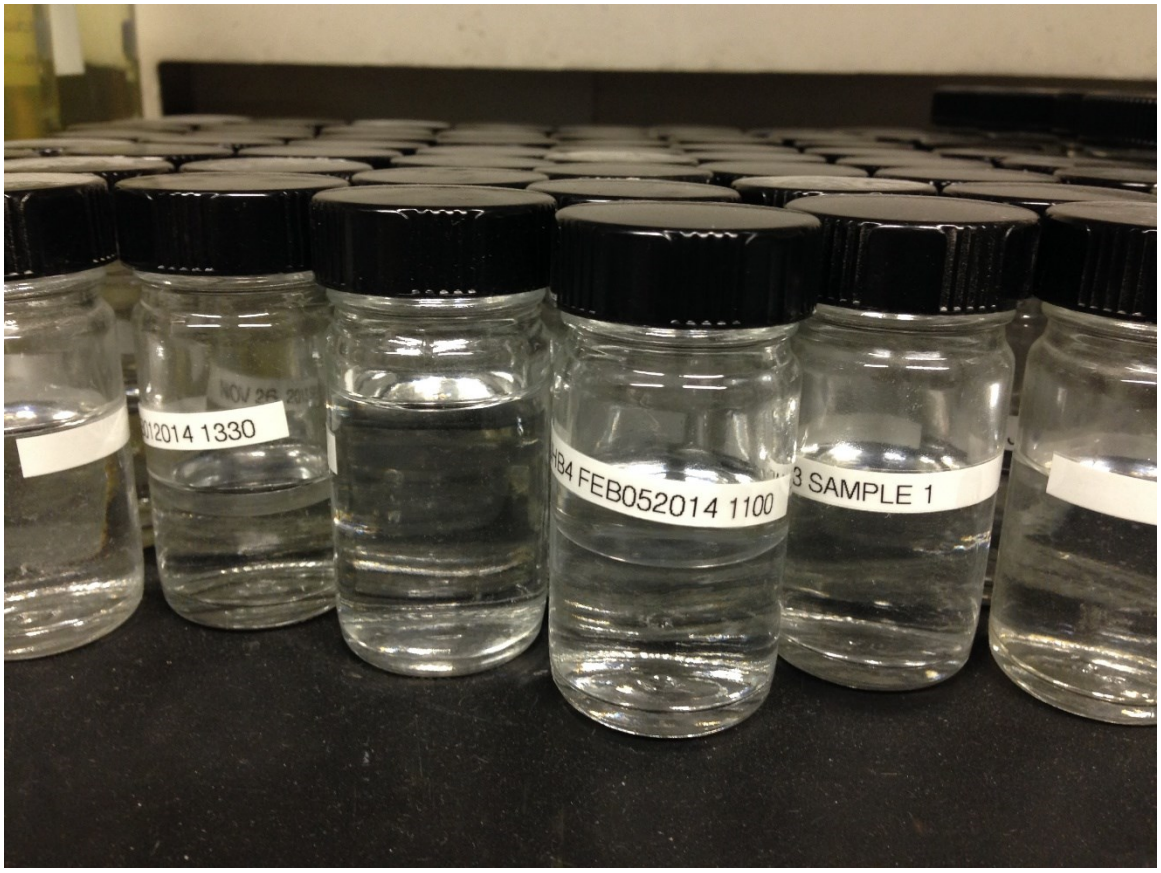

Figure 19: FTS liquid product samples collected from the bottom of the cold trap.

III.2 Cobalt Catalyst Preparation

The (15 wt% Co/Al_2O_3) catalyst used in the FTS experiments was prepared in our lab using the impregnation technique. The method described below is used for the preparation of 15 wt% Co/Al_2O_3 catalyst. Nevertheless, for the detailed description of the calculations used for the catalyst preparation, refer to Appendix A.

Firstly, high purity γ-alumina support (Alfa Aesar, surface area 255 m^2/g, median pore 70 micron and 5000 Å, total pore volume 1.14 cm^3/g, packing density 0.395 kg/L) (as shown in Figure 20 a) was crushed, then sieved (75-150 μm) (as shown in Figure 20

b). The support was then thoroughly washed with deionized water. After this, the support was calcined under airflow at 700 °C for 5.0 h at a heating ramp of 10 °C/min. The calcined support was then cooled down to room temperature before stopping the airflow.

Secondly, an aqueous 2 molar cobalt (2 M Co) solution was prepared by dissolving 7.41 g of cobalt nitrate precursor (Alfa Aesar, 99.999 % $Co(NO_3)_2 \bullet 6H_2O$) in 12.7 ml of deionized water while stirring at room temperature. After a clear solution was formed, 8.5 g of Al_2O_3 were added gradually under constant stirring in order to avoid lumps formation. Stirring and mixing were continued for 24 hours until a thick paste was formed. Afterwards, the formed catalyst paste was dried at 60 °C for 6 hours under mild stirring. The dried catalyst was then crushed and sieved (150 - 250 μm), as shown in Figure 20 c.

Thirdly, the catalyst powder formed was calcined in a rotary oven (Thermcraft, XSL-3-0-12-1C with 1-1-20-230-E15SK), as illustrated in Figure 21, under an airflow of 50 ml/min while gradually ramping the temperature at a rate of 3.0 °C/min to a maximum of 350 °C and then holding the temperature for about 6 hours. The catalyst was then allowed to cool to room temperature.

To reduce local overeating, the calcined catalyst was diluted by mixing 0.5 g of the prepared catalyst with 10 g of quartz sand (Sigma Aldrich, 50-70 mesh), as shown in Figure 20 d. The catalyst and quarts were vigorously mixed to assure homogeneous catalyst distribution.

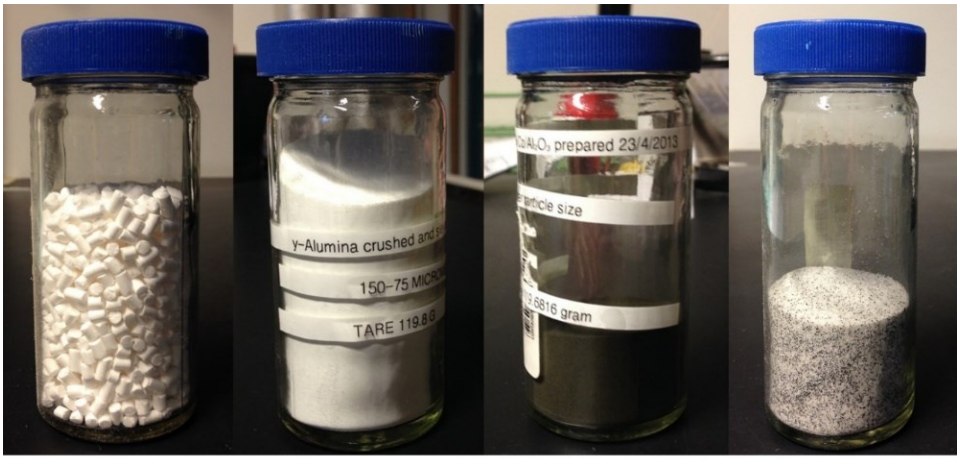

Figure 20. Cobalt-based catalyst preparation. (a) Al_2O_3 support, (b) crushed and sieved Al_2O_3, (c) impregnated Co/Al_2O_3 catalyst, (d) quartz diluted Co/Al_2O_3 catalyst.

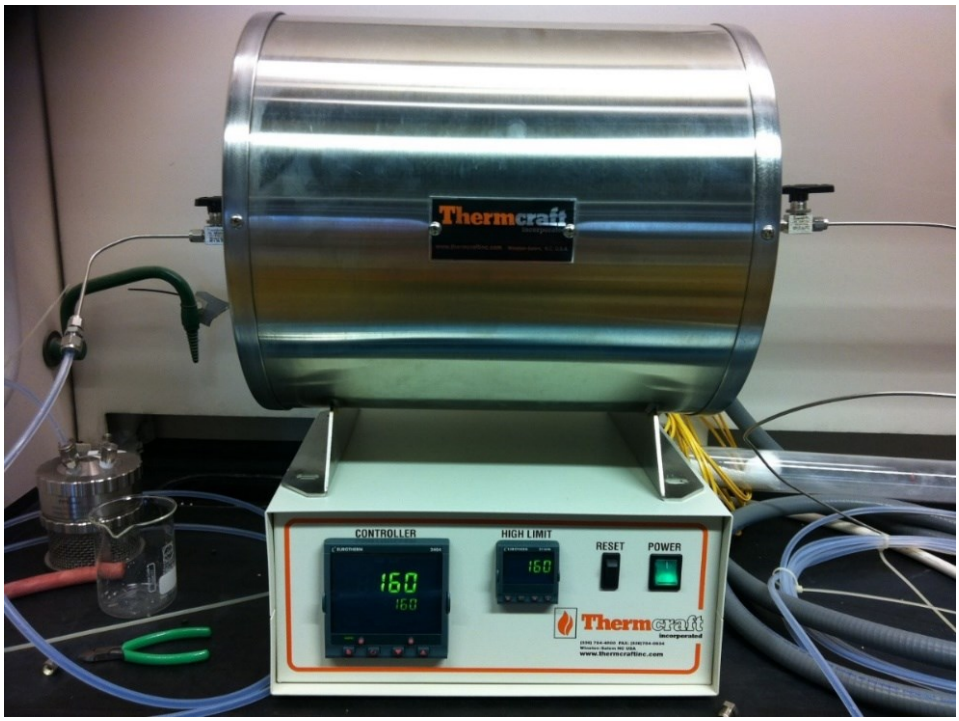

Figure 21. Utility furnace setup, used for drying and calcination of catalysts and adsorbers.

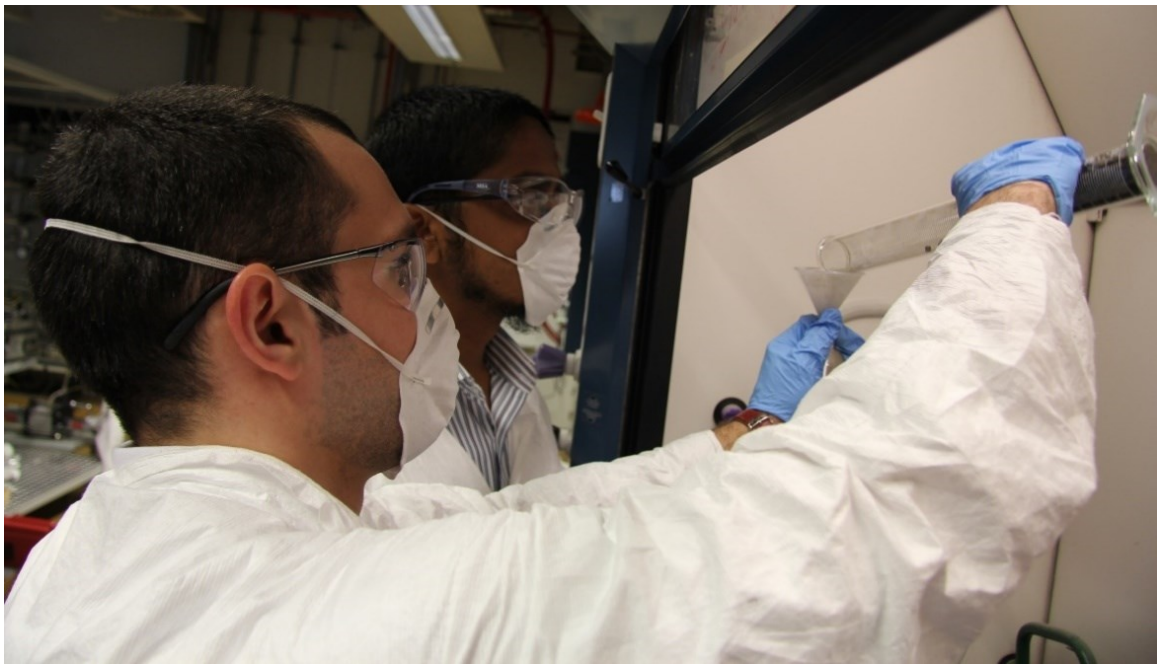

Figure 22. Cobalt-based catalyst loading into the reactor tube.

Finally, 1.0, 0.5 or 0.25 grams of the diluted catalyst were loaded into the reactor tube on top of 5.0 grams of quartz, as shown in Figure 22. The catalyst bed was held in place using glass wool (Supelco) and stainless steel sintered frits located at both ends.

III.3 Feed Purification System Pretreatment

III.3.1 PuriStar R3-15 Activation

Before using the PuriStar R3-15 catalyst, it needs to be reduced and dried. The reduction process took place in a setup similar to that used for Co catalyst calcination, described in section III.2, using a rotary furnace as shown in Figure 21. The required amount of PuriStar (150 ml approx.) was placed and plugged with glass wool on both sides, in a hollow glass tube connected to H_2 and N_2 sources from one end, and to a vent from the other end. The rotary oven temperature was slowly raised to 230 °C at a rate of

2.0 °C/min while purging the system with 200 nmL.min N_2. After, 230 °C was achieved, N_2 flow was replaced with 80 nmL/min flow of H_2 and then temperature was held for 2.0 hours. A noticeable amount of water was formed during the reduction process, which needs to be removed before PuriStar can be used. To dry the formed water, the H_2 source was replaced by N_2 source flowing at around 100 nmL/min at the same temperature for another 2.0 hours when no more water was observed. After that, the furnace was set to ambient temperature and PuriStar was allowed to cool under N_2 flow. Finally, PuriStar was added to each feed purification vessel as necessary.

III.3.2 E-315 Activation

The reduction and dehydration process for E-315, followed the same procedure used for PuriStar R3-15 reduction and dehydration, explained previously in section III.3.1.

III.3.3 Selexsorb COS Dehydration/Regeneration

During storage and handling, Selexsorb adsorb moisture from the atmosphere. Thus, it must be regenerated. The regeneration process took place in a setup similar to that used for Co catalyst calcination, described in section III.2, as shown in Figure 21. Selexsorb sample was placed in a hollow glass tube connected to an air source from one end and a vent from the other end. The rotary oven temperature was slowly raised under an N_2 flow of about 300 nmL/min to 230 °C at a rate of 2.0 °C/min and then temperature was held for 2 hours. A noticeable amount of water vapor was observed to desorb from the Selexsorb, indicating that the dehydration process was effectively implemented. After that, the furnace was set to ambient temperature and Selexsorb was allowed to cool under

N_2 flow. Finally, Selexsorb was added to each feed purification vessel supported on a layer of glass wool.

III.4 High-Pressure Reactor Unit Commissioning and Troubleshooting

A number of design flaws and operational problems were identified during reactor unit commissioning and operation. These problems begin with gas leaks, mainly from connection points. To overcome this problem, the system was tested for leaks using inert N_2 at 10, 50 and 90 bar while monitoring the pressure drop in the system. Additionally, liquid leak detector (Swagelok, Snoop) was used to precisely identify the leak source/point, and all leaks were fixed before starting the FTS reaction experiments.

Another problem faced was passing pressure control valve (PV-115, Badger Meter, 1001GCN36SVOSP01ST), due to the accumulation of some wax in the valve preventing the needle to close properly. This was investigated; efficient measures that include flushing the valve with hexane to remove accumulated wax, tightening the valve spring from the gland nut, and enhancing the heating tape wrapping and insulation around the valve were able to resolve this problem.

The same problem was faced in the GC system, where wax kept accumulating in the sample lines, causing abnormalities in the GC data. Similarly, this problem was solved by flushing the GC lines with hexane after each experimental set and improving the heat tape wrapping and insulation around the lines.

Wax also accumulated in the lines connecting the bottom of the hot trap and the wax collector resulting in severe tube blockage. This time the unit had to be shut down in order to remove the blocked lines that were heated and cleaned with hexane flow. The

lines were then reinstalled and the reactor was again started while the lines this time were kept under constant hot argon purge and the heat tape wrapping and insulation around the lines were improved.

Reactor temperature control proved to be very difficult to manage. On a number of occasions, control over the reactor temperature was lost resulting in reaction runaway. This was found to be caused by a malfunction and miss placement of the temperature probe inside the reactor bed. The probe was replaced, and a method was developed to slowly ramp the reactor temperature. In addition, the catalyst was further diluted, which minimized the chance of such incidents. However, controlling the reactor temperature remained a difficult task. Additionally at the initial startup phase, there were some difficulties in reaching the required reactor temperature. This was found to be caused by the high heat loss to the surroundings; providing better thermal insulation at the reactor inlet and outlet was sufficient to solve the problem.

Running out of feed gases, solvent and helium for the analysis system while running the reactor was an additional problem faced. This caused operational interruptions and instability in the measured analyzer data. In the future, this problem can be solved by providing a backup gas cylinder for each gas and creating an on-line hexane filling/makeup system, which should minimize operational interruptions.

Furthermore, malfunctions in the H_2, N_2 and air generators caused abnormalities in the FID operation, while a malfunction in the air generator caused total system shutdown due to loss of pneumatic air causing shut-off valves to go to the fail-to-close state. Thus, continuous monitoring of generators operation and proper preventative

maintenance were required. In addition, an air supply line from TAMUQ utility station was connected to the system, so it can be used in case of air generator failure.

Moreover, the MFCs, flow meter FQI-800 and cold trap level meter needed to be recalibrated at initial reactor startup. In addition, Proportional Integral Derivative (PID) controllers needed to be tuned (gain K, rate I and reset D) in order to obtain optimum controller behavior.

In one incident, the actual set point of a pressure safety valve was found to be less than the specified one, resulting in gas venting and loss of pressure. The problem was quickly identified and rectified by adjusting the PSV set point.

Finally, a pressure transducer (PT-126, WIKA, S10/0-3000 psi) was once damaged due to high operational temperature (above design specifications). The tubing connecting the transducer to the process line was extended to allow for temperature reduction by natural cooling, and this prevented the problem from reoccurring.

III.5 High-Pressure Reactor Unit Operation

III.5.1 High-Pressure Reactor Unit Startup

Firstly, the reactor catalyst bed was prepared by adding 2.0 cm of glass wool (Supelco) followed by 0.3 g of quartz sand (Sigma Aldrich, 50-70 mesh). Then, the diluted catalyst mixture was poured on top of the sand layer and after that, the mixture was topped with a plug of glass wool. After that, the reactor was carefully connected back to the unit.

During initial reactor startup, the entire system was purged with N_2 to remove air and other contaminants that may have entrained into the system. The unit was then leak tested at 10, 50 and 90 bars of N_2, and after the leak test, the unit was depressurized and

prepared for startup. After that, the water chiller (WC-501, Thermo Scientific, NESLAB RTE 10) and the HPLC solvent pump (P-101, LabAlliance, P40SFT01) were primed and tested. The water chiller was switched on at a set point of 4.0 °C, while the hot trap, GC transfer lines and wax collector heat tapes (HT-108, 110, 115 and 116) were switched on to 150 °C at 5.0 °C/min. The solvent pump was then started at 1.0 mL/min to flush and clean the reactor; this was performed for 1 hour after each experimental set. After this, N_2 was used to purge the solvent remaining in the system. Next, argon was allowed into the system from the cylinder at 80 bar. Its pressure was then reduced via (PCV-104, GO Regulator, PR-57-1A11C5N141) to 10 bar.

III.5.2 Cobalt Catalyst Activation

Before initiating the FTS reactions, the prepared catalyst must be reduced at elevated temperatures. This step is necessary in order to remove the water absorbed by the highly hygroscopic Co/Al_2O_3 and to bring Co into an active form, which is required to obtain high activity, desired selectivity and achieve high catalyst stability.

The catalyst activation took place *in-situ* in the fixed bed reactor. At first, the catalyst was subjected to H_2 flow at 100 nmL/min and then increased to 350 nmL/min. The reactor temperature was then ramped to 180 °C at 5.0 °C/min, and hydrogen flow was dropped back to 100 nmL/min after the temperature reached the desired set point and stabilized. After that, the reactor temperature was increased to 350 °C at 2.0 °C/min and held at this point for 12 hours.

III.5.3 Fischer-Tropsch Synthesis Experiments

After activating the cobalt catalyst, the reactor temperature was set at 180 °C, H_2 flow was stopped and replaced with a flow of N_2 to cool and purge the catalyst bed. In a typical FTS run where supercritical solvent was utilized. The solvent pump was first switched on and the solvent flow was gradually increased to the desired flow rate. Argon was also introduced to the system at controlled flow rates in order to be used as an internal standard and to continuously purge the wax collection lines. Next, the reactor pressure was ramped up slowly to the desired set pressure, while the reactor temperature was slowly raised (to avoid hot spot formation and reaction runaway) from 180 °C to the desired reaction temperature. After the reactor temperature and pressure had been stabilized, syngas was allowed at the desired flow rate. Each experimental set was allowed to reach steady state conditions in terms of conversion and product distribution, as indicated by the on-line GC. After reaching steady state, wax and liquid samples were collected for further off-line analysis.

III.5.4 High-Pressure Reactor Unit Shutdown

After each experimental set, the syngas flow was stopped, while the flow of hexane continued at 2.0 nmL/min to flush and clean the reactor and the GC lines. Hexane flow was stopped when no FTS products other than hexane were detectable by the on-line GC. Then, N_2 flow was introduced at 50 nmL/min to purge the remaining hexane from the system. Meanwhile, the reactor temperature and pressure were gradually reduced (to avoid wax condensation) to ambient conditions. Subsequently, the hot trap and cold traps were emptied in order to obtain a good baseline reading and to have fresh samples without

interference from previous runs/conditions. Finally, the power to the heating tapes and reactor furnace was turned off, nitrogen flow was stopped, and the system was depressurized. After shutting down the reactor unit, the reactor tube was disassembled and the used catalyst was collected for future analysis and characterization.

IV. RESULTS AND DISCUSSION

IV.1 Fischer-Tropsch Product GC Peak Identification

The exact and detailed identification of the FTS product can be hindered by the large number of compounds involved [60]. One method for identifying FTS products is to use standard solutions that include FTS products (paraffins, α-olefins, β-olefins, branched and oxygenates of C_1-C_{34}) to obtain a satisfactory Gas Chromatograph (GC) calibration. This is a far too complex and cumbersome process; thus a GC/Mass Spectroscopy (GC/MS) analyzer (Agilent, 7890A) was used for compound identification in the range of C_5-C_{34}.

For the identification of C_1-C_4 hydrocarbons and permanent gases (CO, CO_2, H_2, Ar) a calibration gas was necessary. Calibration gas (National Industrial Gas Plants, 53 bar, 50 L) with known molar percentages (Table 3) was injected into the on-line GC (Shimadzu, GC-2014). Additionally, normal alcohols (methanol – hexanol) were injected to identify the alcohol peaks. The retention time and peak area for each gas concentration were predetermined by Shimadzu FID detector; thus an adequate peak identification for C_1-C_4 was possible. A sample peak identification for C_4 group is shown in Figure 23.

As illustrated in Figure 24, for the TCD 1 signal (channel 2), helium was used as the carrier gas. Thus, any gas slower than C_2 was back-flushed. The peak order obtained from the detector as shown in Figure 24 started with H_2 (small peak), Argon and O_2 (they do not separate), N_2, CH_4, CO, ethylene, ethane and CO_2. The identification and quantification process of TCD peaks is crucial for the activity and selectivity calculations as discussed in the Result and Discussion Section IV.2, Appendices A and B.

Table 3. Calibration gas molar percentages.

Component	Composition %
Carbon monoxide	10
Carbon dioxide	3
Methane	4
Ethane	1.5
Ethylene	3
Propane	1
Propylene	2
Iso-Butane	0.5
N-Butane	0.5
N-Butene	0.5
Iso-Butylene	0.5
Trans-2-Butene	0.5
Cis-2-Butene	0.5
Nitrogen	Balance

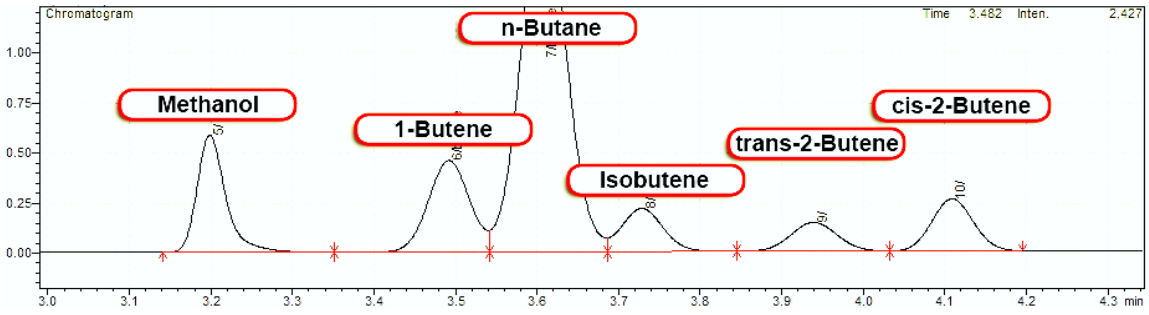

Figure 23. Peak identification for C_4 FTS product range, using Shimadzu FID predetermined retention times.

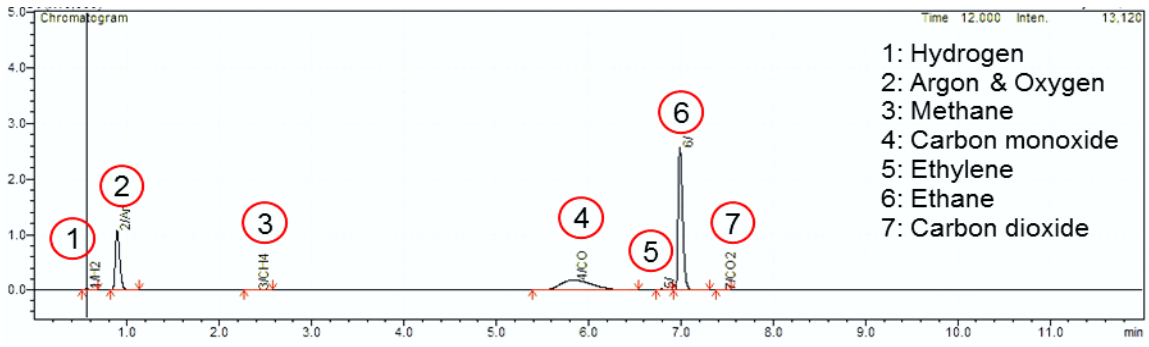

Figure 24. Peak identification of permanent gases on the Shimadzu TCD**.**

The identification of C_5-C_{34} hydrocarbon compounds was carried out off-line by injecting liquid samples into the GC/MS. The off-line GC/MS analysis of liquid products provided the full product distribution upon accurate identification of all hydrocarbons between C_5 and C_{34}. Most hydrocarbons (isomers, olefins and oxygenates) between C_5 and C_{25} were easily identified with high accuracy by the GC/MS. However, higher molecular weight branched isomers and high molecular weight olefins were more problematic to identify.

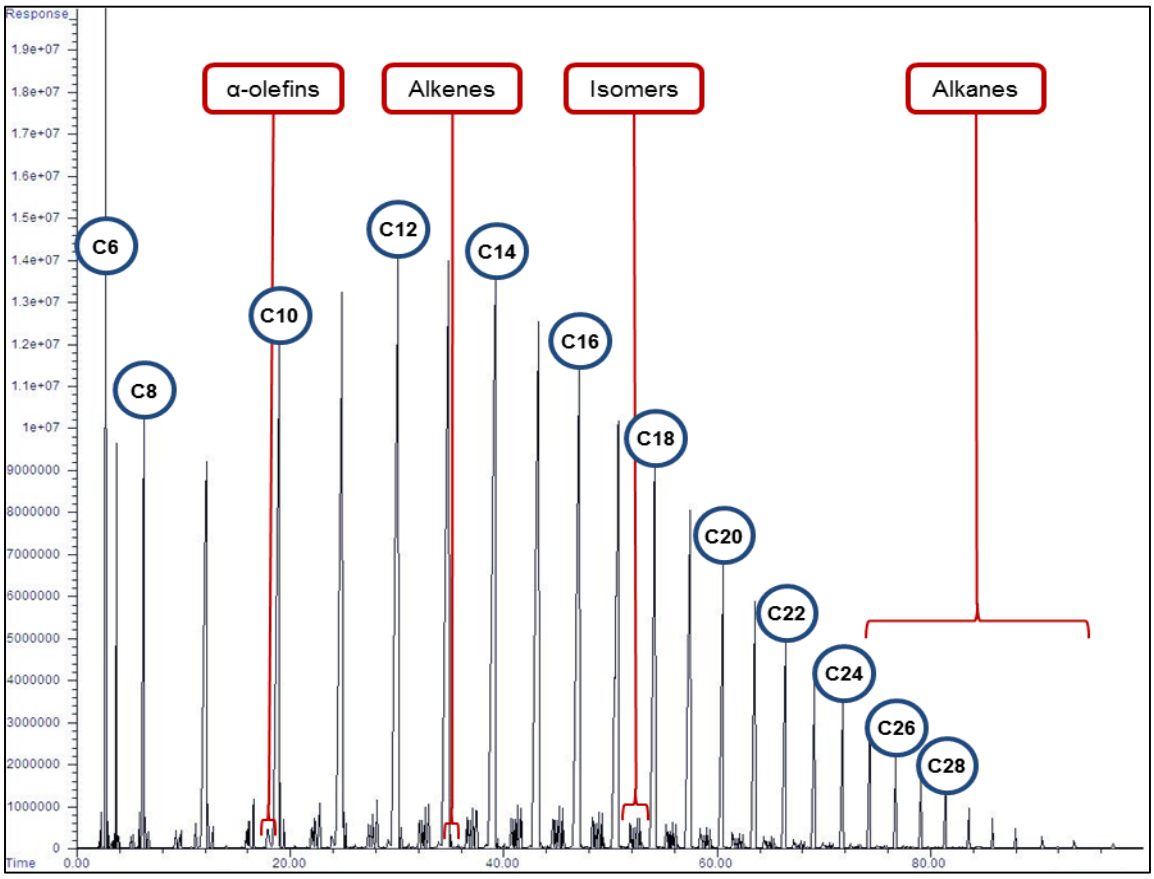

Figure 25. Overall FTS product spectrum obtained using the off-line Agilent FID analysis, for cobalt-based, gas phase FTS at 240 °C and 20 bar with H_2:CO of 2:1 feed ratio.

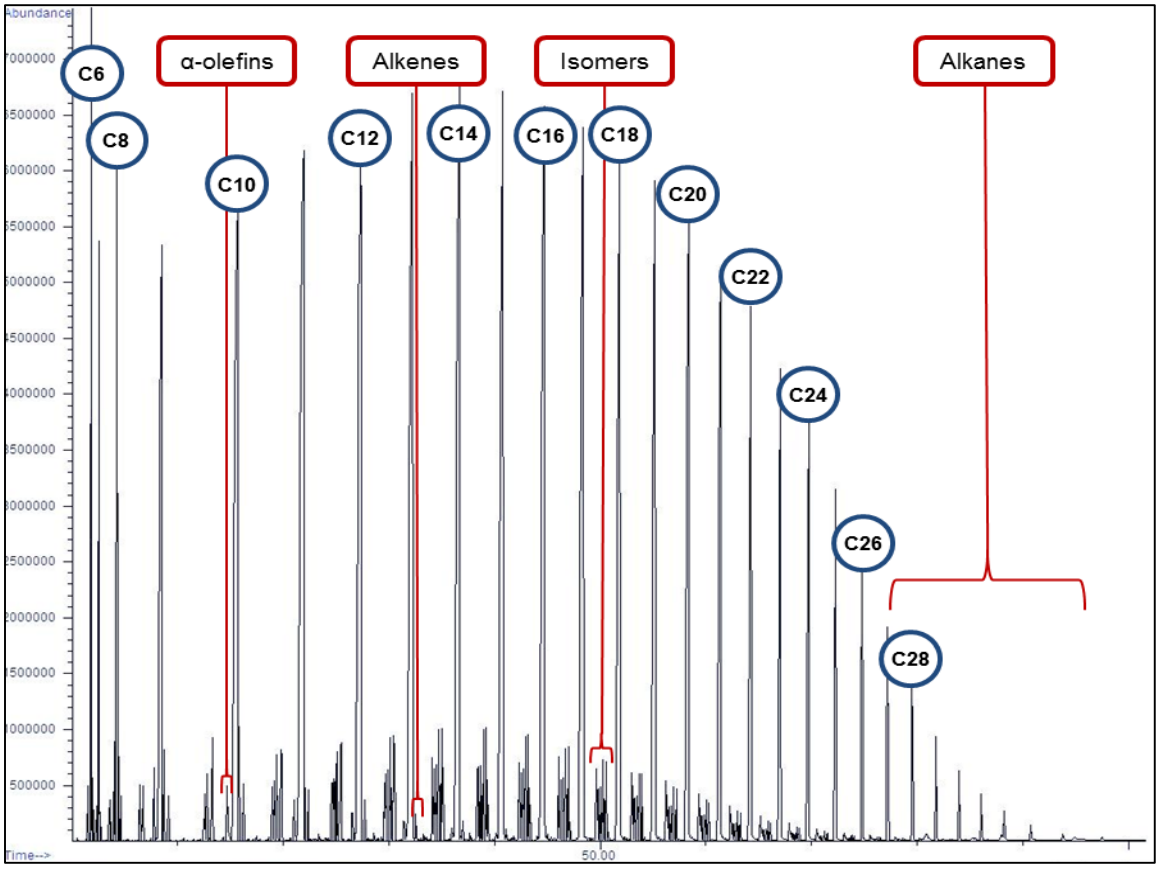

Figure 26. Overall FTS product spectrum obtained using off-line Agilent MS analysis, for cobalt-based, gas phase FTS at 240 °C and 20 bar with H_2:CO of 2:1 feed ratio.

A sample of compounds (C_7 range) identified using the GC/MS is shown in Table 4. The sample retention time on both FID and MS were identified while the molecule identity was determined utilizing the MS (database), as shown in Figures 27-29. Then, the retention time for each compound was inserted manually into the Agilent GC software (Enhanced Data Analysis), for automatic report generation with defined components, as illustrated in Figure 30. This process is of high importance since product distribution and selectivity studies depend on the accuracy of the peak identification process.

Table 4. C_7 FTS product range as identified by the off-line Agilent GC/MS, for cobalt-based, gas phase FTS at 240 °C and 20 bar with H_2:CO of 2:1 feed ratio.

FID Retention Time	Peak Area	MS Retention Time	Compound Name	Compound Group	Compound Branch
3.218	612711	2.228	1-butanol	C_4	Alcohol
3.258	2065458	2.252	2-methyl hexane	C_7	Isomer
3.367	2459938	2.328	3-methyl hexane	C_7	Isomer
3.572	10665767	2.471	1-heptene	C_7	α-Olefin
3.708	154553134	2.559	n-heptane	C_7	Normal
3.766	855344	2.605	3-methyl-2-hexane-Cis	C_7	Alkene
3.812	7000586	2.638	2-heptene-Cis	C_7	Alkene
3.957	4094594	2.739	2-heptene-Trans	C_7	Alkene

The FTS product followed a similar pattern for each hydrocarbon group (C_X), where it begins with (C_X) isomers (increasing in number as X increases). The peaks follow the aforementioned C_X of α-olefins (from 1-3), the normal (C_X) alkane (normally the peak with the highest area, which is common for cobalt-based catalyst). After the normal alkane peak comes, the cis and then the trans (C_X) alkenes peaks, as demonstrated in Figures 27 and 28. On the other hand, the location of (C_{X-3}) alcohol peaks changed as the carbon number increased. For lighter alcohols (C_3 – C_7), the alcohol peak was located before the C_X isomers, for (C_8 – C_{13}) alcohols, the alcohol peaks were located between C_X isomers and for (C_{14} – C_{20}) alcohols, the alcohol peaks were found after the isomers and before the α-olefins peaks. It is also noticeable that, α-olefins were not detectable by the Agilent GC/MS beyond (C_{17}), alcohols beyond 1-eicosanol (C_{20} alcohol) were not detectable, while cis and trans alkenes were not detectable beyond (C_{22}). All observations mentioned earlier agree well with the profile of FTS hydrocarbon product distribution obtained from cobalt-based catalysts tested under similar conditions [47, 60].

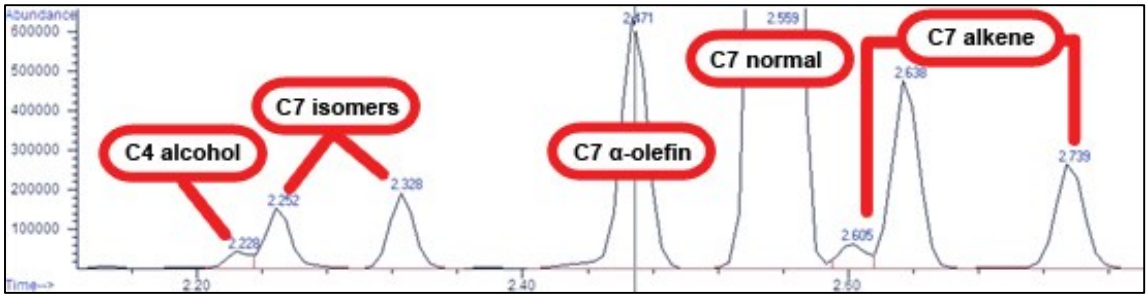

Figure 27: C_7 FTS product range on the MS, as identified by the off-line Agilent GC/MS, for cobalt-based, gas phase FTS at 240 °C and 20 bar with H_2:CO of 2:1 feed ratio.

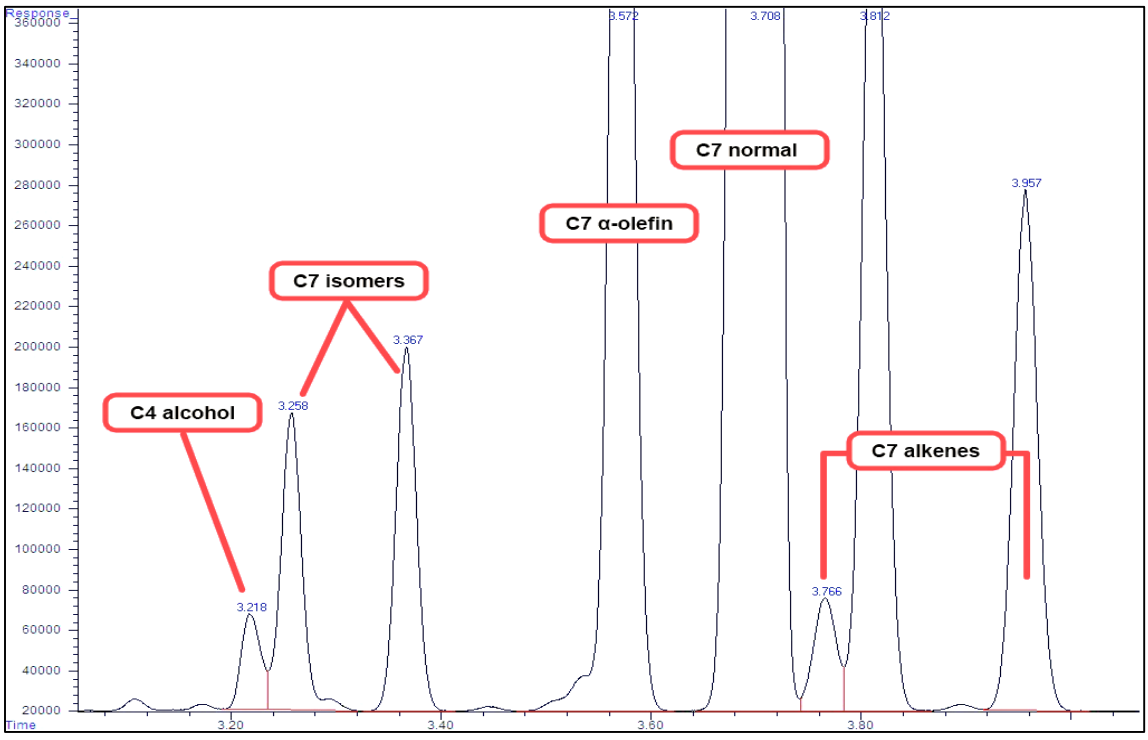

Figure 28. C_7 FTS product range on the FID, as identified by the off-line Agilent GC/MS, for cobalt-based, gas phase FTS at 240 °C and 20 bar with H_2:CO of 2:1 feed ratio.

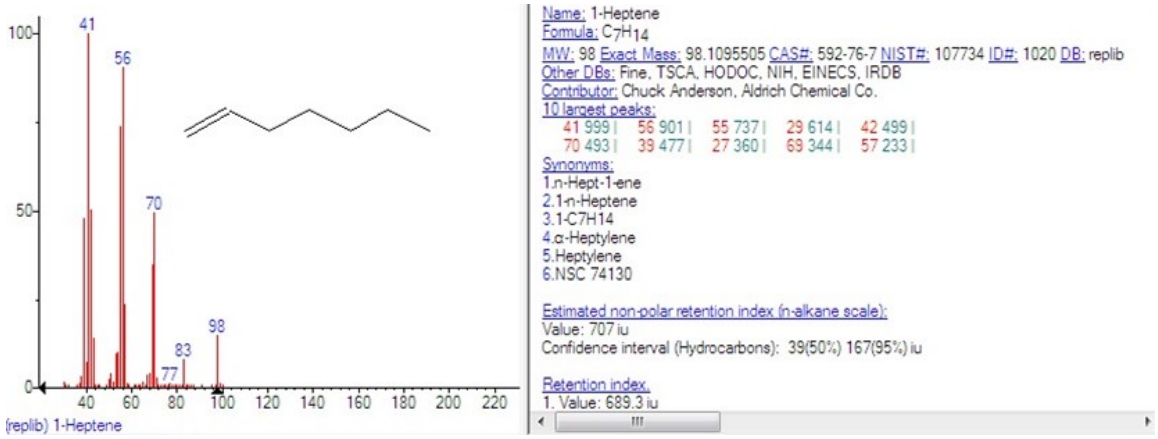

Figure 29. Example of MS peak identification for C7 peak # 4 (1-heptene) using the off-line Agilent GC/MS, for cobalt-based, gas phase FTS at 240 °C and 20 bar with H_2/CO feed ratio of 2.

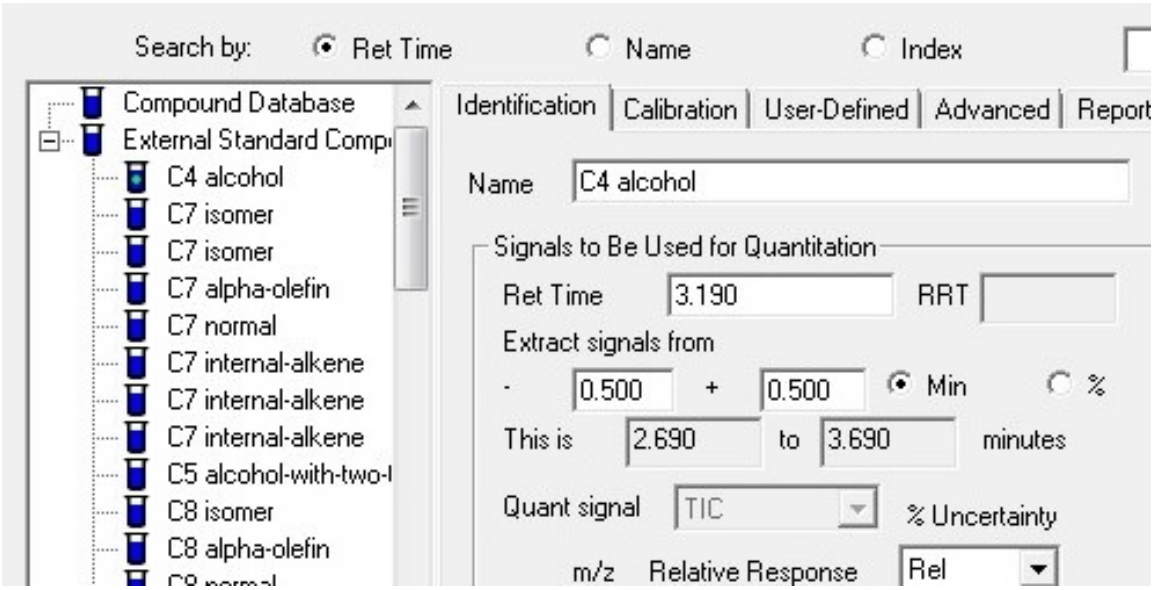

Figure 30. Manual retention time insertion of identified compounds, for automated Agilent off-line FID report generation.

IV.2 Steady-State Fischer-Tropsch Synthesis Reaction Studies

The FTS reaction was performed in the commissioned high-pressure reactor unit described in Chapter III over the prepared cobalt-based catalyst (15 wt% Co/Al_2O_3). Through the experimental run, the same catalyst was used; however, different catalyst loadings of 1.0, 0.5 and 0.25 grams were used for selected conditions. The experimental run was carried over a period of six months (October 2013 – May 2014) for a total of 1360 hours time-on-stream (TOS). A total of 28 different experimental conditions were used, as shown in Table 5.

CO consumption (activity) and conversion, CH_4 formation rate, olefin formation rate, the hydrocarbon product distribution, and the chain growth probability (α-value) were measured and analyzed under different reaction conditions. The method and equations used to conduct the carbon balance and to calculate the CO activity, CO conversion, CH_4 formation rate, CH_4 selectivity, product distribution and olefin formation rate are discussed in detail in Appendices B - E. These parameters are dependent on several factors as some are straightforward such as pressure and temperature, and some are more complex such as reactor type, catalyst type, promoters used, and the reaction medium [61]. In order to accomplish the research project objectives, the FTS reaction was carried out in gas phase media and SCF media, while varying the reaction temperature (210 – 240) °C, pressure (20 – 80) bar, syngas feed ratio (H_2/CO) from 0.6/1 to 2/1, syngas flow rate (50 – 150) nmL/min, and solvent flow rate (2.43 and 2.74) nmL/min.

Table 5. Experimental conditions used in the FTS experimental campaign.

Experimental Set	A1	A2	A3	A4	A5	A6	B1	B2	B3	B4	B5	B6	B7	B8
T (°C)	230	230	230	230	230	230	240	240	240	240	240	240	240	240
P (Bar)	80	80	80.3	81.24	80.3	19	20	20	50	80	80	20	65	20
Qsyngas.in (nmL/min)	138	84	138	152	138	68	70	65	85	85	140	65	55	65
Q_{CO}.in (nmL/min)	0	0	0	0	0	0	0	0	0	0	0	0	0	0
Q_{H2}.in (nmL/min)	0	0	0	0	0	0	0	0	0	0	0	0	0	0
Q_{Ar}.in (nmL/min)	10	10	10	10	10	10	10	10	10	10	10	10	10	10
Q_{Hex}.in (nmL/min)	2.43	0	2.43	0	2.43	0	0	0	0	0	2.43	0	2.74	0
Q_{N2}.in (nmL/min)	0	218.7	0	124	0	100	0	0	110	220	0	0	0	0
H_2/CO Feed Ratio	2	2	2	2	2	2	2	2	2	2	2	2	2	2
Solvent/Syngas Ratio	3	0	3	0	3	0	0	0	0	0	3	0	6	0
Reaction Medium	SCF	N_2 Balance	SCF	N_2 Balance	SCF	N_2 Balance	Gas	Gas	N_2 Balance	N_2 Balance	SCF	Gas	SCF	Gas

Table 5. Continued.

Experimental Set	C1	C2	C3	C4	C5	C6	C7	D1	D2	D3	D4	D5	D6	D7
T (°C)	240	240	240	240	240	240	240	210	210	220	220	220	220	230
P (Bar)	20	80	80	20	20	20	20	20	20	20	20	20	20	25
Qsyngas.in (nmL/min)	65	85	140	65	75	50	100	100	50	50	0	0	0	50
Q_{CO}.in (nmL/min)	0	0	0	0	0	0	0	0	0	0	25	22	33	0
Q_{H2}.in (nmL/min)	0	0	0	0	0	0	0	0	0	0	32	15	21	0
Q_{Ar}.in (nmL/min)	10	10	10	10	10	10	10	15	15	15	15	10	15	15
Q_{Hex}.in (nmL/min)	0	0	0	0	0	0	0	0	0	0	0	0	0	0
Q_{N2}.in (nmL/min)	0	220	100	0	0	0	0	0	0	0	0	0	0	0
H_2/CO Feed Ratio	2	2	2	2	2	2	2	2	2	2	1.3	0.65	0.6	2
Solvent/Syngas Ratio	0	0	0	0	0	0	0	0	0	0	0	0	0	0
Reaction Medium	Gas	N_2 Balance	N_2 Balance	Gas	Gas	Gas	Gas	Gas	Gas	Gas	Gas	Gas	Gas	Gas

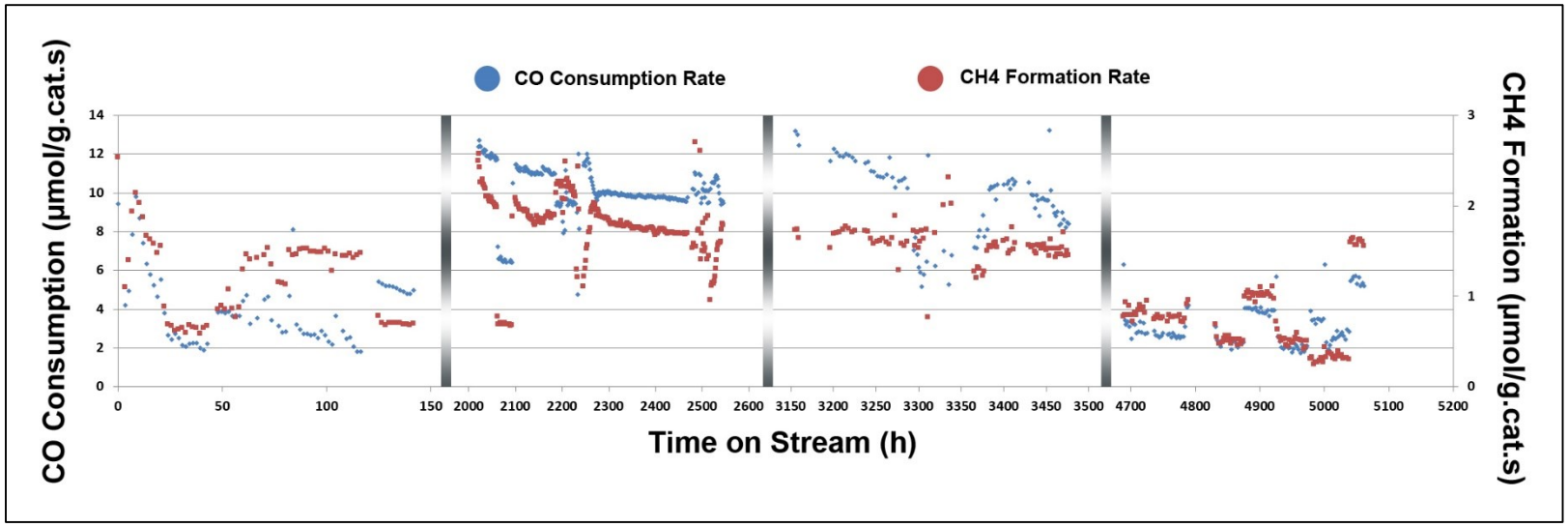

Figure 31. CO consumption rate (activity) and CH_4 formation rate, in (µmol/g.cat.s), for the entire FTS experimental campaign.

Each experimental set was allowed to reach steady state conditions, at which the conversion and the hydrocarbon product distribution became stable with TOS. After reaching steady state, the experiment was continued for about 15 hours and the steady state data was used for the comparative studies. Figure 31 shows the activity (primary axis; left y-axis) and CH_4 formation rate (μmol/g.cat.s) (secondary axis; right y-axis) for the entire experimental campaign.

IV.2.1 Supercritical FTS versus Gas Phase FTS

In this section, a comparison study between the conventional gas phase FTS and the supercritical FTS was conducted by investigating and validating the potential enhancements in terms of conversion, selectivity, hydrocarbon product distribution, α-value and olefin formation when performing the FTS reaction under near and supercritical conditions. The reactor was operated at 20 bar for the gas phase FTS while the temperature was varied at 210, 220, 230 and 240 °C. On the other hand, the reactor was operated at 65 and 80 bar for the supercritical FTS conditions while varying the temperature at 230 and 240 °C. In both cases, the syngas partial pressure was kept at 20 bar.

The CO conversion and the CH_4 selectivity were measured based on the TCD analysis from the on-line Shimadzu GC. The hydrocarbon product distributions and olefin selectivity were measured based on the FID analysis from both the on-line Shimadzu GC and off-line Agilent GC/MS, as previously discussed in section IV.1. The hydrocarbon formation rate (g/g.cat.h) was calculated as the sum of formation rate of all species (isomers, normal, olefins, alcohols) with "n" carbon number. Then, the normalized weight percentages (W_n) of each carbon number was calculated from the ratio of the hydrocarbon

formation rate of carbon number "n" to the total weight of hydrocarbons formed as detected by the FID, the detailed method used for generating the hydrocarbon product distributions can be found in Appendix D.

The on-line and off-line GC FTS product analysis confirmed a yield of a complex mixture of C_1 to C_{34} hydrocarbons and C_1 to C_{17} oxygenates, in addition to H_2O, CO_2 and unreacted syngas. The predominant FTS products were linear alkanes (*n*-paraffins), while branched (isomers), oxygenates (alcohols), α-olefins, and alkenes (cis and trans) hydrocarbons were produced to a lesser extent, as previously shown in Figures 25-28; this product distribution is typical for cobalt-based catalysts.

It was difficult to determine the exact amount of C_6 hydrocarbons produced when running the FTS reaction under near and supercritical conditions since large quantities of n-hexane were present in the feed. This resulted in a very large n-hexane peak absorbing nearby peaks within the C_6 range. Thus, calculating the formation rate of C_6 hydrocarbons was impractical. Hence, the hydrocarbons within the C_6 product range were emitted from the product distribution and were not included in the ASF calculations. Additionally, for consistency purposes, C_6 hydrocarbons were also emitted in the gas phase FTS when comparing the performance under the two reaction mediums.

In this comparative study, the focus was on two main reaction conditions. The first was conducted at 240 °C and 20 bar with only syngas (gas phase). In the second set, SCF (hexane) was introduced at 240 °C, with 20 bar syngas partial pressure and the total reactor pressure was set at 65 bar. Figures 32-36 compare the FTS performance under the two different reaction mediums at the aforementioned conditions.

Starting with Figure 32, which compares the CO conversion percent for the two reaction mediums. It was noticed that CO conversion increased by about 14 % upon the introduction of supercritical hexane where the steady state CO conversion was about 71 % compared to 57 % under conventional gas phase FTS.

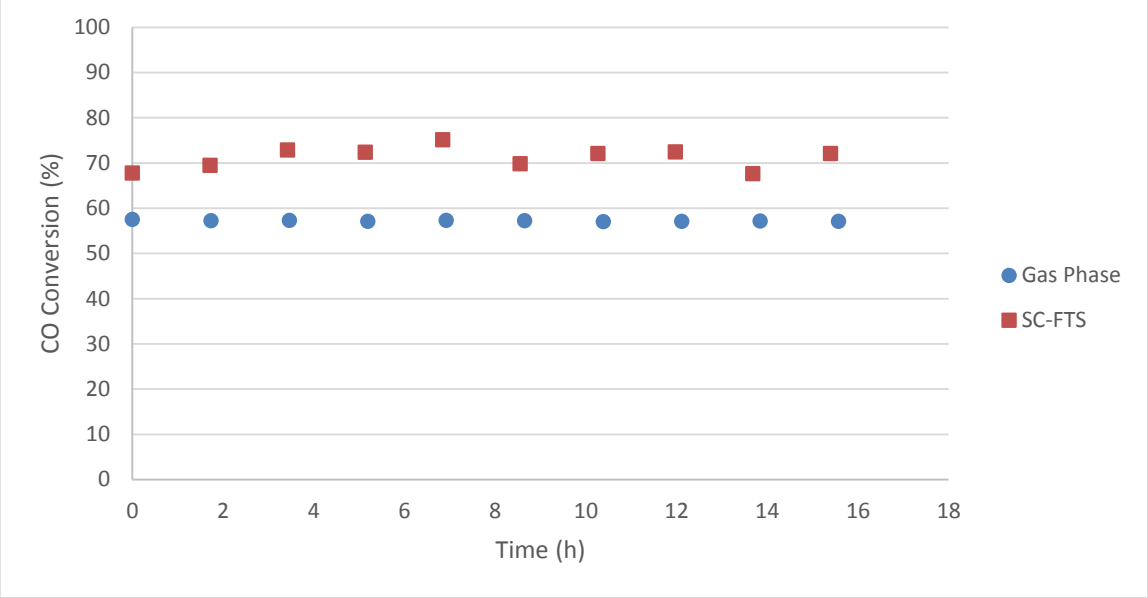

Figure 32. Reaction medium effect on CO conversion, over 15 wt% Co/Al_2O_3, under the following conditions: temperature 240 °C, pressure 65 bar for SC-FTS and 20 bar for gas phase FTS, and H_2:CO of 2:1 feed ratio.

In literature [41, 56, 58], the experimental data concerning CO conversion under the different reaction media is contradictory. On one hand, Fujimoto et al. [56], found that the conversion under supercritical conditions was to some extent lower than that in the gas phase. They attributed this to the difference in syngas diffusion rate in the different reaction media where the diffusion rate in supercritical fluids is slower than that in the gas phase. On the other hand, Huang and Roberts [41] showed that conversion in supercritical

hexane is higher (70 %) than that in the gas phase (60 %). Using an iron-based catalyst, Bukur and et al. [58], showed that conversion under supercritical phase was similar to that under the gas phase FTS.

Since the diffusion of reactants (syngas) is relatively higher in the gas phase than that in SCF, higher conversion rates are theoretically expected under the gas phase FTS. However, increased CO conversion was observed in our study as well as those conducted by Huang and Roberts [41], when the SCF was introduced. The rise in CO conversion after the introduction of SCF could be attributed to the enhanced *in-situ* extraction of heavy hydrocarbons (wax) that accumulates inside the catalyst pores [2]. The accumulation of wax inside the catalyst pores reduce the availability of active sites and increase the diffusional limitations (film resistance) [62]. Whereas, the *in-situ* wax extraction and removal of carbonaceous deposits from the catalyst pores by the SCF improve the reactants' accessibility to the active sites and alleviate the diffusional limitations resulting from wax buildup [36, 43, 44].

Next, in Figure 33 the selectivity towards specific fuel cuts under the two reaction media was compared. The hydrocarbon fuel cuts illustrated in Figure 33 are light hydrocarbons (LHC) represented by C_1-C_4, gasoline fraction represented by C_5-C_{10}, jet fuel fraction C_9-C_{13}, diesel fraction C_{13}-C_{18}, middle distillates (MD) by C_{11}-C_{22}, and light wax by C_{23}-C_{32} [21]. From Figure 33 it is apparent that the product distribution shifted towards the production of heavier hydrocarbons (especially within the middle distillates range) when shifting the reaction medium from the gas phase to the supercritical phase. Through the application of SCF, the selectivity towards light hydrocarbons was

significantly reduced by about 78 %, while jet fuel, diesel, middle distillates, and light wax selectivities were increased by about (15, 37, 35 and 76) %, respectively. Huang et al. [59] and Elbashir [63] reported similar results utilizing a fixed bed reactor with a cobalt-based catalyst (15 wt% Co/Al_2O_3) and operating the FTS reaction under similar conditions (240 °C, and 65 bar for the SC-FTS and 20 bar for the gas phase FTS). In addition to the aforementioned increase in heavy hydrocarbons selectivity at supercritical conditions, more wax was collected from the bottom of the hot trap under supercritical operation, about 2 to 3 times more in weight, for the same time on stream.

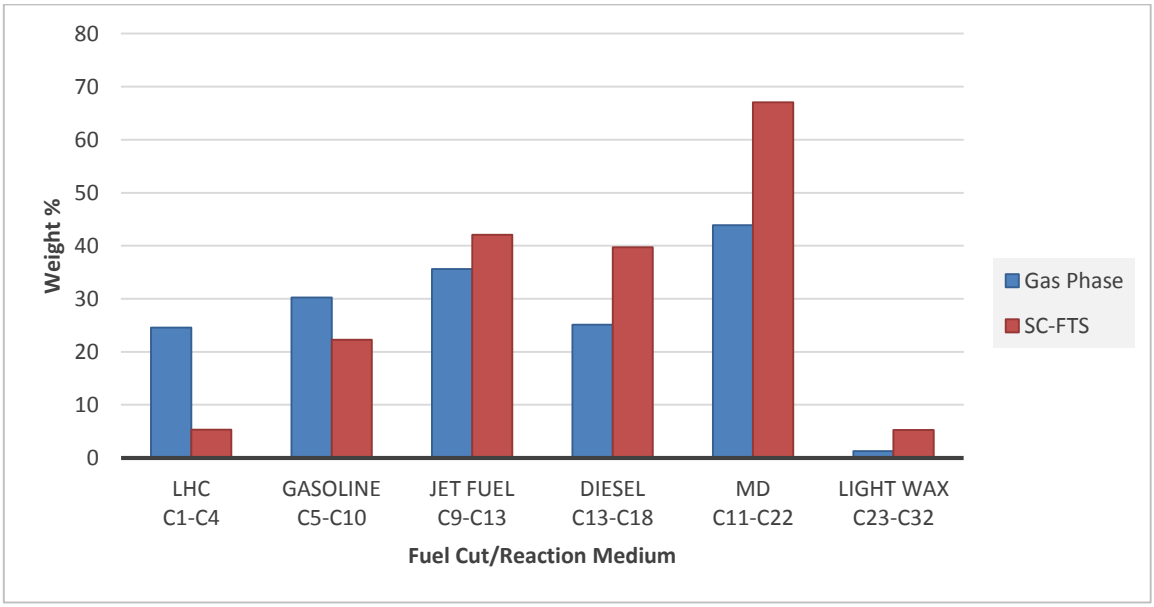

Figure 33. Reaction medium effect on hydrocarbon cut selectivity, over 15 wt% Co/Al_2O_3, under the following conditions: temperature 240 °C, pressure 65 bar for SC-FTS and 20 bar for gas phase FTS, and H_2:CO of 2:1 feed ratio.

The observed reduction in light hydrocarbons can be related to the increased heat capacity of the supercritical reaction medium compared to the gas phase. The liquid-like heat capacity of supercritical fluids provides better heat removal and minimizes hot spot formation, which suppresses the formation of light hydrocarbons [36, 41, 43]. Furthermore, the SCF liquid-like solubility enhances the *in-situ* extraction of waxy products from the catalyst pores, hence freeing more active sites for primary products to incorporate in the chain growth process, and thus improving the selectivity towards heavier fuel cuts and yielding more wax [2, 36, 41, 43, 46, 63].

The overall hydrocarbon product distributions from C_1-C_{32} under the previously mentioned conditions (240 °C, with 65 bar for the SC-FTS and 240°C with 20 bar for the gas phase FTS) were compared as shown in Figure 34. The overall product distribution figure elucidates the shift towards the production of heavier hydrocarbons under the SCF reaction medium. For instance, middle distillates (C_{11}-C_{22}) constituted about 67 % of the normalized product weight under the SC-FTS compared to 44 % in the gas phase FTS. In addition, a substantial drop in methane selectivity was observed when shifting the FTS reaction medium from the gas phase to the supercritical phase.

A number of studies [36, 41, 56, 64] also reported a suppression of methane formation when applying SCF as a reaction media for the FTS. This suppression can be attributed to the liquid-like heat transfer properties in SCF medium that results in better heat removal from the catalyst bed and thus minimize hot spots formation. This as well helps in reducing the rate of cracking reactions, thus suppressing methane formation and simultaneously increasing the production of heavier hydrocarbons [36, 41, 43, 51, 64].

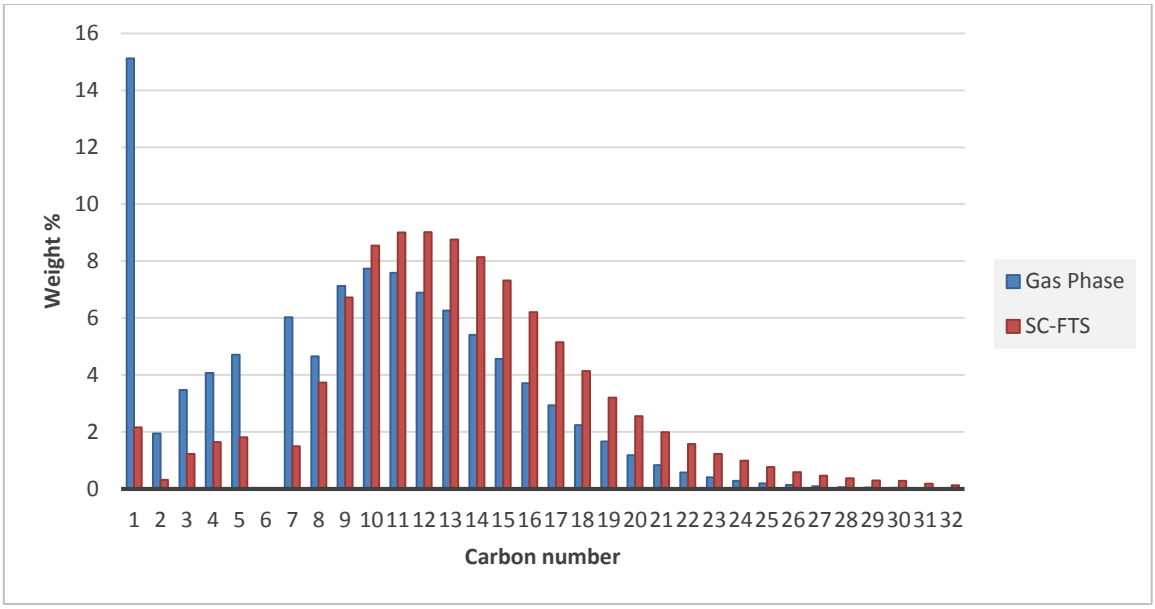

Figure 34. Reaction medium effect on product distribution, over 15 wt% Co/Al_2O_3, under the following conditions: temperature 240 °C, pressure 65 bar for SC-FTS and 20 bar for gas phase FTS, and H_2:CO of 2:1 feed ratio.

Different mathematical models have been proposed and developed to predict the FTS product distribution. The simplest and most widely used model is the Anderson-Schulz-Flory (ASF) product distribution, which can be represented in mass basis as follows:

$$W_n = n(1-\alpha)^2 \alpha^{n-1} \quad (1)$$

Where W_n is the mass fraction of hydrocarbon molecules with "n" carbon atoms. "n" is an integer representing the number of carbon atoms that begins with C_1 and ends with the highest molecular weight hydrocarbon detected by the GC. α-value is the chain growth

probability, which is the probability that a molecule keeps reacting with other carbon-containing molecules to form longer chains.

The model assumes that the FTS follows the style of a polymerization reaction, by which the reaction is initiated on the catalyst active site by a single carbon atom monomer. Then, the chain growth process occurs by consecutively adding a single monomer molecule at a time. Eventually, the chain growth process ends, by either the addition or subtraction of a hydrogen molecule. Following this, the molecule produced desorbs from the catalyst pore and leaves a free active site for further reactions [63]. The ASF model assumes that the carbon number product distribution is governed by a factor called the chain growth probability (α-value) that does not depend on the number of carbon atoms in the product.

A plot of $\ln(W_n/n)$ versus "n" results in a straight line, where α-value can be calculated from the slope of that line, see Appendix D. Higher α-value indicates higher selectivity towards heavier hydrocarbon production and vice versa. Figure 35 shows the ASF plots of the FTS under either reaction media (supercritical hexane and gas phase). From the ASF plots, it was first noticed that lower selectivities towards methane and light hydrocarbons were achieved under supercritical conditions, while the selectivity towards middle distillates and heavy hydrocarbons was increased (this is in agreement with the previous discussion). The improved product selectivities when shifting the FTS from the gas phase media to supercritical hexane medium resulted in a significant increase in chain growth probability from 0.76 to 0.85. The increase in chain growth probability under

supercritical conditions was observed by others including Bochniak and Subramaniam [44], Tsubaki et al. [65], and Elbashir et al. [47, 54].

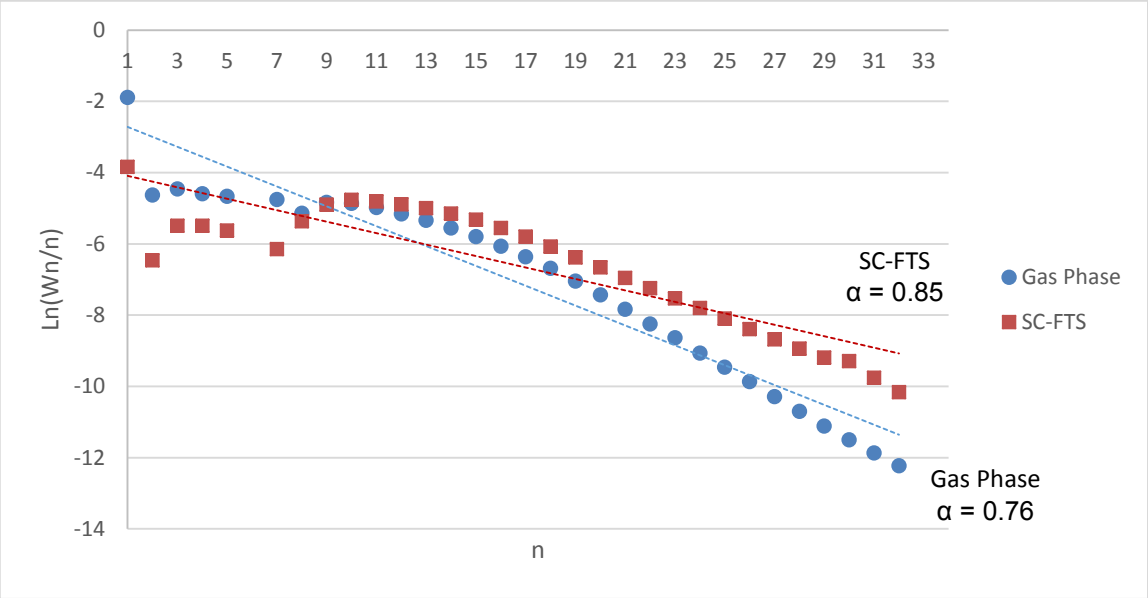

Figure 35. Anderson–Schulz–Flory (ASF) plots showing the reaction medium effect on the hydrocarbon product distribution and chain growth probability (α-value), over 15 wt% Co/Al_2O_3, under the following conditions: temperature 240 °C, pressure 65 bar for SC-FTS and 20 bar for gas phase FTS, and H_2:CO of 2:1 feed ratio.

The reason behind the increase in chain growth probability after introducing the SCF can be attributed to higher diffusivities and desorption rates of heavy hydrocarbons in the SCF. The liquid-like density and solubility of supercritical hexane enhance the extraction of heavy hydrocarbons from the catalysts pores, thus minimizing wax accumulation in these pores resulting in better diffusion rates of both reactant and products [2, 36, 43, 44, 46]. SCF are also capable of extracting olefins from the catalyst pores prior hydrogenation (termination of the chain growth). This increases the chance for olefins

readsorption and their incorporation in the chain growth process, thus yielding heavier FTS products [44, 54, 65].

Another observation from Figure 35 is the deviation from the straight-line ASF model. The ASF model overestimates the selectivity of light hydrocarbons (C_3-C_7) and heavy hydrocarbons (C_{27}-C_{32}) while the selectivity of hydrocarbons within the middle distillates range (C_{11}-C_{22}) were underestimated. Additionally, higher CH_4 yield was obtained experimentally than that predicted by the ASF model (especially for gas phase FTS). Typically, CH_4 yield is always higher than that predicted by the ASF model due to the parallel methanation reaction, it is noteworthy to mention here that the methanation reaction is usually treated separately from the FTS propagation reaction and therefore cannot be easily predicted by the ASF model. On the other hand, C_2 products were well below the ideal ASF line. The decrease in C_2 selectivity is probably because C_2 species are extremely active. They are considered as chain initiators where they compete with hydrogen molecules for reactants and strongly participate in the chain growth process [66]. As discussed before, the supercritical reaction media suppress methane formation and enhance the formation of olefins and long chain hydrocarbons. This could result in additional deviations from the ideal ASF. Such deviations were previously reported by several experimental FTS studies carried at supercritical conditions [17, 47, 54, 65].

Since olefins hold great value as a feedstock for lubricating oils, detergents and polymers [50], it is highly desirable to be able to control the selectivity towards olefins by reducing their secondary reactions. However, this cannot be achieved under conventional gas phase FTS where the catalyst pores are filled over time with the produced liquids and

heavy wax [2, 39, 50], which could result in a reduction of the desorption rate of olefins from the catalyst pores. Hence, this increases the probability of their participation in secondary reactions. It has been previously reported [2, 50] that conducting the FTS under supercritical conditions may enhance olefins selectivity due to the increased solubility of olefins in the SCF.

Figure 36 compares the olefin formation rate under two different reaction media (20 bar gas phase and 65 bar SC-hexane, with 20 bar syngas partial pressure). From Figure 36, it was noticed that shifting the reaction medium from the gas phase to supercritical hexane had a significant increase in the olefin formation rate resulting in 62 % increase in total olefin formation. Furthermore, up to C_{24} olefins were detected by the GC under supercritical conditions compared to C_{15} olefins in the gas phase FTS.

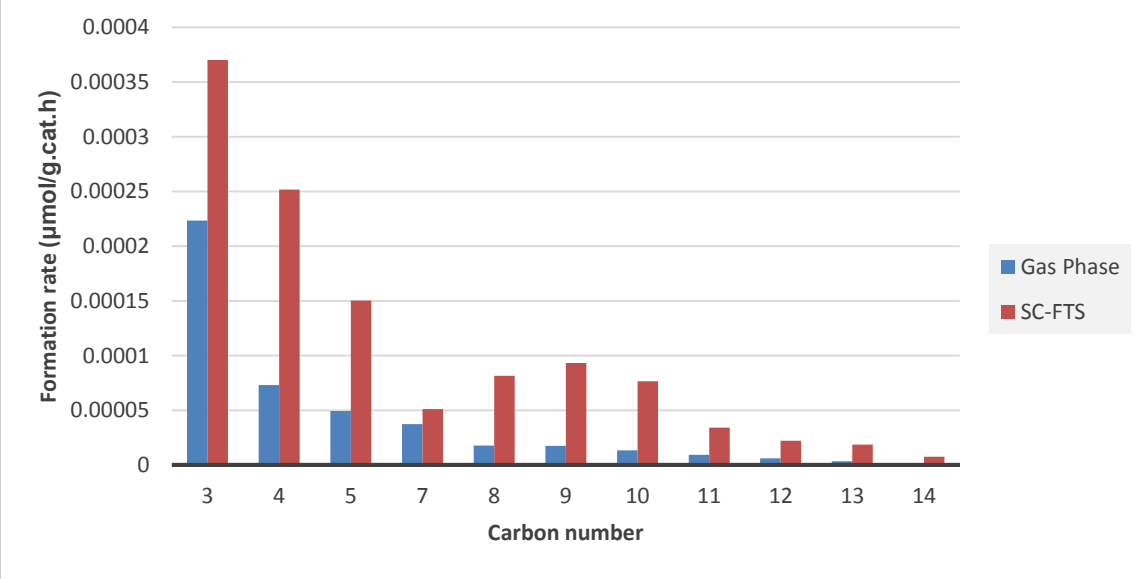

Figure 36. Reaction medium effect on olefin formation rate, over 15 wt% Co/Al_2O_3, under the following conditions: temperature 240 °C, pressure 65 bar for the SC-FTS and 20 bar for the gas phase FTS, and H_2:CO of 2:1 feed ratio.

Yokota, Fan and Fujimoto [48, 67] used three different FTS reaction media: n-hexadecane (liquid-phase), N_2 (gas phase) and n-hexane (supercritical phase). They operated the reactor at a bed temperature between 220 and 240 °C and maintained a total reactor pressure of 45 bar, with syngas H_2:CO ratio of 2:1 and syngas partial pressure of 10 bar. Eventually, they also concluded that higher olefin selectivities were achieved when supercritical hexane was used as a reaction media. Similar results were attained by Huang and Roberts [41] using Co/Al_2O_3 catalyst, as well Bukur and co-researchers [39, 50] used Fe catalyst and also reported an increase in olefin selectivity under supercritical propane FTS.

In the gas phase FTS where severe mass transfer limitations are present, olefins (especially heavy olefins) are not able to desorb out from the catalyst pores as soon as they are produced. As a result, they are subjected to hydrogenation reactions, resulting in lower olefin selectivity. On the other hand, using supercritical fluids as a reaction media for the FTS can alleviate these mass transfer limitations and thus enhance olefin selectivity. The improved selectivity towards olefins under supercritical conditions can be explained by the increased solubility of olefins in the supercritical medium. This increased solubility facilitates the desorption (reduce intra-particle diffusion limitations) of olefins and results in faster diffusion rates (extraction) from the pores, which decrease the residence time of olefins inside the catalyst pores, hence reducing the probability of their readsorption and participation in secondary (hydrogenation to paraffins) reactions [39, 44, 48-51].

IV.2.2 Fischer-Trospch Synthesis Parametric Studies

In this section, the reactor unit was utilized further to conduct a number of FTS studies to prove the functionality and abilities of the new reactor unit. In the current section, the effect of temperature, pressure and syngas molar feed ratio on the catalyst activity and methane formation rate will be studied under the gas phase FTS. Each experimental set was continued to reach steady state conditions, and after reaching steady state, the experiment was continued for another 15 hours before shifting to the next conditions. The steady state data were used in the following studies.

To begin with, the temperature effect on the catalyst activity and methane formation rate was studied. Figures 37 and 38 show the relationship between temperature and the consumption rate of carbon monoxide (catalyst activity) under the gas phase FTS while Figures 39 and 40 give the relationship between temperature and CH_4 formation. Four reaction temperatures 210, 220, 230 and 240 °C were applied, and it is clearly visible that temperature had a significant impact on both the catalyst activity and selectivity. As predicted, increasing the reactor bed temperature resulted in an increase in catalyst activity and at the same time an increase in CH_4 formation. Activity increased from around 2.6 to 4.0, 5.5 and 9.8 μmol/g.cat.s, while methane formation increased from 0.8 to 1.0, 1.6 and 1.8 μmol/g.cat.s when increasing the temperature from 210 to 220, 230 and 240 °C, respectively.

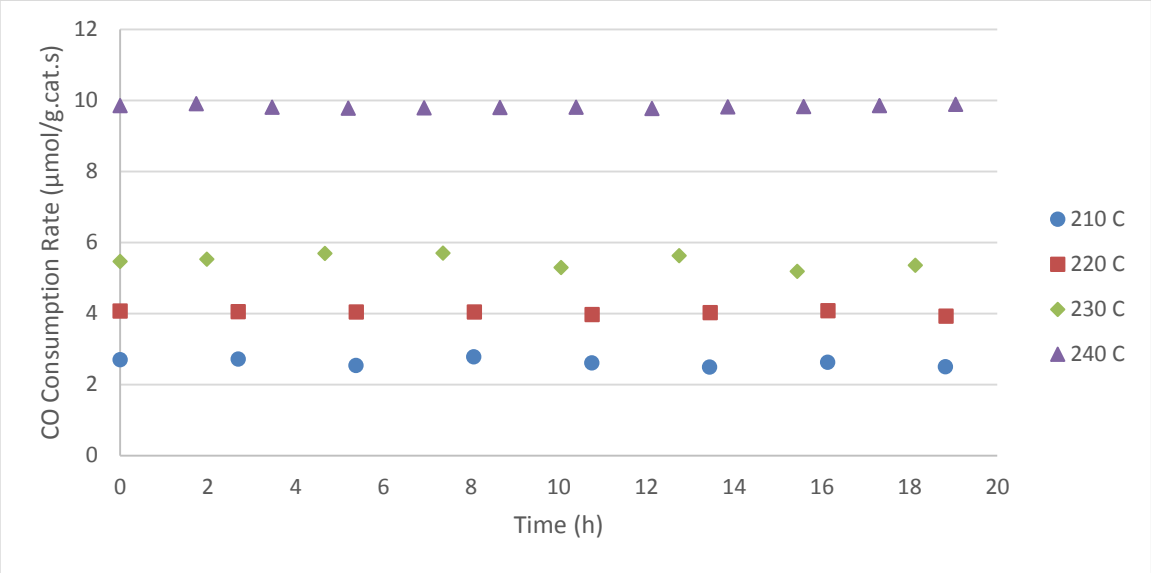

Figure 37. Steady-state variations in catalyst activity as a function of reaction temperature, over 15 wt% Co/Al_2O_3, under the following conditions: gas phase FTS, temperature 210, 220, 230 and 240 °C, pressure 20 bar, and H_2:CO of 2:1 feed ratio.

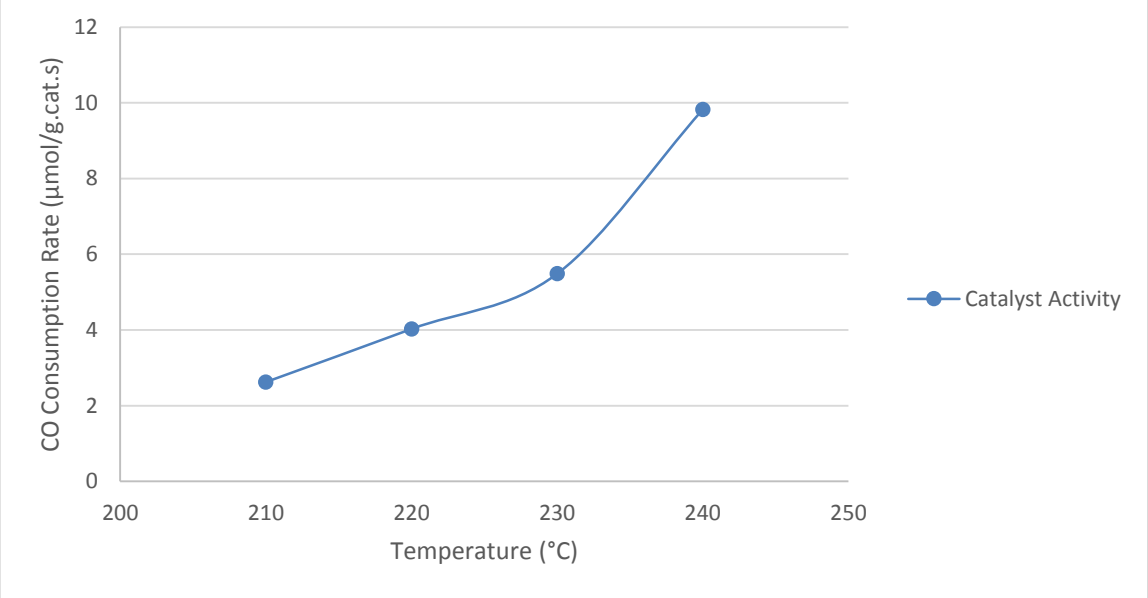

Figure 38. Reaction temperature effect on catalyst activity, over 15 wt% Co/Al_2O_3, under the following conditions: gas phase FTS, temperature 210, 220, 230 and 240 °C, pressure 20 bar, and H_2:CO of 2:1 feed ratio.

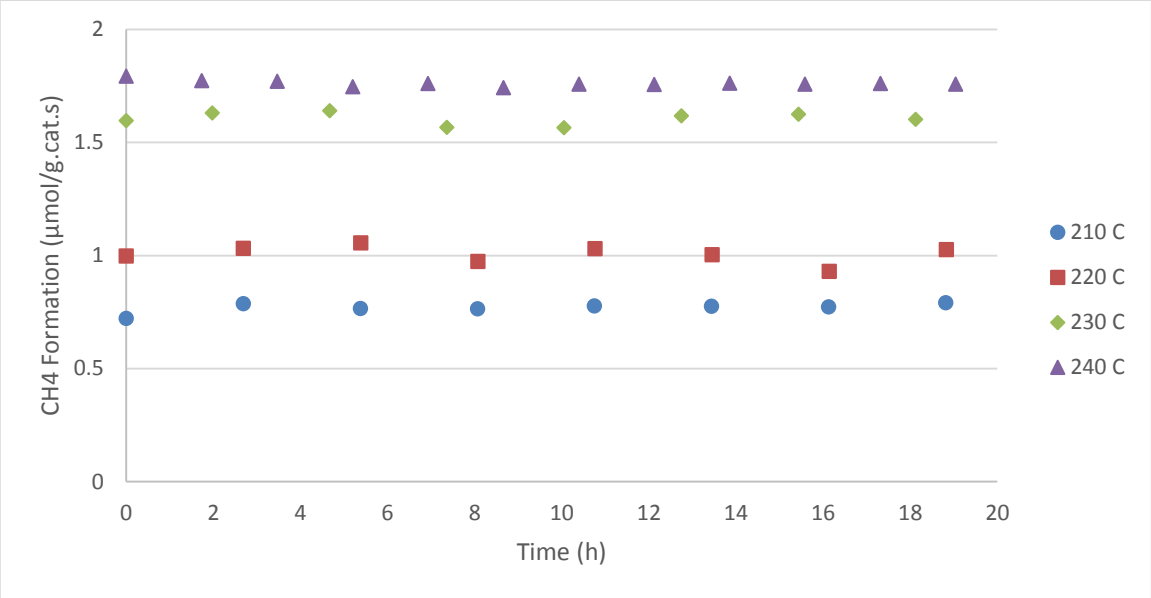

Figure 39: Steady-state variations in CH_4 formation as a function of reaction temperature, over 15 wt% Co/Al_2O_3, under the following conditions: gas phase FTS, temperature 210, 220, 230 and 240 °C, pressure 20 bar, and H_2:CO of 2:1 feed ratio.

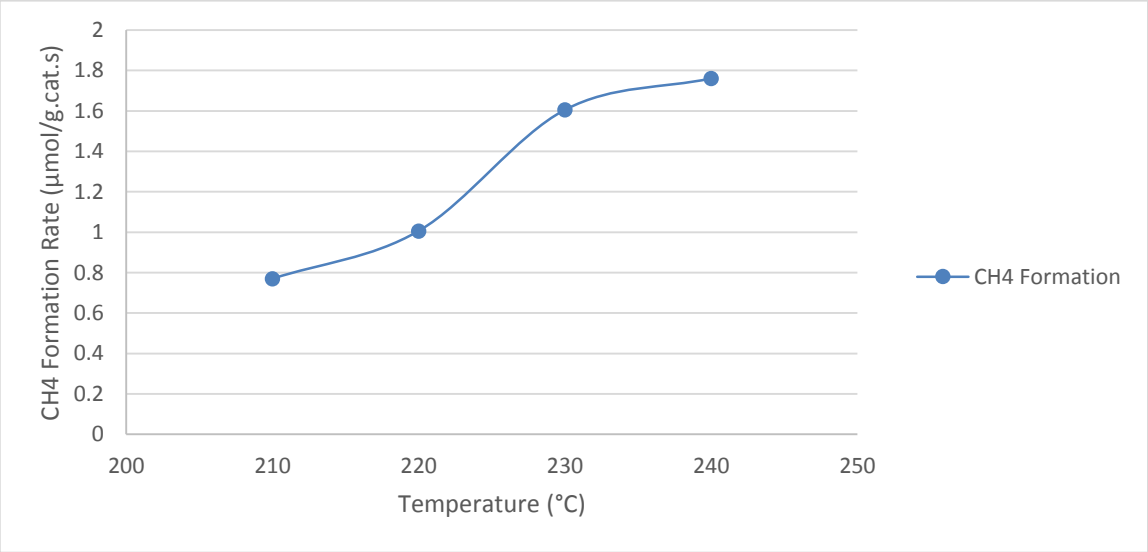

Figure 40. Reaction temperature effect on CH_4 formation rate, over 15 wt% Co/Al_2O_3, under the following conditions: gas phase FTS, temperature 210, 220, 230 and 240 °C, pressure 20 bar, and H_2:CO of 2:1 feed ratio.

Higher reaction temperatures would result in faster reaction rates, thus higher productivity. However, operating the FTS at higher temperature favors methane formation and results in lower chain growth probabilities and lower selectivities toward the desired product range (middle distillates). Hence, a fine tune between the desired high activity and undesirable methanation reaction is necessary, and that is why gas phase FTS is regularly operated in the low temperature range (180 – 220) °C for the cobalt-based catalysts. In addition, as seen in Figure 38 and 40, it should be noted that the changes in activity and CH_4 formation with reaction temperature were non-linear and perhaps followed more closely an exponential behavior. For instance, increasing the reactor temperature by 10 °C from (220 to 230) °C, resulted in a 27 % increase in CO activity, while the activity increased as high as 44 % when temperature was again raise by 10 °C from (230 to 240) °C.

Next, the pressure effect on catalyst activity and methane formation is discussed. In these experimental sets, nitrogen was used as a balance gas to pressurize the system up to 50 and 80 bar while keeping syngas partial pressure constant at 20 bar. Figures 41 and 42 present the relationship between the reaction pressure and the catalyst activity. From these figures, it was noticed that increasing the reaction pressure had a negative effect on the catalyst activity. The activity decreased from 12 to 11 and 9.5 μmol/g.cat.s when pressure was increased from 20 to 50 and 80 bar, respectively. At gas phase FTS operation, increasing the total reactor pressure beyond the optimum pressure would result in the condensation of liquid and even solid hydrocarbons that are normally gases at lower

pressures. This will lead to the saturation of the catalyst pores with the formed hydrocarbons, thus increasing mass transfer (pore diffusion) limitations [9].

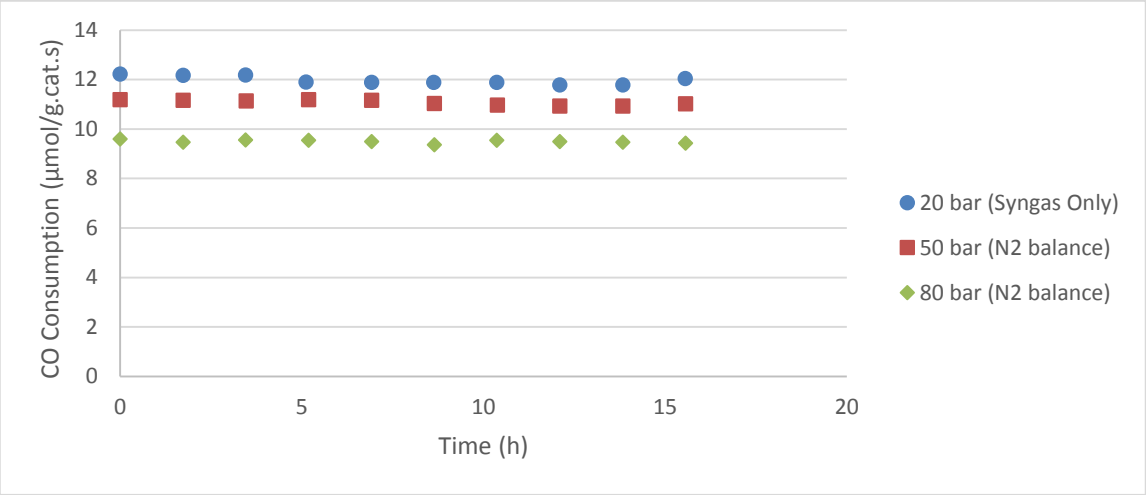

Figure 41. Steady-state variations in catalyst activity as a function of reaction pressure, over 15 wt% Co/Al_2O_3, under the following conditions: gas phase FTS, temperature 240 °C, pressure 20, 50 and 80 bar, and H_2:CO of 2:1 feed ratio.

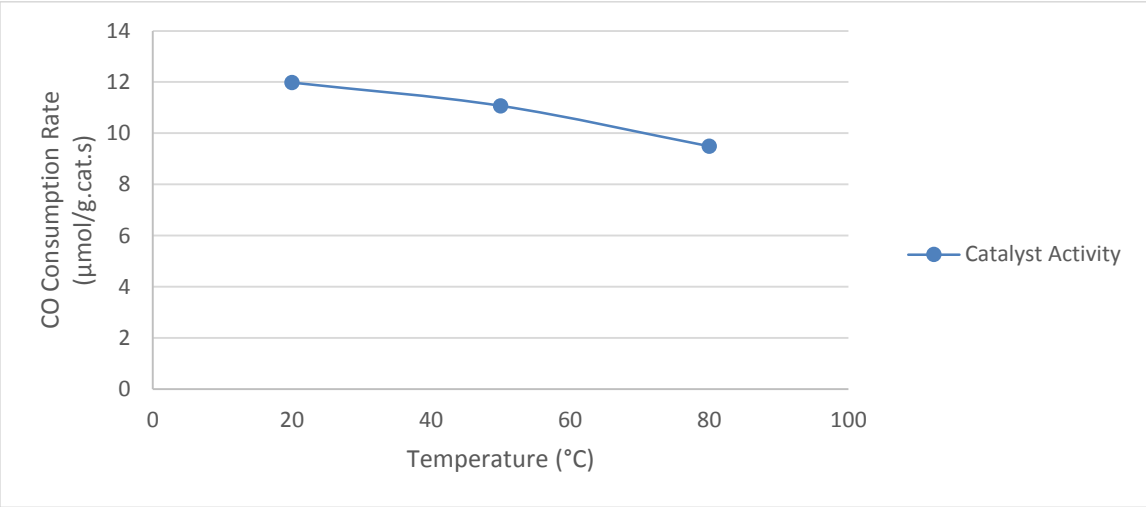

Figure 42. Reaction pressure effect on catalyst activity, over 15 wt% Co/Al_2O_3, under the following conditions: gas phase FTS, temperature 240 °C, pressure 20, 50 and 80 bar, and H_2:CO of 2:1 feed ratio.

On the other hand, methane formation was reduced when the total reaction pressure was increased from (20 to 80) bar, as seen in Figure 43. This is possibly caused by the dilution of reactants (reduced molar concentration of CO and H_2 in the feed gas) as the nitrogen partial pressure is increased. This dilution will reduce the residence time and slow down the methanation reaction rate, thus lower the reaction exotherm. Consequently, coke formation and hot spots formation are expected to be reduced as well. Overall, this would hinder methane formation and lead to lower activity.

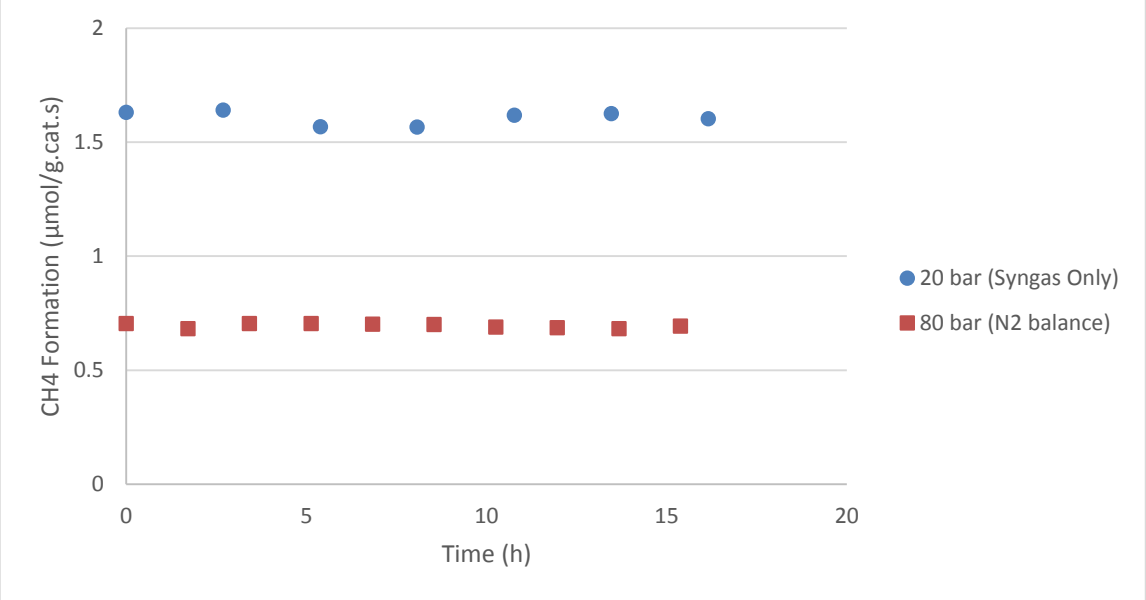

Figure 43. Steady-state variations in CH_4 formation rate as a function of reaction pressure, over 15 wt% Co/Al_2O_3, under the following conditions: gas phase FTS, temperature 230 °C, pressure 20 and 80 bar, and H_2:CO of 2:1 feed ratio.

At the end of this section, the effect of syngas feed molar ratio on the catalyst activity and CH_4 formation was studied. As shown in Figure 44, a considerable decrease was observed in the steady state catalyst activity as the hydrogen to carbon monoxide

molar ratio in the feed syngas was reduced from 2.0 to 0.6. Additionally as it can be observed from Figure 45, higher H_2 partial pressures favor methane formation while lower H_2 to CO ratio favors the production of heavy hydrocarbons. This is because higher H_2 partial pressure would stimulate the termination reactions of the carbon-hydrogen monomer to produce either methane or paraffins, which are irreversible reactions and have an adverse impact on the product selectivity and the chain growth process [47].

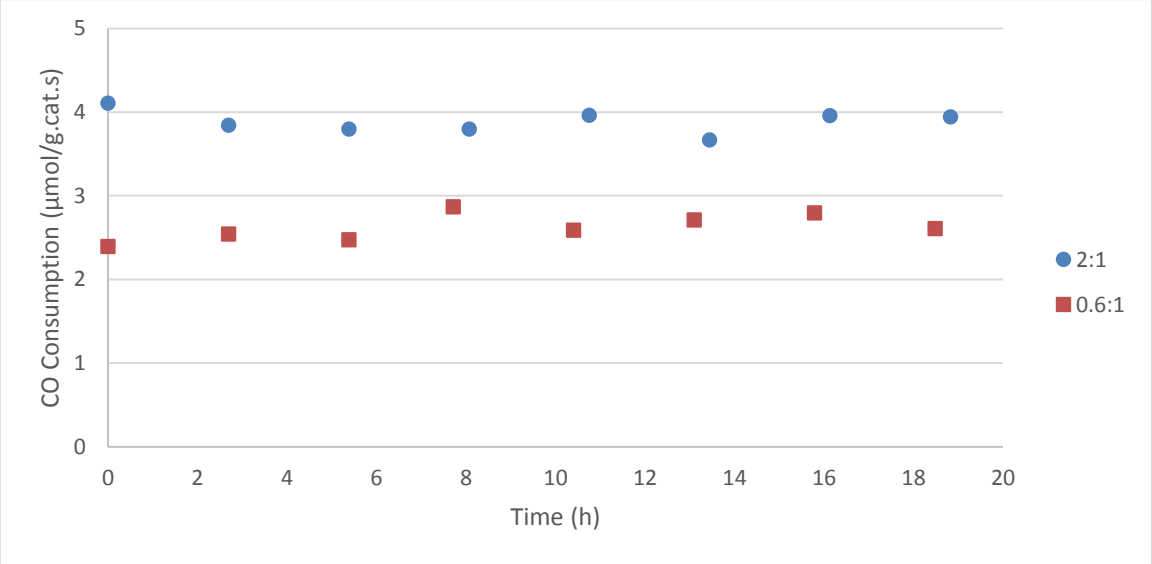

Figure 44. Steady-state variations in catalyst activity as a function of syngas molar feed ratio, over 15 wt% Co/Al_2O_3, under the following conditions: gas phase FTS, temperature 240 °C, pressure 20 bar, and H_2:CO of 2:1 and 0.6:1 feed ratio.

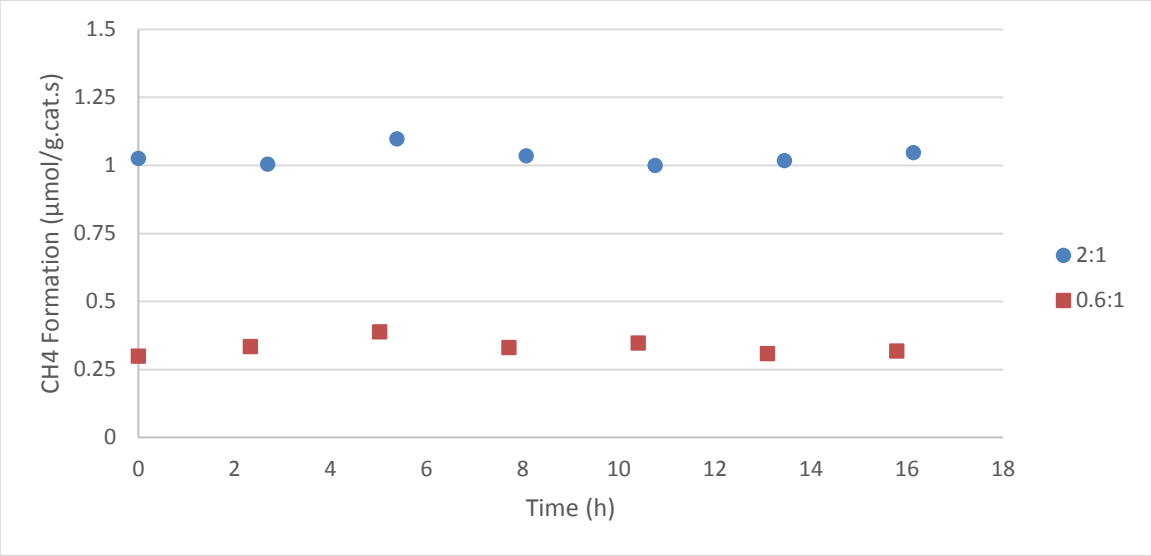

Figure 45. Steady-state variations in CH_4 formation rate as a function of syngas molar feed ratio, over 15 wt% Co/ Al_2O_3, under the following conditions: gas phase FTS, temperature 240 °C, pressure 20 bar, and H_2:CO of 2:1 and 0.6:1 feed ratio.

IV.2.3 Alcohol Analysis in the FTS Product

Through the experimental campaign, a cobalt-based catalyst (15 wt% Co/Al_2O_3) was used to conduct the FTS reactions. During the off-line FTS product peak identification using the Agilent (GC/FID/MS) system, considerable amounts of several alcohols were identified in the organic FTS product samples. This is uncommon for cobalt-based low-temperature FTS; thus, further investigation was required.

A typical liquid sample of the gas phase FTS (240 °C, 20 bar, 65 nmL/min syngas flow with 2:1 H_2:CO molar feed ratio) was collected from the bottom of the cold trap. Then the organic phase from that sample was injected into the Agilent GC/MS for analysis. The alcohols identified within the sample's organic phase are given in Table 6.

Table 6. Peak list for the alcohols identified in the gas phase FTS (240 °C, 20 bar, 65 nmL/min syngas flow with H_2:CO of 2:1 molar feed ratio) organic phase liquid sample, injected into Agilent GC/MS/FID system.

Alcohol	Retention time (min)	Response
1-Propanol	2.457	276259
1-Butanol	3.203	467519
1-Hexanol	9.666	4132448
1-Heptanol	16.473	25329552
1-Octanol	22.644	36927076
1-Nonanol	28.049	41910385
1-Decanol	32.923	33100899
1-Undecanol	37.417	32615101
1-Dodecanol	41.619	31647273
1-Tridecanol	45.578	29650492
1-Tetradecanol	49.331	27495369
1-Pentadecanol	52.892	22176038
1-Hexadecanol	56.279	13716154

To further investigate these results, the aqueous phase from the same sample was injected into the Agilent GC/MS, where the resulting MS spectrum is shown in Figure 46, labelled with the identities of the peaks, as determined by the MS [68]. The MS analysis of the aqueous phase clearly shows that C_1-C_6 alcohols were present in the FTS product.

As a double check and to confirm the MS results, a reference sample was prepared by mixing a small amount (~5 μL) of a mixture of C_1-C_6 alcohols diluted with 1.5 mL of n-hexane (Sigma Aldrich, >=95% purity, with the rest composed of small amounts of C_6 *iso* and *cyclic* hydrocarbons). The reference sample was then injected into the GC/MS, and the obtained MS spectrum is shown in Figure 47. By comparing Figure 46 and 47, it can be concluded that the reference sample confirms that the Agilent GC/MS correctly identified the alcohol peaks. Nevertheless, this finding requires further detailed investigation since such amounts of alcohol products are not typical for cobalt-based

catalyst low-temperature FTS; however such oxygenates are common for iron-based catalysts.

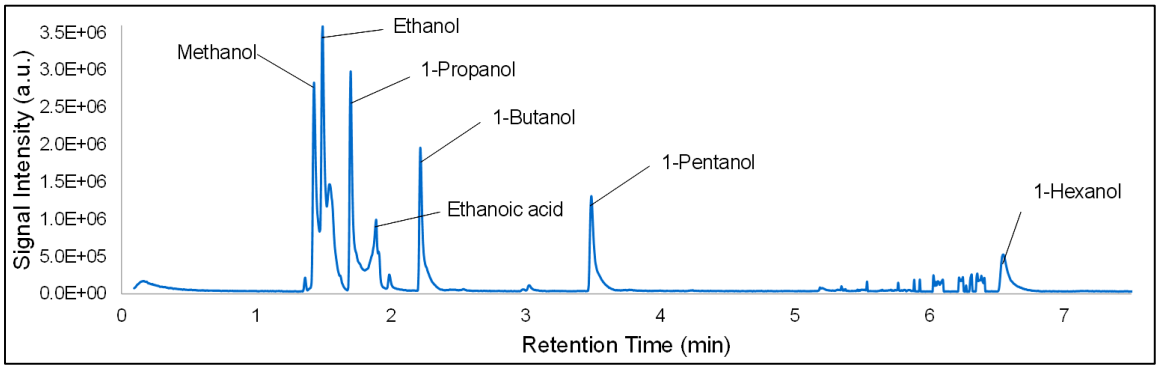

Figure 46. GC/MS spectrum for the aqueous FTS (240 °C, 20 bar, 65 nmL/min syngas flow with 2:1 H2:CO molar feed ratio) sample, with compound identities labeled.

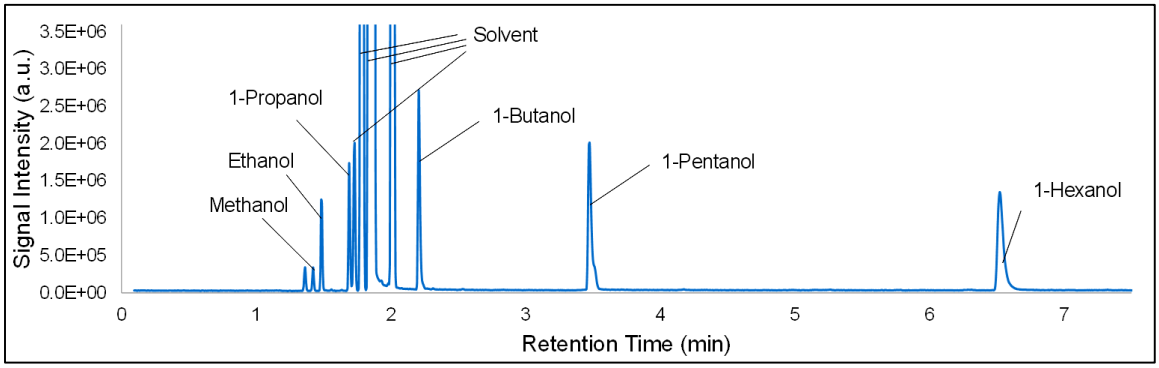

Figure 47. GC/MS spectrum of the prepared reference sample, consisting of C_1-C_6 alcohols dissolved in n-hexane, with compound identities labelled.

V. CONCLUSION, RECOMMENDATIONS AND FUTURE WORK

V.1 Conclusion

After more than 20 years of research focused on the implementation of supercritical fluids as a reaction media for the FTS, the development of this novel technology has not moved beyond the lab-scale reactor. Many obstacles face scaling-up this technology because of the non-ideality of the reaction mixture that requires both micro and macro scale investigations for the reaction kinetics, phase behavior, physiochemical properties under supercritical conditions, energy and mass integration as well as reactor and process configuration.

In this project, a high pressure, state-of-the-art, bench-scale reactor unit was commissioned. The unit is capable of running the FTS reaction in the conventional gas phase and the novel supercritical phase. Such scaled-up design would provide the means necessary to study and gain better understanding of the FTS reaction when carried under supercritical conditions, optimize the reaction behavior for typical large-scale FTS processes and verify the possibility of building a pilot-scale reactor for this process. The unit can also aid in developing more predictive reactor models, as well as investigate and validate the proposed enhancements by applying SCF as a FTS reaction media. This thesis described the methods followed in designing, commissioning and operating the bench-scale reactor unit, the process followed to prepare the cobalt-based (15 wt% Co/Al_2O_3) utilized to conduct the FTS reactions, the technique applied in identifying the FTS products using the on-line and off-line GC analysis systems, and finally the methods used to analyze the collected reaction data.

The results obtained in this project showed that the introduction of SCF in the FTS carried the following benefits:

- Firstly, a 14 % increase in CO conversion was achieved when changing the reaction medium from gas phase (240 °C reaction temperature, 20 bar syngas partial pressure with 2:1 H_2:CO feed ratio) to SCF (240 °C reaction temperature, 65 bar total reactor pressure, 20 bar syngas partial pressure with H_2:CO of 2:1 feed ratio). This was attributed to the increased reactants accessibility to the active sites after the *in-situ* wax extraction by the SCF.
- Secondly, methane and light hydrocarbons selectivities were significantly reduced. Under the aforementioned reaction conditions, the selectivity towards light hydrocarbons was reduced by 78 wt%, while methane selectivity was reduced from 15 wt% under the gas phase FTS to 2.2 wt% under the supercritical conditions. The reduction in methane and light end fuel cuts was attributed to the liquid-like heat capacity of the SCF. The enhanced heat capacity improves the reaction heat removal, minimizes hot spots formation, and reduces the rate of cracking reactions, which in turn suppress the formation of methane and light hydrocarbons [36, 41, 43].
- Thirdly, a shift towards the production of heavier hydrocarbons was observed when shifting the reaction medium from the gas phase to near and supercritical phase. For instance, middle distillates (C_{11}-C_{22}) selectivity increased from (67 to 44) wt% while light wax (C_{23}-C_{32}) selectivity was increased by 76 %. In addition, the chain growth probability (α-value) increased under supercritical operation by

10.6 %. The observed enhancements in the chain growth and the selectivity towards heavy hydrocarbons were explained by the ability of the SCF to extract the wax formed inside the catalyst pores, thus freeing more actives sites for primary products to incorporate in the chain growth process [2, 36, 41, 43, 44, 46, 63]. Moreover, SCF are capable of extracting olefins prior to undergoing hydrogenation reactions, which increase the chance of their readsorption and incorporation in the chain growth, thus yielding heavier FTS products [44, 54, 65].

- Fourthly, conducting the FTS under SC reaction medium resulted in an increase in the formation rate of olefins. This was attributed to the increased solubility of olefins in the supercritical medium, which facilitates olefins desorption from the catalyst pores before excess hydrogenation [39, 44, 48-51].

V.2 Recommendations and Future Work

From the obtained experimental results and the previous discussion, it can be concluded that the SC-FTS technology has the potential to be considered as an alternative to the conventional gas phase FTS, with improved selectivity towards the desired products (less light hydrocarbons, more heavy hydrocarbons and olefins). Nevertheless, further studies must be carried out in the future to:

- Gain better understanding of the reaction mechanisms and properties associated with operating under non-conventional supercritical conditions. Additionally, the temperature and pressure effects on the SC-FTS kinetics needs to be evaluated, and thus additional experimental sets/data has to be generated at smaller intervals.

- Confirm the alcohol analysis obtained in this project. As previously discussed in section IV.2.3, considerable amounts of several alcohols were identified in the organic FTS product samples. This is uncommon for cobalt-based low-temperature FTS, and thus an investigation was performed to confirm these results using reference samples. Even though the investigation confirmed the presence of alcohols, however this requires further analysis using different GC setups and analysis techniques.
- Characterize and compare between catalysts used for conventional gas phase FTS and catalysts used for SC-FTS. This would validate the *in-situ* wax extraction capabilities of supercritical fluids and justify the extended catalyst life under SC-FTS as observed in a number of studies [2, 36, 39, 54].
- Obtain meaningful kinetic and reactor models that take into account the effect of running the FTS reaction at supercritical conditions and the associated thermodynamic non-ideality of the supercritical reaction mixture. The models need to predict the influence of temperature, pressure, syngas partial pressures, syngas flow rate and syngas to supercritical solvent ratio on conversion, selectivity and hydrocarbon product distribution. The developed models shall be used to give insight into the FTS reaction mechanism under supercritical phase, optimize the SC-FTS process, and give confidence for potential scale-up and commercialization of the SC-FTS technology.
- Investigate the applicability of a solvent recovery system and the use of mixed solvents. A solvent recovery system needs to be designed, connected to the reactor

unit, tested and then tuned for optimum performance. Furthermore, a single hydrocarbon solvent (n-hexane) was used in this project; however, under typical commercial conditions this might not be technically nor economically viable. Elfatih et al. [45] have previously examined a list of potential FTS solvents, and a number of mixed solvents such as naphtha were found to be thermo-physically and techno-economically feasible for the SC-FTS. These mixed solvents need to be experimentally tested to know whether they can actually be applied as supercritical solvents for the FTS.

- Judge the techno-economic viability of the SC-FTS technology. The several advantages resulting from shifting the reaction medium from conventional gas phase to near and supercritical phase needs to be evaluated against the increased capital and operational costs associated with the need for higher operating temperatures and pressures, and a solvent recovery system.
- Investigate the potential process safety hazards that can be brought to the FTS process by the use of supercritical fluids. A commercial SC-FTS plant would require large (flammable) solvent storage tanks and the FTS reactor would be operated at higher temperatures and pressures to achieve supercritical conditions. These alterations increase the risk associated with the FTS process. Hence, comprehensive safety studies must be conducted before scaling-up the SC-FTS technology.

During the commissioning and operation stage of the high-pressure bench-scale reactor unit, a number of problems were faced. Hence, a list of technical, operational and safety improvements/recommendations was compiled:

- Firstly, a Programmable Logic Controller (PLC) code for automated reactor startup and shutdown is suggested to be written. This would take full advantage of the automation system, ensure safe startup and shut down operations, and minimize operational errors.
- Secondly, a backup gas cylinder for each gas and an on-line solvent filling/makeup system needs to be provided. In addition, a pressure transducer with low-pressure alarm can be placed on each gas line to indicate when a gas cylinder is getting low in pressure. This would prevent operational interruptions and minimize instability in the measured analyzer (GC) data, which are caused by running out of feed gases, solvent and helium carrier gas.
- Thirdly, repeated failure in the air generator caused serious problems, as pneumatic air failure would lead to total failure and shutdown the entire system. Thus, an emergency switch mechanism that can automatically switch the instrument air supply source from the air generator to TAMUQ utilities in case of air generator failure needs to be installed. This will enhance process reliability and reduce downtime caused by air generator failure.
- Fourthly, adequate cold insulation for the cold trap needs to be provided. This will improve energy efficiency and prevent pipe sweating (condensation of water on the surface) that may lead to corrosion with prolonged operation and damage

sensitive equipment near the cold trap. Condensed water may form spills on the unit floor generating slip hazard. In addition, the condensed water may lead to algae and bacterial formation causing health hazards.

- Fifthly, the system needs to be provided with additional sampling points (each feed stream before the MFC, at the reactor inlet, at the top of the liquid collection tank to analyze the permanent gases).
- Sixthly and more importantly, safety wise, the reactor unit was classified as a high hazard unit since it handles toxic and flammable gases (carbon monoxide, hydrogen, methane) at high temperatures and pressures. Thus, the reactor unit will be moved from its current location at the Fuel Characterization Lab to the High Hazard Lab at Texas A&M University at Qatar. Other than that, the lab should be provided with additional personal protective equipment (PPEs) including rubber and leather gloves that are used when handling electrical lines and devices, and mechanical equipment. Since the reactor unit runs at high electrical power, the reactor unit and all its components must be earthed. In addition, anti-static lab coats or coveralls and dissipative safety shoes are preferred to be used when working on the reactor unit. The lab coats or coveralls need also to be flame resistant since the unit handles highly flammable gases. Other than this, noise from the nitrogen and air generators as well as the gas booster can cause hearing damage and headache with prolonged exposure. Thus, it is recommended to supply earplugs or earmuffs for those working in the lab.

In the end, this work is an initial step in the effort to develop a novel FTS technology that has the potential for commercialization upon proof of concept. Thus, research efforts must carry on and substantial funding needs to be provided. This is where collaboration with major industrial corporations in the field become of crucial importance, and that is why conducting this project and related future projects in the State of Qatar "The World Capital of GTL" is highly advantageous. In all, the research team is confident that the successful completion of the ongoing experimental and modeling research studies will lay the foundation for an advanced and economical FTS process and give a reasonable level of confidence for commercializing this technology.

REFERENCES

[1] N.O. Elbashir, F.T. Eljack, A Method to Design an Advanced Gas-to-Liquid Technology Reactor for Fischer-Tropsch Synthesis, in: F. Benyahia, F.T. Eljack (Eds.) 2nd Annual Gas Processing Symposium, Elsevier, Doha, Qatar, 2010, pp. 369-377.

[2] N.O. Elbashir, D.B. Bukur, E. Durham, C.B. Roberts, Advancement of Fischer-Tropsch Synthesis via Utilization of Supercritical Fluid Reaction Media, AIChE Journal, 56 (2009) 997-1015.

[3] N.O. Elbashir, Prospect of Success in Scaling-up Fischer-Tropsch Synthesis Reactor Operates in Near-Critical and Supercritical Phase Media, in, Texas A&M University at Qatar, Doha, 2012.

[4] B. Bao, M.M. El-Halwagi, N.O. Elbashir, Techno-Economic Analysis of Gas-to-Liquid Process, in: F. Benyahia, F.T. Eljack (Eds.) 2nd Annual Gas Processing Symposium, Elsevier, Doha, Qatar, 2010, pp. 287-297.

[5] M.E. Dry, Fischer-Tropsch Reactions and the Environment, Applied Catalysis A: General, 189 (1999) 185-190.

[6] M.E. Dry, The Fischer-Tropsch Process: 1950–2000, Catalysis Today, 71 (2002) 227-241.

[7] Y.N. Wang, Y.Y. Xu, Y.W. Li, Y.L. Zhao, B.J. Zhang, Heterogeneous Modeling for Fixed-Bed Fischer-Tropsch Synthesis: Reactor Model and its Applications, Chemical Engineering Science, 58 (2003) 867-875.

[8] A. Steynberg, M. Dry, Fischer-Tropsch Technology: Studies in Surface Science and Catalysis, Elsevier, New York, 2004.

[9] A.Y. Khodakov, W. Chu, P. Fongarland, Advances in the Development of Novel Cobalt Fischer-Tropsch Catalysts for Synthesis of Long-Chain Hydrocarbons and Clean Fuels, Chemical Reviews, 107 (2007) 1692-1744.

[10] D. Leckel, Diesel Production from Fischer-Tropsch: The Past, the Present, and New Concepts, Energy & Fuels, 23 (2009) 2342-2358.

[11] P. Schubert, S. LeViness, K. Arcuri, A. Stranges, Development of the Modern Fischer-Tropsch Process (1958-1999), in, Syntroleum, 2001.

[12] M.A. Marvast, M. Sohrabi, S. Zarrinpashne, G. Baghmisheh, Fischer-Tropsch Synthesis: Modeling and Performance Study for Fe-HZSM5 Bifunctional Catalyst, Chemical Engineering Technology, 28 (2005) 78-86.

[13] J. Sheehan, V. Camobreco, J. Duffield, M. Graboski, H. Shapouri, Life Cycle Inventory of Biodiesel and Petroleum Diesel for Use in an Urban Bus, in, U.S. Department of Energy, U.S. Department of Agriculture, Colorado, 1998.

[14] R.G. Hay, D.G. Demianiw, G R Lappin, L.H. Nemec, J.D. Sauer, J.D. Wagner, Olefins Higher, in: Kirk-Othmer (Ed.) Kirk-Othmer Encyclopedia of Chemical Technology, John Wiley & Sons, 2007, pp. 1028-1046.

[15] B. Bao, M.M. El-Halwagi, N.O. Elbashir, Simulation, Integration, and Economic Analysis of Gas-to-Liquid Processes, Fuel Processing Technology, 91 (2010) 703-713.

[16] F. Fischer, H. Tropsch, The Synthesis of Petroleum at Atmospheric Pressures from Gasification Products of Coal, Brennstoff-Chemie, 7 (1926) 97-104.

[17] R. Hussain, J.H. Blank, B. Todic, N.O. Elbashir, D.B. Bukur, Development of Gas-to-Liquid Technologies from Micro- to Macro-scale, in: Excellence and Impact of Research, Texas A&M University at Qatar, Doha Qatar, 2014.

[18] A. Moutsoglou, P.P. Sunkara, Fischer-Tropsch Synthesis in a Fixed Bed Reactor, Energy & Fuels, 25 (2011) 2242-2257.

[19] A.A. Adesina, Hydrocarbon Synthesis via Fischer-Tropsch Reaction: Travails and Triumphs, Applied Catalysis A: General, 138 (1996) 345-367.

[20] A. Jess, C. Kern, Modeling of Multi-Tubular Reactors for Fischer-Tropsch Synthesis, Chemical Engineering Technology, 32 (2009) 1164-1175.

[21] J.W. Pratt, A Fischer-Tropsch Synthesis Reactor Model Framework for Liquid Biofuels Production, in, Sandia National Laboratories: Energy Systems Engineering & Analysis Department, California, 2012.

[22] R.J. Madon, E. Iglesia, S.C. Reyes, Non-Flory Product Distributions in Fischer-Tropsch Synthesis Catalyzed by Ruthenium, Cobalt, and Iron, in: Selectivity in Catalysis, American Chemical Society, Washington DC, 1993, pp. 383-396.

[23] H. Schulz, M. Claeys, Kinetic Modelling of Fischer-Tropsch Product Distributions, Applied Catalysis A: General, 186 (1999) 91-107.

[24] M.R. Rahimpour, M.H. Khademi, A.M. Bahmanpour, A Comparison of Conventional and Optimized Thermally Coupled Reactors for Fischer-Tropsch Synthesis in GTL Technology, Chemical Engineering Science, 65 (2010) 6206-6214.

[25] A.R. Mirolaei, F. Shahraki, H. Atashi, R. Karimzadeh, Comparison of CFD Results and Experimental Data in Fixed Bed Fischer-Tropsch Synthesis Reactor, Industrial and Engineering Chemistry, 18 (2012) 1912-1920.

[26] N.O. Elbashir, B. Bao, M.M. El-Halwagi, An Approach to the Design of Advanced Fischer-Tropsch Reactor for Operation in Near-Critical and Supercritical Phase Media, in: H. Alfadala, G.V.R. Reklaitis, M.M. El-Halwagi (Eds.) 1st Annual Gas Processing Symposium, Elsevier, Doha, Qatar, 2009.

[27] B. Jager, Development of Fischer Tropsch Reactors, in: AIChE Spring meeting, Sasol Technology Netherlands BV, New Orleans, 2003.

[28] T.S. Lee, J.N. Chung, Mathematical Modeling and Numerical Simulation of a Fischer-Tropsch Packed Bed Reactor and its Thermal Management for Liquid Hydrocarbon Fuel Production using Biomass Syngas, Energy & Fuels, 26 (2012) 1363-1379.

[29] E.E. Elmalik, E. Torab, M. El-Halwagi, N.O. Elbashir, A Method for Solvent Selection for Supercritical Fischer-Tropsch Synthesis Process, American Chemical Society Division of Fuel Chemistry, 55 (2010).

[30] N. Hooshyar, D. Vervloet, F. Kapteijn, P.J. Hamersma, R.F. Mudde, J.R.v. Ommen, Intensifying the Fischer-Tropsch Synthesis by Reactor Structuring - A Model Study, Chemical Engineering Journal, 207-208 (2012) 865-870.

[31] C. Maretto, R. Krishna, Design and Optimisation of A Multi-Stage Bubble Column Slurry Reactor for Fischer-Tropsch Synthesis, Catalysis Today, 66 (2001) 241-248.

[32] D. Stern, A.T. Bell, H. Heinemann, Effects of Mass Transfer on the Performance of Slurry Reactors used for Fischer-Tropsch Synthesis, Chemical Engineering Science, 38 (1983) 597-605.

[33] C.H. Bartholomew, R.J. Farrauto, Fundamentals of Industrial Catalytic Processes, 2nd ed., Wiley, Hoboken, New Jersey, 2006.

[34] B. Jager, R. Espinoza, Advances in Low Temperature Fischer-Tropsch Synthesis, Catalysis Today, 23 (1995) 17-28.

[35] D.B. Bukur, C. Sivaraj, Supported Iron Catalysts for Slurry Phase Fischer-Tropsch Synthesis, Applied Catalysis A: General, 231 (2002) 201-214.

[36] G. Jacobs, K. Chaudhari, D. Sparks, Y. Zhang, B. Shi, R. Spicer, T.K. Das, J. Li, B.H. Davis, Fischer-Tropsch Synthesis: Supercritical Conversion using a Co/Al_2O_3 Catalyst in a Fixed Bed Reactor, Fuel, 82 (2003) 1251-1260.

[37] J.J.C. Geerlings, J.H. Wilson, G.J. Kramer, H.P.C.E. Kuipers, A. Hoek, H.M. Huisman, Fischer-Tropsch Technology - From Active Site to Commercial Process, Applied Catalysis A: General, 186 (1999) 27-40.

[38] H.A. Jakobsen, Fixed Bed Reactors, in: Lecture Notes in Subject TKP4145 Reactor Technology, Norwegian University of Science and Technology NTNU, Trondheim, 2011.

[39] X. Lang, A. Akgerman, D.B. Bukur, Steady State Fischer-Tropsch Synthesis in Supercritical Propane, Industrial & Engineering Chemical Research, 34 (1995) 72-77.

[40] M.E. Dry, Practical and Theoretical Aspects of the Catalytic Fischer-Tropsch Process, Applied Catalysis A: General, 138 (1996) 319-344.

[41] X. Huang, C.B. Roberts, Selective Fischer-Tropsch Synthesis over an Al_2O_3 Supported Cobalt Catalyst in Supercritical Hexane, Fuel Processing Technology, 83 (2003) 81-99.

[42] R.M. de-Deugd, F. Kapteijn, J.A. Moulijn, Trends in Fischer-Tropsch Reactor Technology - Opportunities for Structured Reactors, Topics in Catalysis, 26 (2003) 29-39.

[43] K. Yokota, Y. Hanakata, K. Fujimoto, Supercritical Phase Fischer-Tropsch Synthesis, Chemical Engineering Science, 45 (1990) 2743-2750.

[44] D.J. Bochniak, B. Subramaniam, Fischer-Tropsch Synthesis in Near-Critical n-Hexane: Pressure Tuning Effects, AIChE, 44 (1998) 1889-1896.

[45] E.E. Elmalik, E. Tora, M. El-Halwagi, N.O. Elbashir, Solvent Selection for Commercial Supercritical Fischer-Tropsch Synthesis Process, Fuel Processing Technology, 92 (2011) 1525-1530.

[46] B. Subramaniam, Enhancing the Stability of Porous Catalysts with Supercritical Reaction Media, Applied Catalysis A: General, 212 (2001) 199-213.

[47] N.O. Elbashir, C.B. Roberts, Enhanced Incorporation of α-Olefins in the Fischer-Tropsch Synthesis Chain-Growth Process over an Alumina-Supported Cobalt Catalyst in Near-Critical and Supercritical Hexane Media, Industrial & Engineering Chemistry Research, 44 (2005) 505-521.

[48] K. Yokota, K. Fujimoto, Supercritical-Phase Fischer-Tropsch Synthesis Reaction. 2. The Effective Diffusion of Reactant and Products in the Supercritical-Phase Reaction, Industrial & Engineering Chemistry Research, 30 (1991) 95-100.

[49] L. Fan, K. Yokota, K. Fujimoto, Supercritical Phase Fischer-Tropsch Synthesis: Catalyst Pore-Size Effect, AIChE, 38 (1992) 1639-1648.

[50] D.B. Bukur, X. Lang, A. Akgerman, Z. Feng, Effect of Process Conditions on Olefin Selectivity during Conventional and Supercritical Fischer-Tropsch Synthesis, Industrial & Engineering Chemical Research, 36 (1997) 2580-2587.

[51] L. Fan, K. Fujimoto, Fischer-Tropsch Synthesis in Supercritical Fluid: Characteristics and Application, Applied Catalysis A: General, 186 (1999) 343-354.

[52] S. Sun, N. Tsubaki, K. Fujimoto, The Reaction Performances and Characterization of Fischer-Tropsch Synthesis Co/SiO_2 Catalysts Prepared from Mixed Cobalt Salts, Applied Catalysis A: General, 202 (2000) 121-131.

[53] K. Yokota, Y. Hanakata, K. Fujimoto, Supercritical Phase Fischer-Tropsch Synthesis Reaction: 3. Extraction Capability of Supercritical Fluids, Fuel, 70 (1991) 989-994.

[54] N.O. Elbashir, P. Dutta, A. Manivannan, M.S. Seehra, C.B. Roberts, Impact of Cobalt-Based Catalyst Characteristics on the Performance of Conventional Gas-Phase and Supercritical-Phase Fischer-Tropsch Synthesis, Applied Catalysis A: General, 285 (2005) 169-180.

[55] X. Huang, C.W. Curtis, C.B. Roberts, Reaction Behavior of Fischer-Tropsch Synthesis in Near Critical and Supercritical Hexane Media, American Chemical Society Division of Fuel Chemistry, 47 (2002) 150-153.

[56] K. Yokota, K. Fujimoto, Supercritical Phase Fischer-Tropsch Synthesis Reaction, Fuel, 68 (1989) 255-256.

[57] W. Linghu, X. Li, K. Asami, K. Fujimoto, Supercritical Phase Fischer-Tropsch Synthesis over Cobalt Catalyst, Fuel Processing Technology, 85 (2004) 1121-1138.

[58] D.B. Bukur, X. Lang, L. Nowicki, Comparative Study of an Iron Fischer-Tropsch Catalyst Performance in Stirred Tank Slurry and Fixed-Bed Reactors, Industrial & Engineering Chemical Research, 44 (2005) 6038-6044.

[59] X. Huang, N.O. Elbashir, C.B. Roberts, Supercritical Solvent Effects on Hydrocarbon Product Distributions from Fischer-Tropsch Synthesis over an Alumina-Supported Cobalt Catalyst, Industrial & Engineering Chemical Research, 43 (2004) 6369-6381.

[60] K. Snavely, B. Subramaniam, On-Line Gas Chromatographic Analysis of Fischer-Tropsch Synthesis Products Formed in a Supercritical Reaction Medium, Industrial & Engineering Chemical Research, 36 (1997) 4413-4420.

[61] C.S. Kellner, A.T. Bell, The Kinetics and Mechanism of Carbon Monoxide Hydrogenation over Alumina-Supported Ruthenium, Journal of Catalysis, 70 (1981) 418-432.

[62] A. Irankhah, A. Haghtalab, Fischer-Tropsch Synthesis Over Co-Ru/γ-Al_2O_3 Catalyst in Supercritical Media, Chemical Engineering Technology, 31 (2008) 525-536.

[63] N.O. Elbashir, Opportunities for Selective Control of Fischer-Tropsch Synthesis Hydrocarbons Product Distribution, in: F. Benyahia, F.T. Eljack (Eds.) 2nd Annual Gas Processing Symposium, Elsevier, Doha, Qatar, 2010, pp. 197-208.

[64] S. Yan, L. Fan, Z. Zhang, J. Zhou, K. Fujimoto, Supercritical-Phase Process for Selective Synthesis of Heavy Hydrocarbons from Syngas on Cobalt Catalysts, Applied Catalysis A: General, 171 (1998) 47-254.

[65] N. Tsubaki, K. Yoshii, K. Fujimoto, Anti-ASF Distribution of Fischer-Tropsch Hydrocarbons in Supercritical-Phase Reactions, Journal of Catalysis, 207 (2002) 371-375.

[66] A.T. Bell, Catalytic Synthesis of Hydrocarbons over Group VIII Metals. In: A Discussion of the Reaction Mechanism, Catalysis Reviews: Science and Engineering, 23 (1981) 203-232.

[67] L. Fan, K. Yokota, K. Fujimoto, Characterization of Mass Transfer in Supercritical-Phase Fischer-Tropsch Synthesis Reaction, Topics in Catalysis, 2 (1995) 267-283.

[68] R. Hussain, Analysis of Alcohols in FTS Product Distribution, in, Texas A&M University at Qatar, Doha, Qatar, 2014.

[69] H.H. Nijs, P.A. Jacobs, On-Line Single Run Analysis of Effluents from a Fischer-Tropsch Reactor, Chromatographic Science, 19 (1980) 40-45.

APPENDIX A

CATALYST PREPARATION CALCULATIONS

10.0 grams of 15 %wt Co/Al_2O_3 catalyst needed to be prepared in order to be used in the FTS reactions. To do so, the weight fraction of cobalt in the cobalt precursor ($Co(NO_3)_2.6H_2O$) used was required.

The molecular weight of $Co(NO_3)_2.6H_2O$ is equal to $MW_{Co(NO_3)_2 \bullet 6H_2O} = 291 g/mol$ Moreover, the molecular weight of Co is $MW_{Co} = 58.93 g/mol$. Thus, the weight of Co in 1.0 gram of $Co(NO_3)_2.6H_2O$ would be 58.93 g/mol. Equivalently the mass fraction of Co is:

$$x = \frac{58.93 gCo}{291 gCo(NO_3)_2 \bullet 6H_2O} = 0.2025 \quad (2)$$

Therefore, to have 1.0 g of Co we need

$$\frac{1.0 gCo}{0.2025 g \, {Co}/{Co(NO_3)_2 \bullet 6H_2O}} = 4.94 gCo(NO_3)_2 \bullet 6H_2O \quad (3)$$

Next, the amount of cobalt and support required to have 15 %wt Co/Al_2O_3 catalyst was determined. The weight of Co required for 10 grams of catalyst was:

$$10gcat * 0.15 \, {gCo}/{gcat} = 1.5gCo \quad (4)$$

Which means that the needed cobalt precursor amount is:

$$1.5gCo * 4.94 \, {gCo(NO_3)_2 \bullet 6H_2O}/{gCo} = 7.41gCo(NO_3)_2 \bullet 6H_2O \quad (5)$$

Similarly, the amount of Al_2O_3 needed is:

$$10gcat * (1 - 0.15) \, {gAl_2O_3}/{gcat} = 8.5gAl_2O_3 \quad (6)$$

The total pore volume of the available Al_2O_3 is 1.14 cm^3/g Al_2O_3 = 1.14 mL/g Al_2O_3, So for the 8.5 grams of Al_2O_3, the total pore volume would be 9.69 mL, which respond to the minimum volume of catalyst solution required to achieve the incipient wetness.

Next, the volume of solution (deionized water) required to prepare the 2 M catalyst solution was estimated. As previously calculated the weight of the catalyst precursor required is 7.41 g. The number of moles of $Co(NO_3)_2.6H_2O$ (the solute) in that is:

$$n_{solute} = \frac{m_{solute}}{MW_{solute}} = \frac{7.41g}{291g/mol} = 0.0255molCo(NO_3)_2 \bullet 6H_2O \quad (7)$$

The volume of solution (deionized water) required can be found next as follow:

$$V_{solution} = \frac{n_{solute}}{M} = \frac{0.0255g}{2.0mol/L} = 0.0127LH_2O = 12.7mLH_2O \quad (8)$$

That is greater than the minimum volume required to achieve incipient support wetness.

APPENDIX B

CALCULATING CO CONSUMPTION RATE AND CONVERSION

The CO inlet flow rate to the FTS reactor was measured and controlled by the MFC; however, CO participates in the FTS reaction, and thus its outlet flow rate cannot be known directly. In order to be able to calculate the outlet CO flow rate, it was necessary to use an inert (argon) as an internal standard. The method adopted herein is similar to that previously used by Nijs and Jacobs [69]. Argon does not participate in the FTS reaction, and thus its inlet and outlet flow rates are equal under steady-state conditions. Hence, it can be used to calibrate the outlet CO flow rate by relating the CO peak area/Ar peak area ratio (found using on-line Shimadzu GC TCD channel 2) to CO flow rate. The trend line (straight-line equation) of the peak area ratio (PA_{CO}/PA_{Ar}) against the CO flow rate can then be used to calculate the CO outlet flow rate as follows:

$$Q_{CO,out} = \frac{\left[\left(\frac{PA_{CO}}{PA_{Ar}}\right) + b\right]}{a} \tag{9}$$

Where "a" is the slope and "b" is the intercept.

For example, syngas with H_2:CO of 2:1 (CO is 1/3 of syngas flow) was allowed into the system at different flow rates (10 – 200) nmL/min. Argon was allowed at constant flow rate (10 or 15) nmL/min. The resulting gas mixture was then directed toward the on-line GC/TCD, where CO and Ar peak areas were determined. CO and Ar peak ratio

(PA_{CO}/PA_{Ar}) was then calculated and plotted against CO flow rate. Figure 48 shows the calibration line for argon flow rate of 15 nmL/min. The resulting straight line equation (y = 0.0548x - 0.0264), where y = PA_{CO}/PA_{Ar} and x = $Q_{co,out}$ can be rearranged to find the outlet CO flow rate as follows:

$$Q_{CO,out} = \frac{\left[\left(\frac{PA_{CO}}{PA_{Ar}}\right) + 0.0264\right]}{0.0548} \tag{10}$$

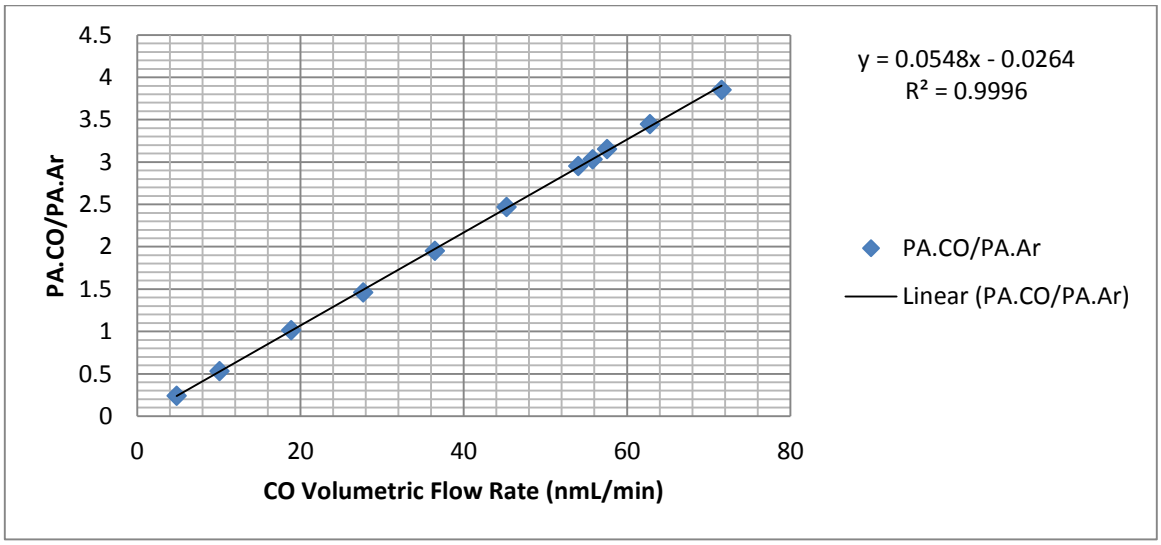

Figure 48. CO/Ar calibration curve at 15 nmL/min Ar flow rate, used to calculate outlet CO flow rate.

The material balance calculation was based on carbon, where the amount of carbon (as CO) entering the reactor is equal to the amount of carbon (as unreacted CO and produced hydrocarbons) leaving it. Therefore, the CO consumption rate and conversion

throughout the experimental run were calculated based on the difference between moles of CO entering the reactor and moles of unreacted CO leaving the reactor, following the below steps (equations). Note that syngas H_2:CO ratio of 2:1 was normally used unless CO, H_2 were introduced separately.

$$Q_{CO,out} = \frac{\left[\left(\frac{PA_{CO}}{PA_{Ar}}\right) + b\right]}{a} \tag{11}$$

$$CO \quad consumption \quad (nmL/\min) = \left(\frac{Q_{syngas,in}}{3} + Q_{CO,in}\right) - Q_{Co,out} \tag{12}$$

$$CO \ consumption\left(\mu mol/g.cat\right) = \frac{CO \ consumption\left(nmL\right)}{\min} \frac{1.01325 bar}{273.15 K} \frac{10^6 \mu mol}{1 mol} \frac{1\min}{60 s} \frac{mol.K}{83.14 bar.mL} \frac{1}{xg.cat} \tag{13}$$

$$CO \quad conversion \quad \% = \frac{CO \quad consumption \quad (nmL/\min)}{\left(\frac{Q_{syngas,in}}{3} + Q_{CO,in}\right)} \times 100\% \tag{14}$$

APPENDIX C

CALCULATING METHANE FORMATION RATE AND SELECTIVITY

To be able to calculate the CH_4 flow rate, a calibration gas with 10.09 CO mol % and 4.00 CH_4 mol % (n_{CH4}/n_{CO} molar ratio = 0.397) was used to find the responding peak area for each component and relate CO flow rate to CH_4 flow rate.

The peak areas for CO and CH_4 were identified by the on-line GC-TCD as 32790 and 10855, respectively. Thus, the CH_4/CO peak area ratio (PA_{CH4}/PA_{CO}) is 0.331.

The molar ratio and peak area ratio were used to calculate CH_4 outlet flow rate as follows:

$$Q_{CH_4,out} = \left(\frac{PA_{CH_4,out}}{PA_{CO,out}} \right) \cdot \left[\frac{\left(\frac{n_{CH_4}}{n_{Co}} \right)}{\left(\frac{PA_{CH_4}}{PA_{CO}} \right)} \right] \cdot Q_{CO,out} \tag{15}$$

The CH_4 formation rate and selectivity throughout the experimental run were calculated using below equations.

$$Q_{CH_4,out} \ \ (CH_4 \ \ formation) \ \ (nmL/\min) = \left(\frac{PA_{CH_4,out}}{PA_{CO,out}} \right) \cdot \left[\frac{\left(\frac{n_{CH_4}}{n_{Co}} \right)}{\left(\frac{PA_{CH_4}}{PA_{CO}} \right)} \right] \cdot Q_{CO,out} \tag{16}$$

$$CH_4 \quad formation \quad (\mu mol / g.cat.s) = \frac{CH_4 \quad formation \quad nmL}{\min} \cdot \frac{1.01325 bar}{273.15 K} \cdot \frac{10^6 \mu mol}{1 mol} \cdot \frac{1 \min}{60 s} \cdot \frac{mol.K}{83.14 bar.mL} \cdot \frac{1}{xg.cat} \quad (17)$$

$$CH_4 \quad selectivity \quad \% = \frac{CH_4 \quad formation \quad (nmL/\min)}{\left(\frac{Q_{syngas,in}}{3} + Q_{CO,in} - Q_{CO,out} \right)} \times 100\% \quad (18)$$

APPENDIX D

PRODUCT DISTRIBUTION, ASF AND CHAIN GROWTH PROBABILITY CALCULATIONS

To start the product distribution calculations, a reference or starting point was needed. For the on-line GC, this was the CH_4 formation rate (g/g.cat.h), previously determined using the GC TCD. The TCD CH_4 formation rate with the CH_4 peak area given by the FID was used as a reference ratio and held constant for each sample. The ratio was then used to calculate the formation rate of hydrocarbons with different carbon numbers. For the off-line GC FID analysis, a similar approach was used, however the CH_4 formation rate (g/g.cat.h) was replaced with *n*-C_7 formation rate, determined using the on-line FID, and the on-line *n*-C_7 formation rate with the off-line *n*-C_7 peak area was used as a reference ratio in this case.

As previously discussed in section IV.1 (Peak Identification), each hydrocarbon present in the FID spectrum was identified and assigned with its distinct carbon number and type (isomer, normal, olefin, alcohol). After that, the peak area for each carbon number with the same type was summed, and then the total peak area for each carbon number was summed. The weighted molecular weight for each carbon number (n) was then estimated as follows:

$$Weighted \quad MW = \frac{\sum\left(PA_{n,Type} \cdot MW_{n,Type}\right)}{Total \quad PA_n} \tag{19}$$

The total hydrocarbon formation rate for each carbon number (n), was then calculated as follows:

$$Hydrocarbon\quad formation\quad (mol/g.cat.h) = \frac{\left[\left(\frac{\$CH_4\quad formation\quad TCD\$}{\$CH_4\quad PA\quad FID\$}\right)\cdot Total\quad PA_n\right]}{\left[\frac{\sum\left(PA_{n,Type}\cdot MW_{n,Type}\right)}{Total\quad PA_n}\right]} \quad (20)$$

$$Hydrocarbon\quad formation\quad (g/g.cat.h) = \left[Hydrocarbon\quad formation\quad (mol/g.cat.h)\right]\cdot\left(Weighted\quad MW_n\right) \quad (21)$$

Parffins formation rate was similarly calculated using below equation.

$$Paraffins\quad formation\quad (mol/g.cat.h) = \left(\frac{\$CH_4\quad formation\quad TCD\$}{\$CH_4\quad PA\quad FID\$}\right)\cdot\left[\frac{\left(PA_{isomers}+PA_{normal}\right)}{MW_{normal}}\right] \quad (22)$$

The weight fraction of hydrocarbons containing "n" carbon atoms (W_n) was then calculated as follows.

$$W_n = \frac{Hydrocarbon\quad formation\quad (g/g.cat.h)\quad for\quad n}{\$\sum\left[Hydrocarbon\quad formation\quad (g/g.cat.h)\right]\$} \quad (23)$$

The natural logarithm of the weight fraction of carbon number "n" over the carbon number [$\ln(W_n/n)$] was calculated in order to plot the ASF distribution, where [$\ln(W_n/n)$] was plotted against "n". The slope of the trend line can then be used to find the chain growth probability as follows.

$$\ln\left(\frac{W_n}{n}\right) = \left[\ln(\alpha)\right] \cdot n + \ln\left[\frac{(1-\alpha)^2}{\alpha}\right] \tag{24}$$

Where $\ln(\alpha)$ is the slope of the trend line and the chain growth probability is equal to the exponential of the slope ($\alpha = e^{slope}$).

APPENDIX E

CALCULATING OLEFINS FORMATION RATE AND WEIGHT CONTENT

The olefin formation rate was calculated using the same technique used to calculate the hydrocarbon and paraffins formation rates. The equation used to calculate olefin formation rate for carbon number "n" is given next.

$$Olefin \quad formation \quad (mol/g.cat.h) = \left(\frac{\$CH_4 \quad formation \quad TCD\$}{\$CH_4 \quad PA \quad FID\$} \right) \cdot \left(\frac{PA_{olefin}}{MW_{n,olefin}} \right) \quad (25)$$

Next, the olefin to paraffin ratio for each carbon number was calculated by dividing the formation rate of olefins over that of paraffins, for the same carbon number. Finally, the olefin content (olefin wt%) was determined as follows.

$$Olefin \quad wt\% = \left[Olefin \quad formation \quad (mol/g.cat.h) \right] \cdot \left[\frac{MW_{olefin} \quad (g/mol)}{Hydrocarbon \quad formation \quad (g/g.cat.h)} \right] \times 100\% \quad (26)$$